Book of abstracts

PHOTONICA2017

The Sixth International School and Conference on Photonics

& COST actions: MP1406 and MP1402

MultiscaleSolar

HERALD

&H2020-MSCA-RISE-2015 CARDIALLY workshop

CARDIALLY

28 August – 1 September 2017

Belgrade, Serbia

Editors

Marina Lekić and Aleksandar Krmpot

Institute of Physics Belgrade, Serbia

Belgrade, 2017

ABSTRACTS OF TUTORIAL, KEYNOTE, INVITED LECTURES, PROGRESS REPORTS AND CONTRIBUTED PAPERS

of

The Sixth International School and Conference on Photonics
PHOTONICA2017

28 August – 1 September 2017
Belgrade Serbia

Editors
Marina Lekić and Aleksandar Krmpot

Technical assistance
Marko Nikolić and Danica Pavlović

Publisher
Institute of Physics Belgrade
Pregrevica 118
11080 Belgrade, Serbia

Printed by
Serbian Academy of Sciences and Arts

Number of copies
300

ISBN 978-86-82441-46-5

Improved thermal and mechanical properties of tot'hema–gelatin eco-friendly films

B. Muric, D. Pantelic, D. Vasiljevic and B. Jelenkovic
Institute of Physics,
Belgrade, Serbia
e-mail:muric@ipb.ac.rs

Today, biodegradable films have known as significant eco-friendly food packaging materials to reduce of plastic wastes [1]. Biodegradable films were mainly made from some biopolymers such as polysaccharides [2], and proteins [3]. Among them, gelatin [4] considered to be the most ideal candidate.
The thermal and mechanical properties of tot'hema-gelatin films were investigated to determine their suitability as eco-friendly films. The influence of different tot'hema concentrations on the physicochemical properties of gelatin films, and consequently on mechanical, and thermal properties was analyzed. A series of tot'hema-gelatin films were made by the gravity settling method. Results showed that prepared films were plasticized by tot'hema adding, and their mechanical properties (tensile strength, elastic modulus, elongation at break) were significantly improved.With the increase of tot'hema content, thickness and tensile strength (TS) of gelatin films increased, and the elongation at break (EB) decreased. Gelatin films containing 30% tot'hema had limit values of the thickness. In addition, thermal properties characterized by differential scanning calorimetry (DSC) showed that the thermal stability of films was better.In the thermograms of gelatin modified films, four endothermic peak can be observed. Briefly, the films prepared from gelatin and tot'hema showed great potential for packaging applications.

REFERENCES

[1] A. Etxabide, I. Leceta, S. Cabezudo, P. Guerrero, K. de la Caba, ACS Sustainable Chem. Eng. 4, 4626 (2016).
[2] C. Li, J. Luo, Z. Qin, H. Chen, Q. Gao, J. Li, RSC Adv. 5, 56518 (2015).
[3] X. Liu, R. Song, W. Zhang, C. Qi, S. Zhang, J. Li, Sci Rep. 7, 44289 (2017).
[4] X. Wu, Y. Liu, W. Wang, Y. Han, A. Liu, J Food Process Eng. 40, e12469 (2017).

Europium and Samarium dopant ions as luminescent sensors of Y_2O_3 phase transitions under high pressure

Ana Vlašić[1], Mihailo Rabasović[1], Branka Murić[1], Vladan Čelebonović[1] and Marko G. Nikolić[1]
[1]*Institute of Physics,*
Belgrade, Serbia
e-mail:vlasic.ana88@gmail.com

Rare earth ions (RE^{3+}) are highly sensitive to local symmetry. Any change in the symmetry is observable in their luminescence spectra [1]. In this work we investigated the photoluminescence properties of cubic and monoclinic Y_2O_3 matrix, doped with either Eu^{3+}or Sm^{3+} ions, under high pressure. Photoluminescence emission measurements for cubic Y_2O_3were recorded in the pressure range from 0 to 20 GPa for Y_2O_3:Sm^{3+}, and from 0 to 15 GPa for Y_2O_3:Eu^{3+}. Measurements for the monoclinic matrix were recorded from 0 to 8 GPa for Y_2O_3:Eu^{3+}.

With varying pressure the intensity ratio of $^4G_{5/2} \rightarrow {}^6H_{7/2}$ and $^4F_{3/2} \rightarrow {}^6H_{7/2}Sm^{3+}$ emission lines has three distinct regions. In the pressure range from 9.2 GPa to 13.1 GPa it has a steep pressure dependence and could be used for detecting a pressure induced phase transition in the Y_2O_3 matrix from cubic to monoclinic crystal structure. Furthermore, the intensity ratio of $^5D_0 \rightarrow {}^7F_1$ and $^5D_0 \rightarrow {}^7F_2Eu^{3+}$ emission lines in the cubic matrix has a similar pressure dependence to the intensity ratio of these Sm^{3+} emission lines. It matches the behavior of the pressure sensitive Sm^{3+} dependence in the range from 9.1 GPa to 11.6 GPa, and is proven to contain a phase transition around 11 GPa [2].

The monoclinic Y_2O_3:Eu^{3+} also has a pressure-sensitive intensity ratio of $^5D_0 \rightarrow {}^7F_1$ and $^5D_0 \rightarrow {}^7F_2$ emission lines. The dependence is unambiguous, without phase transitions in the measured region. The definitive nature and high sensitivity suggests that this dependence can be used as an efficient high pressure sensor.

REFERENCES

[1] G. Blasse, B. C. Grabmaier, Luminescent Materials, Berlin, Springer Verlag (1994).
[2] J. Zhang, H. Cui, P. Zhu, C. Ma, X. Wu, H. Zhu, Y. Ma, Q. Cui, J. Appl. Phys. 115, 023502 (2014).

Application of Tot'hema Eosin Sensitized Gelatin Film for Adaptive Microlenses

BRANKA D. MURIĆ, University of Belgrade,
Institute of Physics, Belgrade
DEJAN V. PANTELIĆ, University of Belgrade,
Institute of Physics, Belgrade
DARKO M. VASILJEVIĆ, University of Belgrade,
Institute of Physics, Belgrade
SVETLANA N. SAVIĆ-ŠEVIĆ, University of Belgrade,
Institute of Physics, Belgrade
BRANISLAV M. JELENKOVIĆ, University of Belgrade,
Institute of Physics, Belgrade

Original scientific paper
UDC: 617.7-76
DOI: 10.5937/tehnika1706787M

In this paper we showed that tot'hema eosin sensitized gelatin (TESG) film can be used for adaptive microlenses fabriacation. The mechanical properties of a pure gelatin film were improved by adding tot'hema solution. We found that the elasticity of TESG film depend on the tot'hema concentration. By stretching the film, the microlenses were deformed uniaxially, and microlenses focal length can be tuned. The achieved microlenses focal lengths range from 0.05 to 0.2 mm.

Key words: *gelatin film, eosin, tot'hema, adaptive microlenses, optical properties, mechanical properties*

1. INTRODUCTION

Optical lenses are widely used in science, industry, and daily life. Microlenses are lenses with dimensions smaller than 1mm. It can be used, either individually or as microlens arrays, in a various applications such as: wavefront sensors, medicine, quantum computer research and so on [1-7].

Direct laser writing, photolithography, and thermal reflow, as well as copying techniques such as hot embossing, and injection molding are various methods of microlens fabrication [8-14].

Various materials such as polymers, photosensitive glass, composites, and many other are used in the microlens fabrication[15-20].

Development of tunable lenses with variable focal lengths is very important for different applications. It can be used in eyeglasses for vision correction, zooming devices in photocameras and integrated in many electrooptical systems. Also, adapive microlenses is significant for tunable photonic waveguides, miniature optical sensing, electronic display, and widezoom cell phone [21-24].

Today, in many cases is necessary to use adaptive microoptical devices, primarily microlenses. In most optical devices, microlenses have an important role in a focusing, imaging, detection, etc. Different variants of adaptive microlenses arrays were proposed [25, 26].

Gelatin is a biocompatible and biodegradable polymer extensively used in food, pharmaceutical, biophysics and biomedical fields. Poor mechanical properties of gelatin film can be improved by crosslinking with various chemical agents such as formaldehyde, epoxy compounds, genipin and glutaraldehyde (GTA) [27–29].

Previously, by modifying the gelatin with tot'hema solution, we improved the mechanical properties of the brittle film of pure gelatin. So we get a film based on gelatin doped with tot'hema and sensitized with eosin dye [30–33], (denoted as tot'hema-eosin sensitized gelatin, abbreviated as TESG.

The TESG film is easy to prepare, low cost nontoxic, and became stretchable by adding tot'hema

Author's address: Branka Murić, University of Belgrade, Institute of Physics, Belgrade, Pregrevica 118
e-mail: muric@ipb.ac.rs
Paper received: 01.12.2017.
Paper accepted: 08.12.2017.

solution. On the film microlenses can be formed by direct laser writing. Our main intention was to use TESG, as biocompatible, thermally stable, soft and elastic material, for tunable microlens fabrication. The microlenses with different diameter and depth were produced on a TESG layer using Nd:YAG laser light (2nd harmonic wavelength of 532 nm).

In this paper, TESG microlenses focal length tunability was obtained by applying controlled strain. The produced adaptive concave TESG microlenses (individual or microlens array) are suitable for numerous applications. Also, they can be copied onto polydimethylsiloxane (PDMS) and used as convex lenses. The shape change of TESG microlenses (and consequently the focal length) was reversibly changed as the applied strain is inside the elastic limit, that be presented in our future work.

2. EXPERIMENTAL PROCEDURE

Film preparation

All chemical components used for the film preparation are easily available, cheap and nontoxic. Tot'hema (Laboratoire Innotech International-France) - the trade name of a mixture of iron gluconate (equivalent to 50 mg iron), manganese gluconate (equivalent to 1.33 mg manganese), copper gluconate (equivalent to 0.7 mg copper) and excipients. It is a drinkable solution frequently used to treat anemia.

The 100 ml of 5% aqueous gelatin (Gelatin from bovine skin gel strength ~225 g Bloom, Type B, Sigma) solution with 20% of sodium chloride (puriss, p.a. Sigma Aldrich) by weight of dry gelatin, and 0.3 ml of 1% aqueous eosin (5wt.% in H_2O, Sigma Aldrich) solution was prepared as describred previously [31, 32]. The five TESG solutions with different tot'hema concentrations (5%, 10%, 15%, 20%, and 30% v/v) were made.

TESG film was prepared by the gravity-settling method pouring 2 ml of TESG solution onto a leveled and cleaned microscope glasses slide covered with a very clean thermoplastic foil. The net result is a film, which is highly absorptive in the green part of the spectrum, permanently soft and elastic. Dried film can be easily removed from the foil. It can be peeled from one substrate and placed on another (plane or curved). The film was dumbbell-shaped specimens cut by the brass mold made according to the standards for elastic materials (ASTM D412).

Microlens fabrication

If TESG film irradiated with laser radiation in the green part of spectrum, (direct, focused or unfocused) laser beam produces lens like-dips. We have shown that concave microlenses can be produced by direct laser writing using second harmonic Nd:YAG laser (wavelength of 532 nm). Microlens formation was followed by the creation of a diffraction picture on a diffuse screen, with millimeter scale, placed behind the film. This pattern was recorded by a CCD camera. The used experimental setup is shown in Figure 1. The laser power of 60 mW and exposure time of 20 s was used in experiment.

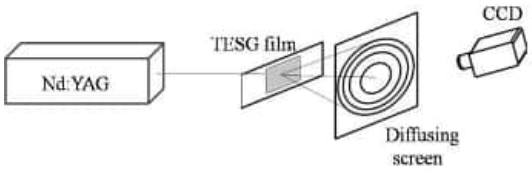

Figure 1 – Experimental setup for microlens fabrication

Film thickness

Film thickness was measured with a digital micrometer with 0.01 mm accuracy. Six thickness measurements were taken for each TESG film, and the averages were taken as the result.

Water content of TESG film

To estimate varying of water content during the film dehydration, the TESG films were weighed (m_w), dried at ambient temperature (20±2°C) for different time, and weighted (m_d) again. Water content (or moisture content) was determined as the percentage of initial TESG film weight lost during drying and reported on a wet basis i.e:

$$\%\, moisture\ content = 100(m_w - m_d)/m_w$$

Triplicate measurements of water content were done for each film, and an average was taken as the result.

Swelling of TESG film

TESG films were weighted in air-dried conditions (W_d). Afterward, they were immersed in a physiological saline solution, containing 9 g/l sodium chloride, for different time periods. Wet samples were wiped with filter paper to remove excess of liquid and reweighted (W_w). The amount of adsorbed water was calculated:

$$W(\%) = 100(W_w - W_d)/W_d$$

Stress−Strain Measurements

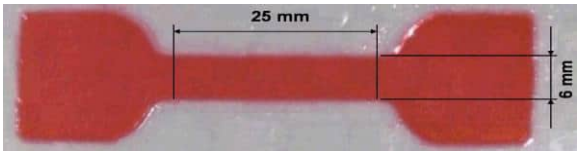

Figure 2 – TESG films used for tensile testing with dimensions according to the ASTM standards (gauge length 25 mm, width 6 mm)

Stress−strain measurements of TESG films were determined in a tensile stress testing machine. Tests were carried out at 25 °C with a strain rate of 20 mm/min, using dumbbell-shaped film (see Figure 2) mounted at a specified gauge length (25 mm) into the system.

Using the appropriate software recorded force and corresponding displacement were recalculated into stress and strain.

The average value of five measurements for every film was calculated. The video camera was used to record the tensile responses of all films.

SEM analysis of microlenses

The morphology of produced TESG microlenses were investigated using a high resolution scanning electron microscope equipped with a high brightness Schottky field emission gun (FEGSEM).

3. RESULTS AND DISCUSSIONS

Variation of water content in TESG films with different tot'hema concentration with drying time is presented in Figure 3.

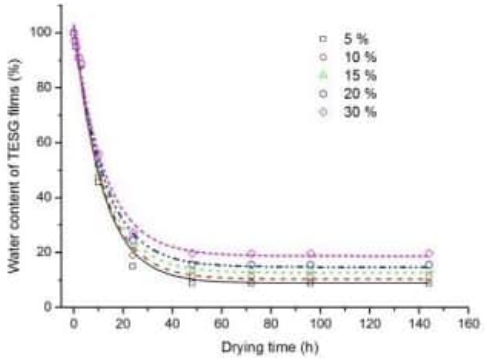

Figure 3 – Variation of water content of TESG films with drying time

It can be seen that the water content of each TESG films decreases with drying time up to 48 hour. After drying of two days, there is no additional change in the water content for all TESG films.

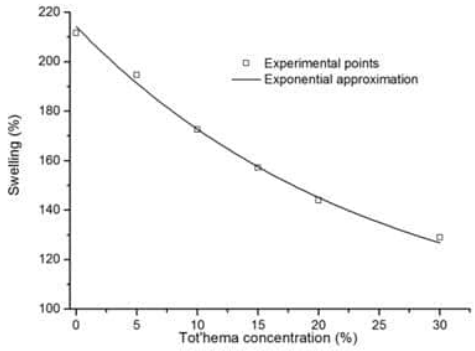

Figure 4 – Swelling of gelatin films as a function of tot'hema concentrations

The degree of swelling of pure gelatin films stored in physiological solution increases up to about 220 % after 24 h. Tot'hema induces a reduction of swelling. From Figure 4 can be seen that swelling of TESG films exponentially decreases with increasing of tot'hema concentration. We found that swelling improve the film elasticity.

During a laser irradiation, eosin bleaches, thus making TESG film colorless. In this case, as result of dye discolouration under the influence of optical radiation the transparent microlenses are formed, as can be seen in Figure 5.

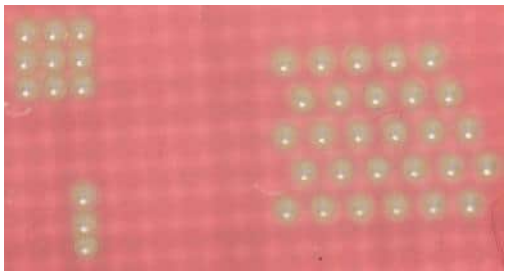

Figure 5 – Transparent 3x3 microlens array, and row of three microlenses (left) and hexagonal microlens array (right) on the TESG film

Figure 6 shows the stretching of microlens formed in the centre of a dumbbell-shaped TESG film.

Figure 6 – The TESG microlens on the dumbbell-shaped TESG film: 1) unstretched; and 2) stretched

The stretching value can be read on the ruler located parallel to film. It can be seen that TESG film stretched from the initial 25 mm to 80 mm.

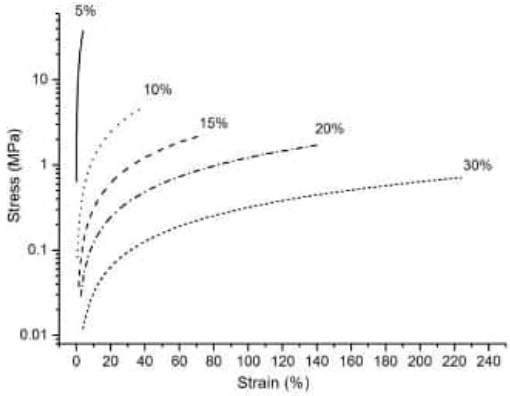

Figure 7 – Stress versus strain curves of TESG films

The results of uniaxial stress–strain measurements for all examined films are shown in Figure 7. The tensile responses of TESG films were measured up to the breaking point. As can be seen, mechanical

properties of TESG films strongly depend on the tot'hema concentrations. The extensibility of the films increases, with increasing of tot'hema concentration up to 250%..

The Young's modulus, the stress at break and the deformation at break of the films were calculated from the stress–strain curves. We found that Young's modulus and stress at break considerably decrease with increasing of tot'hema concentration.

Further we investigated the microlenses uniaxial stretching. Microlenses fabrication is followed by formation of diffraction picture on the diffuse screen. The recorded diffraction pictures extensions on a screen with a millimeter scale are shown in Figure 8.

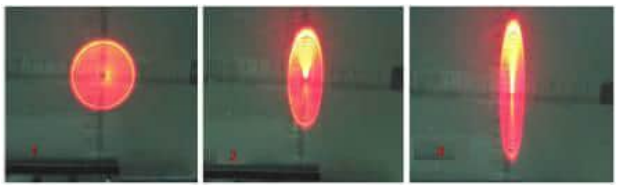

Figure 8 – Diffraction picture recorded after the TESG microlens was: 1) formed; 2) and 3) stretched in one direction. Millimeter scale is visible.

The toric microlenses were produced due to the uniaxial strain. The astigmatic microlenses have two focal lengths along orthogonal directions. For uniform extension (along x and y direction) sphericity of microlenses can be retained.

It was shown that produced TESG microlenses change their optical properties, for example focal length, in response to material elasticity.

The relation between the focal length and strain is shown in Figure 9.

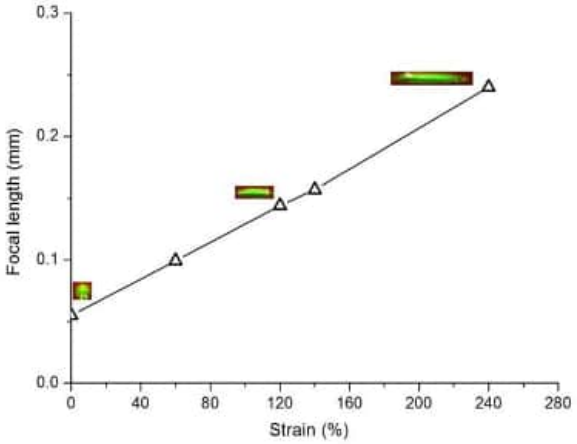

Figure 9 – TESG microlens focal length versus strain

The microlens focal length exponentially increases with increasing strain of TESG film. The focal length was reversibly changed as long as the applied strain is inside the elastic limit. It was noticed that there is a linear dependence between the microlens focal length and diffraction pattern width (see Figure 10).

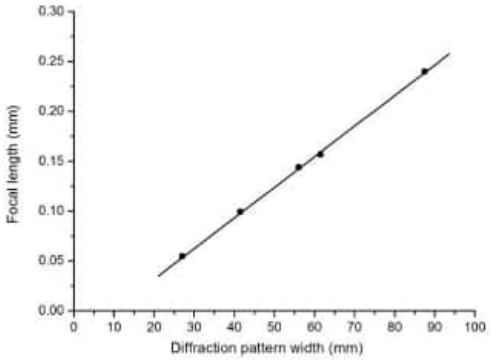

Figure 10 – TESG microlens focal length versus diffraction patern width

The strain responsive, transparent TESG microlenses offer interesting possibilities in tunable optical devices and sensors. Also, closely packed (hexagonal or square) microlenses arrays can be used to mimicking biological structure such as compound eyes. Hexagonal TESG microlenses arrays observed with an electron microscope is shown in Figure11.

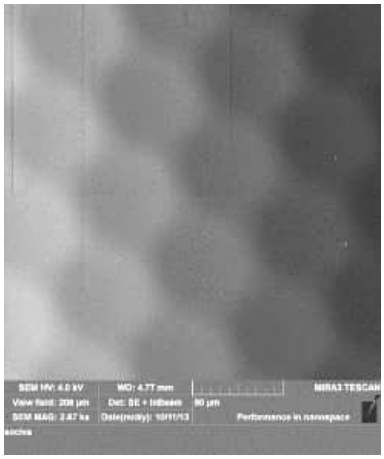

Figure 11 – Image of hexagonal TESG microlenses array is recorded using a field-emission gun scanning electron microscope (FEGSM)

Using of microlenses for visualization it is possible to obtain high-quality images. The picture of hexagonal TESG microlenses arrays with observed milimeter paper at its centre is shown in Figure 12.

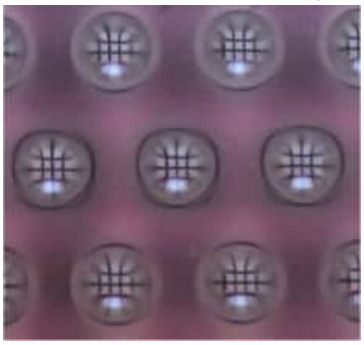

Figure 12 – Image of hexagonal TESG microlenses array recorded using an optical microscope

4. CONCLUSION

Tunable (strain responsive) microlenses were prepared on elastic TESG film. Stretching the film of about 250%, microlenses are uniaxial deformed so that the focal lengths were changed.The microlenses focal lengths from 0.05 mm to 0.2 mm were obtained. As TESG proved to be a good material for adaptive microlensess, we plan to retain sphericity of microlenses in the future and to achieve uniform stretching along both axes.

The TESG microlenses show good optical and imaging properties. The individual concave microlenses can be used. Also, the large-area square or hexagonal close-packed microlenses array can be used for various applications such as: medical laser, optical sensors, light-field cameras, biological structures. Convex microlenses can be produced by coping TESG lenses onto polydimethylsiloxane (PDMS).

5. ACKNOWLEDGEMENT

This paper was written as a part of research on the projects ON 171038 and III 45016 supported by the Ministry of Education, Science and Technological Development of the Republic of Serbia.

REFERENCES

[1] Liang W. L, Su G. D. J, Wide-angle and ultrathin camera module using a curved hexagonal microlens array and all spherical surfaces, *Appl. Opt.* Vol. 53, No 29, pp. H121-H128, 2014.

[2] Deng Z, Chen F, Yang Q, Bian H, Du G, Yong J, Shan C, Hou X, Dragonfly-eye-inspired artificial compound eyes with sophisticated imaging, *Adv. Funct. Materials* Vol 26, No 12, pp. 1995-2001, 2016.

[3] Zhang H, Li L, McCray D. L, Scheiding S, Naples N. J, Gebhardt A, Risse S, Eberhardt R, Yi A. Y, Development of a low cost high precision three-layer 3D artificial compound eye, *Opt. Express* Vol. 21, No 19, pp. 22232-22245, 2013.

[4] Zhang W, Zappe H, Seifert A, Wafer-scale fabricated thermo-pneumatically tunable microlenses, *Light: Science & Applications* Vol. 3, pp. e145, 2014.

[5] Varshney A, Gohil S, Tadavani S. K, Yethiraj A, Bhattacharya S, Ghosh S, Large scale arrays of tunable microlenses, *Lab Chip* Vol. 4, pp. 1330-1335, 2014.

[6] Lu D. X, Zhang Y. L, Han D. D, Wang H, Xia H, Chen Q. D, Ding H, Sun H. B. J, Solvent-tunable PDMS microlens fabricated by femtosecond laser direct writing, *Mater. Chem. C* Vol. 3, pp. 1751-1756, 2015.

[7] Pavia J. M, Wolf M, Charbon E, Measurement and modeling of microlenses fabricated on single-photon avalanche diode arrays for fill factor recovery, *Opt. Express* Vol. 22, No 4, pp. 4202-4213, 2014.

[8] Sadasivuni K. K, Ponnamma D, Ko H. U, Zhai L, Kim H. C, Kim J, J, Electroactive and optically adaptive bionanocomposite for reconfigurable microlens, *Phys. Chem. B* Vol. 120, No 20, pp. 4699-4705, 2016.

[9] Kim S, Kang S, Replication qualities and optical properties of UV-moulded microlens arrays, *J. Phys. D:Appl. Phys.* Vol. 36, No 20, pp. 2451–2456, 2003.

[10] Naessens K, Ottevaere H, Baets R, Van Daele P, Thienpont H, Direct writing of microlenses in polycarbonate with excimer laser ablation, *Appl. Opt.* Vol. 42, No 31, pp. 6349–6359, 2003.

[11] Wu M. H, Park C, Whitesides G. M, Fabrication of arrays of microlenses with controlled profiles using gray-scale microlens projection photolithography, *Langmuir* Vol. 18, No 18, pp. 9312–9318, 2002.

[12] Lee B. K, Kim D. S, Kwon T. H, Replication of microlens arrays by injection molding, *Microsyst. Technol.* Vol. 10, No 6-7, pp. 531–535, 2004.

[13] Ong N. S, Koh Y. H, Fu, Y. Q, Microlens array produced using hot embossing process, *Microelectron. Eng.* Vol. 60, No 3-4, pp. 365–379, 2002.

[14] PericetCamera R, Best A, Nett S. K, Gutmann J. S, Bonaccurso E, Arrays of microlenses with variable focal lengths fabricated by restructuring polymer surfaces with an ink-jet device, *Opt. Express* Vol. 15, No 15, pp. 9877–9882, 2007.

[15] Calixto S, Scholl M. S, Relief optical microelements fabricated with dichromated gelatin, *Appl. Opt.* Vol. 36, No 10, pp. 2101–2106,1997.

[16] Jones C. D, Serpe M. J, Shroeder L, Lyon L. A, Microlens formation in microgel/gold colloid composite materials via photothermal patterning, *J. Am. Chem. Soc.* Vol. 125, No 18, pp. 5292–5293, 2003.

[17] Jung H, Jeong Ki-H, Monolithic polymer microlens arrays with high numerical aperture and high packing density, *ACS Appl. Mater. Interfaces* Vol. 7, No 4, pp. 2160–2165, 2015.

[18] Wu M. H, Park C, Whitesides G. M, Fabrication of arrays of microlenses with controlled profiles using

gray-scale microlens projection photolithography, *Langmuir* Vol. 18, No 24, pp. 9312–9318, 2002.

[19]Fu Y, Bryan N. K, Semiconductor microlenses fabricated by one-step focused ion beam direct writing, *IEEE Trans.Semicond. Manuf*. Vol. 15, No 2, pp. 229–231, 2002.

[20]He M, Yuan X. C, Ngo N. Q, Bu J, Tao S. H, Single-step fabrication of a microlens array in sol–gel material by direct laser writing and its application in optical coupling, *J. Opt. A: Pure Appl. Opt*.Vol. 6, No 1, pp. 94–97, 2004.

[21]Peer A, Biswas R, Park J-M, Shinar R, Shinar Light management in perovskite solar cells and organic LEDs with microlens arrays, *Opt. Express* Vol. 25, No 9, pp. 10704–10709, 2017.

[22]Wrzesniewski E, Eom S.H, Cao W, Hammond W.T., Lee S, Douglas E.P, Xue J, Enhancing light extraction in top-emitting organic light-emitting devices using molded transparent polymer microlens arrays, *Small* Vol. 8, No 17, pp. 2647–2651, 2012.

[23]Tvingstedt K, Zilio S. Dal, Inganńs O, Tormen M, Trapping light with micro lenses in thin film organic photovoltaic cells, *Opt. Expr*ess Vol. 16, No 26, pp.21608–21615, 2008.

[24]Chen Y, Elshobaki M, Ye Z, Park J.M, Noack M.A, Ho K. M, Chaudhary S, Microlens array induced light absorption enhancement in polymer solar cells, *Phys. Chem. Chem. Phys*. Vol.15, pp. 4297–4302, 2013.

[25]Song Y. M, Xie Y, Malyarchuk V, Xiao J, Jung I, Choi K.J, Liu Z, Park H, Lu C, Kim R. H, Li R, Crozier K. B, Huang Y, Rogers J. A, Digital cameras with designs inspired by the arthropod eye, *Nature* Vol. 497, pp. 95–99, 2013.

[26]Li Z, Xiao J, Mechanics and optics of stretchable elastomeric microlens array for artificial compound eye camera, *J. Appl. Phys*. Vol. 117, pp. 014904, 2015.

[27]Bigi A, Bracci B, Cojazzi G, Panzavolta S, Roveri N., Drawn gelatin films with improved mechanical properties, *Biomaterials* Vol.19, No 24, pp. 2335–2340, 1998.

[28]Bigi A, Cojazzi G, Panzavolta S, Roveri N, Rubini K, Mechanical and thermal properties of gelatin films at different degrees of glutaraldehyde crosslinking, *Biomaterials* Vol. 22, No 8, pp. 763–768, 2001.

[29]Bigi A, Cojazzi G, Panzavolta S, Roveri N, Rubini K, Stabilization of gelatin films by crosslinking with genipin, *Biomaterials* Vol. 23, No 24, pp. 4827–4832, 2002.

[30]Muric B. D, Pantelic D. V, Vasiljevic D. M, Panic B. M. Properties of microlenses produced on a layer of tot'hema and eosin sensitized gelatin, *Appl. Opt*. Vol. 46, No 35, pp. 8527–8532, 2007.

[31]Muric B, Pantelic D, Vasiljevic D, Panic B, Microlens fabrication on tot'hema sensitized gelatin, *Opt. Mater*. Vol. 30, No 7, pp. 1217–1220, 2008.

[32]Muric B, Pantelic D, Vasiljevic D, ZarkovB, Jelenkovic B, Pantovic S, Rosic M, Sensitized gelatin as a versatile biomaterial with tailored mechanical and optical properties, *Phys. Scr*. Vol. T157, pp. 014018, 2013.

[33]Muric B, Pantelic D, Vasiljevic D, Panic B, Jelenkovic B, Thermal analysis of microlens formation on a sensitized gelatin layer, *Appl. Opt*. Vol. 48, No 19, pp. 3854–3859, 2009.

REZIME

PRIMENA FILMA ŽELATINA SENZIBILIZOVANOG TOT' HEMOM I EOZINOM ZA ADAPTIVNA MIKROSOČIVA

U ovom radu smo pokazali da se film želatina dopiran tot'hemom i senzibilizovan eozinom (TESG) može koristiti za proizvodnju adaptivnih mikrosočiva. Mehaničke osobine čistog želatinskog filma poboljšane su dodavanjem rastvora tot'heme. Utvrdili smo da elastičnost TESGfilma zavisi od vrednosti koncentracije tot'heme. Istezanjem filma, mikrosočiva su deformisana duž jedne ose, pa se žižna daljina mikrosočiva može podešavati. Postignute vrednosti žižne daljine kreću se od 0.05 do 0.2 mm.

Ključne reči: *film želatina, eozin, tot'hema, adaptivna mikrosočiva, optičke osobine, mehaničke osobine*

Serbian Ceramic Society Conference
ADVANCED CERAMICS AND APPLICATION VII
New Frontiers in Multifunctional Material Science and Processing

Serbian Ceramic Society
Institute of Technical Sciences of SASA
Institute for Testing of Materials
Institute of Chemistry Technology and Metallurgy
Institute for Technology of Nuclear and Other Raw Mineral Materials

PROGRAM AND THE BOOK OF ABSTRACTS

Serbian Academy of Sciences and Arts, Knez Mihailova 35
Serbia, Belgrade, 17-19. September 2018.

Serbian Ceramic Society Conference

ADVANCED CERAMICS AND APPLICATION VII

New Frontiers in Multifunctional Material Science and Processing

/ Serbian Ceramic Society / Institute of Technical Science of SASA /
/ Institute for Testing of Materials / Institute of Chemistry Technology and Metallurgy /
/ Institute for Technology of Nuclear and Other Raw Mineral Materials /

PROGRAM AND THE BOOK OF ABSTRACTS

Serbian Academy of Sciences and Arts, Knez Mihailova 35
Serbia, Belgrade, 17-19. September 2018

Book title:
Serbian Ceramic Society Conference -
ADVANCED CERAMICS AND APPLICATION VII
Program and the Book of Abstracts

Publisher:
Serbian Ceramic Society, Belgrade, 2018.

Editors:
Prof. dr Vojislav Mitić
Dr Lidija Mančić
Dr Nina Obradović

Technical Editors:
Ivana Dinić
Marina Vuković

Printing:
Serbian Ceramic Society, Belgrade, 2018.

Edition:
130 copies

CIP - Каталогизација у публикацији - Народна библиотека Србије, Београд
666.3/.7(048)
66.017/.018(048)

SRPSKO keramičko društvo. Conference Advanced Ceramics and Application : New Frontiers in Multifunctional Material Science and Processing (7 ; 2018; Beograd)
Program ; and the Book of Abstracts / Serbian Ceramic Society
Conference Advanced Ceramics and Application VII : New Frontiers in Multifunctional Material Science and Processing, Serbia, Belgrade, 17-19. September 2018 ; [organized by] Serbian Ceramic Society ... [et al.] ; [editors Vojislav Mitić, Lidija Mančić, Nina Obradović]. - Belgrade : Serbian Ceramic Society, 2018 (Belgrade : Serbian Ceramic Society). - 106 str. : ilustr. ; 30 cm
Tiraž 130.
ISBN 978-86-915627-6-2
a) Керамика - Апстракти b) Наука о материјалима - Апстракти c) Наноматеријали - Апстракти

COBISS.SR-ID 267569676

INV-OGE 3

Detection of high pressure phase transitions in RE^{3+} doped Y_2O_3 and Y_2MoO_6 through luminescence measurements

Marko G. Nikolić[1], Ana Vlašić[1], Mihailo Rabasović[1], Branka Murić[1], Vladan Čelebonović[1], Nadežda Stanković[2], Branko Matović[2] and Branislav Jelenković[1]

[1] *Institute of Physics, Belgrade University, Belgrade, Serbia*
[2] *Institute of Nuclear Sciences "Vinča", Belgrade University, Belgrade, Serbia*

Rare earth ions (RE^{3+}) are highly sensitive to local symmetry so changing the symmetry is reflected in their luminescence spectra. In this work we investigated the high pressure photoluminescence properties of cubic and monoclinic Y_2O_3, as well as, monoclinic Y_2MoO_6, doped either with Eu^{3+} or Sm^{3+} ions.

Photoluminescence emission of cubic Y_2O_3:Sm^{3+} and Y_2O_3:Eu^{3+} phases were recorded up to the pressure of 20 GPa and 15 GPa, respectively. With varying pressure, the intensity ratio of $^4G_{5/2} \rightarrow {}^6H_{7/2}$ and $^4F_{3/2} \rightarrow {}^6H_{7/2}$ Sm^{3+} emission shows three distinct regions. Furthermore, the intensity ratio of $^5D_0 \rightarrow {}^7F_1$ and $^5D_0 \rightarrow {}^7F_2$ Eu^{3+} emission of the cubic matrix has similar pressure dependence as Sm^{3+} doped phase. A steep pressure dependence evident in the range of 9.2-13.1 GPa could be used for detecting a pressure induced cubic to monoclinic phase transition of Y_2O_3 matrix. It matches well the behavior of the pressure sensitive Sm^{3+} spectra in the range of 9.1-11.6 GPa, which is proven to appear due to a phase transition at ~ 11 GPa.

The monoclinic Y_2O_3:Eu^{3+} also has a pressure-sensitive intensity ratio of $^5D_0 \rightarrow {}^7F_1$ and $^5D_0 \rightarrow {}^7F_2$ emission lines. Measurements for the monoclinic Y_2O_3:Eu^{3+} matrix were recorded up to 8 GPa. The dependence is unambiguous, without any phase transitions in the measured region. The nature and high sensitivity suggests that this dependence can be used as an efficient high pressure sensor.

Photoluminescence emission measurements of Y_2MoO_6:Sm^{3+} and Y_2MoO_6:Eu^{3+} phases were recorded up to 12 and 11.5 GPa, respectivelly. Intensity ratio variation of $^4G_{5/2} \rightarrow {}^6H_{5/2}$ and $^4G_{5/2} \rightarrow {}^6H_{7/2}$ Sm^{3+} emission lines, as well as of $^5D_0 \rightarrow {}^7F_1$ and $^5D_0 \rightarrow {}^7F_2$ Eu^{3+} emission lines as a function of pressure can be also used for detection of the Y_2MoO_6 phase transition. The accomplished results demonstrate the properties of Y_2MoO_6:Sm^{3+} and Y_2MoO_6:Eu^{3+} inorganic phosphors, with emmision linear dependance of the intensity ratio on the pressure up to 8 GPa, could be used as an efficient high pressure sensor.

INV-OGE 4

Optical and stryctural properties of nanostructured semiconductors

Martina Gilić and Milica Ćurčić

Institute of Physics Belgrade, University of Belgrade, 11080 Belgrade, Serbia

Science and technologyof nanostructures is a broad and interdisciplinary area of research and development activity that has been growing explosively worldwide in the past decade. Ongoing studies cover not only basic research but also the broad applications range.

Book of abstracts

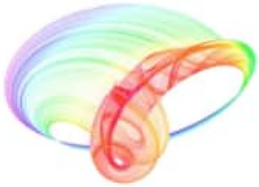

PHOTONICA2019

The Seventh International School and Conference on Photonics, 26 August – 30 August 2019, Belgrade, Serbia

& Machine Learning with Photonics Symposium (ML-Photonica 2019)

& ESUO Regional Workshop

& COST action CA16221

Editors: Milica Matijević, Marko Krstić and Petra Beličev

Belgrade, 2019

ABSTRACTS OF TUTORIAL, KEYNOTE, INVITED LECTURES, PROGRESS REPORTS AND CONTRIBUTED PAPERS

of

The Seventh International School and Conference on Photonics
PHOTONICA2019, 26 August – 30 August 2019, Belgrade, Serbia

and
Machine Learning with Photonics Symposium

and
ESUO Regional Workshop

Editors
Milica Matijević, Marko Krstić and Petra Beličev

Technical Assistance
Danka Stojanović and Goran Gligorić

Publisher
Vinča Institute of Nuclear Sciences
Mike Petrovića Alasa 12-14, P.O. Box 522
11000 Belgrade, Serbia

Printed by
Serbian Academy of Sciences and Arts

Number of copies
300

ISBN 978-86-7306-153-5

Negative thermal expansion of pullulan multilayers

S. Savic-Sevic[1], D. Pantelic[1], B. Muric[1], D. Vasiljevic[1], B. Kolaric[1] and B. Jelenkovic[1]
[1]*Institute of Physics, Belgrade, Serbia*
e-mail: savic@ipb.ac.rs

The change of temperature leads to thermal expansion. Most materials expand, but, some materials contract upon heating, characterized by negative thermal expansion [1]. Such negative thermal expansion material have various applications such as photoelectric devices, fillers in controlled thermal expansion composites, aerospace technology, as dental fillings [2].

We combine holography and phase separation [3] to design complex photonic structures that exhibit negative thermal expansion behavior. The structures were recorded in pullulan, (linear polysaccharide) doped with ammonium dichromate, and consist of a multilayer composed of pullulan and air.

We study optical response during heating and cooling of the synthesized pullulan nanostructures. The reflection wavelength of the hologram was used to characterize the temperature dependence of their shrinkage and swelling behavior. By heating and cooling the sample partially reversible shifts of the photonic band gap could be observed. We have observed that heating leads to a reduction in the thickness of the structure, resulting in the reflectance peak shift towards shorter wavelengths. With temperature decreasing the band gap position shifts back towards longer wavelengths. We reveal temperature sensitive responses of the structure, which are the consequence of the mechanical deformation of air nanolayers upon heating or cooling. The temperature change leads to the increased permeability of air molecules through the pullulan nanolayers, which causes mechanical changes.

REFERENCES

[1] J. Paul Attfield, Front. Chem. 6, 371 (2018).
[2] D. Tam Ho et al., Nano Lett. 17, 5113 (2017).
[3] S. Savic-Sevic et al., Soft Matter 14, 5595 (2018).

One-step fabrication large area of microlens arrays

B. Muric, D. Pantelic, D. Vasiljevic and B. Jelenkovic
Institute of Physics, Belgrade, Serbia
e-mail: muric@ipb.ac.rs

The microlens arrays (MLAs) are greatly used in medical lasers, optical fiber sensors, light-field cameras, biochemical systems, biological structures... Numerous methods such as: hot embossing, thermal reflow, droplet process, grayscale photolithography… are used for the microlens fabrication [1-4].

One step fabrication of low-cost concave microlens arrays on tot'hema tartrazine sensitized gelatin layer (TTSG) was developed. The layer is easy to prepare, elastic, biocompatible, thermally stable and nontoxic [5, 6]. MLAs were produced by direct diode-pumped solid state laser writing, operating at 473 nm. In addition, the microlens diameter, depth, and distance between two adjacent microlenses were controlled by changing the laser power, exposure time and dye concentration. The large area of hexagonally or square-packed microlenses was made for a short time. The concave MLA is suitable as a master mold for the further fabrication of convex arrays onto the polydimethylsiloxane (PDMS) or dental composite. The results were showed that the closely packed microlenses possess high-quality surface morphology, good optical and imaging properties. Using MLAs clear and uniform images were observed. Potentially applications MLAs are artificial compound eyes, Gabor superlens, optofluidic system, etc. [7].

REFERENCES

[1] F. Zhang et al., Sci. Rep. 8, 2419 (2018).
[2] T. J. Li et al., Opt. Express 25, 8274 (2017).
[3] H. Bian et al., Appl. Phys. Lett. 109, 221109 (2016).
[4] M. Elsherif et al., Lab chip 19, 2060 (2019).
[5] B. D. Murić et al., Appl. Opt. 46, 8527 (2007).
[6] B. D. Murić et al., Curr. Appl. Phys. 16, 57 (2016).
[7] G. Holzner et al., Lab chip 18, 3631 (2018).

Temperature Effects on Luminescent Properties of $Sr_2CeO_4:Eu^{3+}$ Nanophosphor: a Machine Learning Approach

DRAGUTIN ŠEVIĆ, University of Belgrade,
Institute of Physics Belgrade, Belgrade
ANA VLAŠIĆ, University of Belgrade,
Institute of Physics Belgrade, Belgrade
MAJA S. RABASOVIĆ, University of Belgrade,
Institute of Physics Belgrade, Belgrade
SVETLANA SAVIĆ-ŠEVIĆ, University of Belgrade,
Institute of Physics Belgrade, Belgrade
MIHAILO D. RABASOVIĆ, University of Belgrade,
Institute of Physics Belgrade, Belgrade
MARKO G. NIKOLIĆ, University of Belgrade,
Institute of Physics Belgrade, Belgrade
BRANKA D. MURIĆ, University of Belgrade,
Institute of Physics Belgrade, Belgrade
BRATISLAV P. MARINKOVIĆ, University of Belgrade,
Institute of Physics Belgrade, Belgrade
JANEZ KRIŽAN, AMI, d. o. o, Ptuj, R. Slovenia

Original scientific paper
UDC: 535.37
DOI: 10.5937/tehnika2003279S

In this paper we analyze possibilities of application of $Sr_2CeO_4:Eu^{3+}$ nanopowder for temperature sensing using machine learning. The material was prepared by simple solution combustion synthesis. Photoluminescence technique has been used to measure the optical emission temperature dependence of the prepared material. Principal Component Analysis, the basic machine learning algorithm, provided insight into temperature dependent spectral data from another point of view than usual approach.

Key words: *Photoluminescence, New materials, Thermographic phosphors*

1. INTRODUCTION

Nowadays, nano materials have more and more advantages over bulk materials. Nano science inevitably entered our world [1]. Thermographic nano phosphors are widely used in many applications [2-7]. They typically consist of a ceramic host and rare-earth dopant. The temperature dependency of their luminescence is used for remote temperature sensing. For obvious reasons, non contact measurements have many advantages. Thermographic remote monitoring of laser cleansing is described in [8].

Strontium cerium oxide (Sr_2CeO_4) nano phosphors doped with europium ions (Eu^{3+}), $Sr_2CeO_4:Eu^{3+}$ are described in many scientific papers. As shown in [9], emission color change in a wide range of temperatures proves a great potential of $Sr_2CeO_4:Eu^{3+}$ nanocrystals for industrial applications, particularly in nanothermometric technology. Moreover, additional application possibilities for this material are provided by the fact that the samples with different grain sizes are characterized by various luminescence colors [9]. The possibility of application of this nanophosphor in single-color and two-color fluorescence thermometry techniques in temperature range of 303–523 K has been proposed in [10]. In [11] it was shown that the Eu^{3+} doped Sr_2CeO_4 phosphors emitting white light (by combining blue, green and red emissions) has potential

Author's address: Dragutin Šević, University of Belgrade, Institute of Physics Belgrade, Belgrade, Pregrevica 118
e-mail: sevic@ipb.ac.rs
Paper received: 26.05.2020.
Paper accepted: 30.05.2020.

applications not only in the fields of lamps and display devices under 280 nm excitation, but also in the field of LEDs under near UV (350 nm) excitation. $Sr_2CeO_4:Eu^{3+}$ considered as a source of anti-stokes white light generated under near infrared excitation was analyzed in [12]. Various methods of synthesis and studies of structural and luminescent characteristics of nanophosphors based on $Sr_2CeO_4:Eu^{3+}$ or nondoped Sr_2CeO_4 are reported in [9-13], and references therein.

In this study, we analyze $Sr_2CeO_4:Eu^{3+}$ nanopowders, efficiently prepared using a solution combustion synthesis (SCS) method [14,15]. The main characteristics of this process are simplicity and low cost. The structure of prepared materials has been confirmed and characterized using X-ray powder diffraction (XRD), scanning electron microscope (SEM) and photoluminescence (PL) techniques [15]. The most of europium luminescence comes from transitions from the $^5D_0$ and $^5D_1$ state; and they are usually used for fluorescence intensity ratio technique for remote temperature sensing.

In our recent publication [16] we have shown that $Sr_2CeO_4:Eu^{3+}$ made by solution combustion synthesis could be used as a red phosphor. In [15] we have studied the possibility of using the synthesized $Sr_2CeO_4:Eu^{3+}$ for temperature measurements, using usual approach of calculating the calibration curves.

However, availability of more and more fast computers, capable of machine learning, gave us an idea of different approach. Here, we analyze the possibilities of training the computer to recognize optical emission spectra of $Sr_2CeO_4:Eu^{3+}$ at different temperatures. So, this paper describes extension of our work presented in [15].

2. EXPERIMENTAL PROCEDURE

The preparation of samples

Europium doped Sr_2CeO_4 nanopowders were prepared by solution combustion method, similarly as described in [14,15]. Stoichiometric quantities of starting chemicals $Sr(NO_3)_2$, CH_4N_2O, $Ce(NO_3)_3{\times}6H_2O$, and $Eu(NO_3)_3{\times}6H_2O$ with the purity of 99.99% were chosen to obtain the Eu^{3+} concentration in Sr_2CeO_4 of 2.5 at.% ($Sr_{2-0.05}Eu_{0.05}CeO_4$). The used chemicals were purchased from ABCR, and urea, $(NH_2)_2CO$, from Sigma-Aldrich.

The dry mixture of 10.32 g (48.75 mmol) of $Sr(NO_3)_2$, 15.015 g (250 mmol) of CH_4N_2O, 10.86 g (25 mmol) of $Ce(NO_3)_3{\times}6H_2O$ and 0.558 g (1.25 mmol) of $Eu(NO_3)_3{\times}6H_2O$ was combined with the mixture of 4.8 g (60 mmol) of ammonium nitrate and 3.003 g (50 mmol) of urea which were used as organic fuels.

The prepared starting reagents were combusted with the flame burner at approximately 500 °C, yielding a voluminous foamy pink powder in an intensive exotermic reaction. After the solution combustion synthesis, the nanopowder was annealed for 2 hours, in air atmosphere, at 900 °C. The annealing of the material is needed to achieve optimal optical characteristics of synthesized material.

Experimental details

As an excitation source for photoluminescence measurements we used the output of the optical parametric oscillator (Vibrant OPO), continuously tunable over a spectral range from 320 nm to 475 nm. Laser pulse duration is about 5 ns, at a repetition rate of 10 Hz. Time-resolved streak images of the luminescence response of $Sr_2CeO_4:Eu^{3+}$ nanopowder excited by the OPO system were acquired by Hamamatsu streak camera equipped with a spectrograph.

Emission spectra of $Sr_2CeO_4:Eu^{3+}$ were also acquired using Ocean Optics USB2000 and AVANTES AvaSpec 2048TEC USB2 spectrometers and continuous laser diode excitation at 405 nm. The experimental setup for luminescence measurement as a function of temperature is described in [17].

For machine learning simulation experiments we have used Solo software package (Version 8.8, Eigenvector Research Inc, USA).

3. RESULTS AND DISCUSSION

The structure of material was confirmed by XRD patterns and SEM images, see [15].

The streak image of the time resolved photoluminescence spectrum of the $Sr_2CeO_4:Eu^{3+}$ using the 330 nm excitation is presented in Figure 1. Horizontal scale of streak image corresponds to wavelength, vertical scale shows development of spectra in time. Images are presented in pseudocolor, where different colors mean different optical intensities.

The $^5D_1$-$^7F_3$ transition (583 nm), located closely between the $^5D_0$-$^7F_0$ (582 nm) and the $^5D_0$-$^7F_1$ (587 nm) transitions is easy to identify on the time resolved image. Its time integrated peak has a comparable intensity to the intensities of peaks originating from nearby $^5D_0$ levels (see the line profile denoted by a red curve in Fig. 4).

The luminescence spectra presented in publications usually do not have the time resolution, so it is hard to guess which transitions are short lived. Streak image presented in Figure 1 shows clearly that the $^5D_1$-$^7F_3$ transition (583 nm) has a much higher intensity and a much shorter lifetime than nearby transitions from $^5D_0$ state.

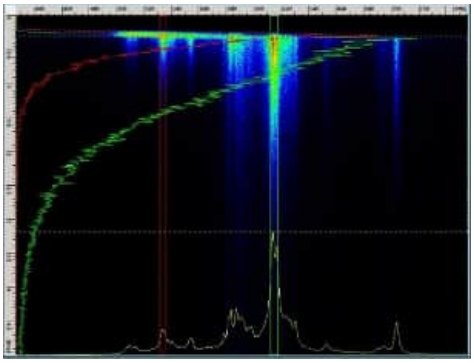

Figure 1 - Streak image of the photoluminescence spectrum of $Sr_2CeO_4:Eu^{3+}$ nanophosphor. (OPO excitation at 330 nm).

The temperature dependency of intensity ratio of spectral lines

The luminescence of samples was measured both using pulsed (OPO) and continuous excitation. The measured luminescence spectra of Eu^{3+} doped Sr_2CeO_4 at various temperatures are presented in Figure 2. The spectra were obtained by using continuous laser diode excitation at 405 nm.

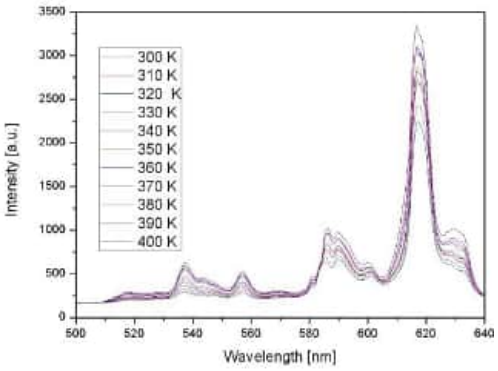

Figure 2 - Luminescence spectra of Eu^{3+} doped Sr_2CeO_4 at various temperatures. (Continuous laser diode excitation at 405 nm).

The fluorescence intensity ratio (FIR) of spectral line intensities from the $^5D_0$ and $^5D_1$ transitions depend on two physical processes: the thermalization of the $^5D_1$ level with rising temperature, where the energy difference to populate the $^5D_1$ level from the $^5D_0$ level is fully covered by phonons; and the nonradiative quenching of the $^5D_0$ and $^5D_1$ levels through the charge transfer state. Looking at Figure 2 we can see that intensity ratio between lines at 614 nm and 537 nm is temperature dependent.

The Principal Component Analysis of temperature dependent $Sr_2CeO_4:Eu^{3+}$ spectra

Principal component analysis (PCA) finds combinations of variables, or *factors*, that describe major trends in the data [18].

If X is a data matrix with *m* rows and *n* columns, each variable being a column and each sample a row, PCA decomposes X as the sum of rt_i and p_i, where *r* is the rank of the matrix X:

$$\boldsymbol{X} = \boldsymbol{t_1 p^T}_1 + \boldsymbol{t_2 p^T}_2 + ... + \boldsymbol{t_k p^T} k + ... + \boldsymbol{t r p^T} r$$

where $r \leq \min\{m,n\}$

The t_i, p_i pairs are ordered by the amount of variance captured. The t_i vectors are known as scores and contain information on how the samples relate to each other. The p_i vectors are known as loadings and contain information on how the variables relate to each other.

For analysis presented here, we use luminescence spectra of Eu^{3+} doped Sr_2CeO_4 at temperatures between 300 and 400 K, measured with the step of 5 K. About a half of the spectral data (measured at 300, 310, 320 ... K) are used to train the PCA algorithm. Another half of the spectral data (measured at 305, 315, 325 .... K) are used to test the obtained PCA model.

Scores on first two principal components of measurement data of temperature dependence of luminescence of $Sr_2CeO_4:Eu^{3+}$ nanophosphor are shown in Figure 3. It could be seen that scores on PC 1 gradually move along the x axis, while scores on PC 2 oscillate along the y axis.

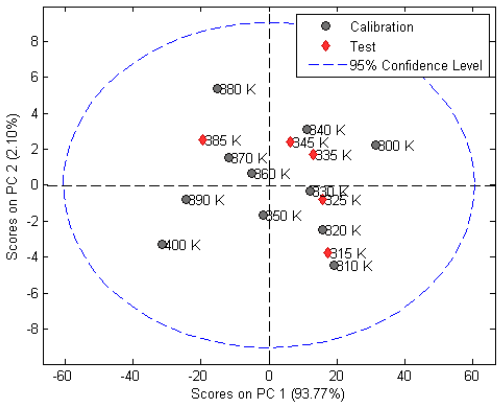

Figure 3 - Scores on first two principal components of measurement data of temperature dependence of luminescence of $Sr_2CeO_4:Eu^{3+}$ nanophosphor.

We see that the predictions for future measurements are well within the 95% confidence level. However, it should be noted that this approach is different, and not necessarily better, than usual method based on fitting the temperature sensing calibration curve. Namely, the machine is trained on restricted size of training data set. The remote temperature estimation is based on classification of newly obtained data in regard the calibrated data. The classification is implemented by comparing the scores distances between the calibrated data and the newly measured ones. So, the larger the training set, the better is resolution of the remote temperature sensing.

4. CONCLUSION

In this paper we have applied the Principal Component Analysis, the basic machine learning algorithm, on temperature dependent Sr_2CeO_4:Eu^{3+} spectral data. We have shown that the machine could be trained to differentiate spectral data obtained on different temperatures. However, the resolution of this remote temperature sensing technique depends on the size of spectral data training set. For relatively small training set, the predicted data are well within the confidence level of 95 %.

5. ACKNOWLEDGEMENT

This work was financially supported by funding provided by the Institute of Physics Belgrade, through the grant by the Ministry of Education, Science, and Technological Development of the Republic of Serbia.

REFERENCES

[1] Uskokovic V, Nanoscience: Whence it entered our World, *Tehnika*, Vol. 22, pp 795-803, 2013.

[2] Jaque D, Vetrone F, Luminescence nanothermometry, *Nanoscale*, Vol. 4, pp 4301-4326, 2012.

[3] Brites C. D. S, Lima P. P, Silva N. J. O, Millan A, Amaral V. S, Palacio F, Carlos L. D, Thermometry at the nanoscale, *Nanoscale*, Vol. 4, pp. 4799-4829, 2012.

[4] Aldén M, Omrane A, Richter M, Särner G, Thermographic phosphors for thermometry: A survey of combustion applications, *Progress in Energy and Combustion Science*, Vol. 37, pp. 422-461, 2011.

[5] Allison S. W, Gillies G. T, Remote thermometry with thermographic phosphors: Instrumentation and applications, *Rev. Sci. Instrum*, Vol. 68, pp 2615-2650, 1997.

[6] Goss L. P, Smith A. A, Post M. E, Surface thermometry by laser-induced fluorescence, *Rev Sci. Instrum*, Vol. 60, pp 3702-3706, 1989.

[7] Heyes A. L, On the design of phosphors for high-temperature thermometry, *Journal of Luminescence*, Vol. 129, pp 2004-2009, 2009.

[8] Ristic S, Polic S, Knjezevic D, Radojkovic B, Linic S, Jegdic B, Termografija u kontroli efikasnosti i bezbednosti laserskog čišćenja, *Tehnika*, Vol. 28, pp 623-629, 2019.

[9] Stefanski M, Marciniak L, Hreniak D, Strek W, Size and temperature dependence of optical properties of Eu^{3+}:Sr_2CeO_4 nanocrystals for their application in luminescence thermometry, *Mat. Res. Bull.*, Vol. 76, pp 133–139, 2016.

[10] Shi L, Zhang H, Li C, Su Q., Eu^{3+} doped Sr_2CeO_4 phosphors for thermometry: single-color or two-color fluorescence based temperature characterization, *RSC Advances*, Vol. 1, pp. 298–304, 2011.

[11] Suresh K, Poornachandra Rao N. V, Murthy K. V. R, Photoluminescent properties of Sr_2CeO_4:Eu^{3+} and Sr_2CeO_4: Eu^{2+}phosphors suitable for near ultraviolet excitation, *Bull. Mater. Sci.*, Vol. 37, pp 1191–1195, 2014.

[12] Stefanski M, Lukaszewicz M, Hreniak D, Strek W, Laser induced white emission generated by infrared excitation from Eu^{3+}: Sr_2CeO_4 nanocrystals, *Jour. Chem. Phys.*, Vol. 146, pp 104705-1-7, 2017.

[13] Stefanski M, Marciniak L, Hreniak D, Strek W, Influence of grain size on optical properties of Sr_2CeO_4 nanocrystals, *Jour. Chem. Phys.*, Vol. 142, pp 184701-1-7, 2015.

[14] Rabasovic M. S, Sevic D, Krizan J, Terzic M, Mozina J, Marinkovic B. P, Savic Sevic S, Mitric M, Rabasovic M. D, Romcevic N, Characterization and luminescent properties of Eu^{3+} doped $Gd_2Zr_2O_7$ nanopowders, *J. Alloys and Compounds* Vol. 622, pp 292-295, 2015.

[15] Vlasic A, Sevic D, Rabasovic M. S, Krizan J, Savic-Sevic S, Rabasovic M. D, Mitric M, Marinkovic B. P, Nikolic M. G, Effects of temperature and pressure on luminescent properties of Sr_2CeO_4: Eu^{3+} nanophosphor, *Journal of Luminescence*, Vol. 199 pp 285–292, 2018.

[16] Rabasovic M. S, Krizan J, Gregorcic P, Rabasovic M. D, Romcevic N, Sevic D, Time-resolved luminescence spectra of Eu^{3+} doped YVO_4, Sr_2CeO_4 and $Gd_2Zr_2O_7$ nanopowders, *Optical and Quantum Electronics*, Vol. 48, pp163-1-4, 2016.

[17] Rabasovic M. D, Muric B. D, Celebonovic V, Mitric M, Jelenkovic B. M, Nikolic M. G, Luminescence thermometry via the two-dopant intensity ratio of Y_2O_3:Er^{3+}, Eu^{3+}, J. *Phys. D: Appl. Phys*., Vol. 49, pp 485104-1-6, 2016.

[1] Hoteling H, Analysis of a Complex of Statistical Variables into Principal Components. *Journal of Educational Psychology*, Vol. 24, 417-441, 1933.

REZIME

TEMPERATURNA ZAVISNOST LUMINESCENTNIH OSOBINA SR_2CEO_4:EU^{3+} NANOFOSFORA: PRISTUP MAŠINSKIM UČENJEM

U ovom radu analizirali smo mogućnosti primene Sr_2CeO_4:Eu^{3+}nanopraha za merenje temperaruture primenom mašinskog učenja. Materijal je pripremljen jednostavnom metodom sinteze sagorevanja rastvora. Fotoluminescentna tehnika je korišćena za merenje temperaturne zavisnosti optičke emisije pripremljenog materijala. Analiza ključnih faktora omogućila nam je uvid u temperaturnu zavisnost spektralnih podataka sa drugačije tačke gledišta nego što je uobičajeni pristup.

Ključne reči: *fotoluminescencija, novi materijali, termografski fosfori*

Institute of Physics Belgrade
University of Belgrade
Kopaonik, March 08-12, 2020

Book of Abstracts

13th Photonics Workshop

(Conference)

PHOTONICS
CENTER

13th Photonics Workshop (2020)

Book of abstracts

Kopaonik, Serbia, March 08-12, 2020

Publisher, 2020:

Institute of Physics Belgrade

Pregrevica 118

11080 Belgrade, Serbia

Editors:

Dragan Lukić, Marina Lekić, Zoran Grujić

ISBN 978-86-82441-50-2

Printed by:

NEW IMAGE d.o.o.

Cara Dušana 212, Zemun, Belgrade

Number of copies: 60

CIP - Каталогизација у публикацији Народна библиотека Србије, Београд

535(048)
681.7(048)
66.017/.018(048)

PHOTONICS Workshop (13 ; 2020 ; Kopaonik)
Book of Abstracts / 13th Photonics Workshop, (Conference), Kopaonik, March 08-12, 2020 ; [editors Dragan Lukić, Marina Lekić, Zoran Grujić]. - Belgrade : Institute of Physics, 2020 (Belgrade : New Image). - 58 str. : ilustr. ; 25 cm

Tiraž 60. - Registar.

ISBN 978-86-82441-50-2

a) Оптика -- Апстракти b) Оптоелектроника -- Апстракти v) Технички материјали -- Апстракти

COBISS.SR-ID 283421708

Negative thermal expansion in nanolayered pullulan

Svetlana Savic-Sevic, Dejan Pantelić, Branka Murić, Darko Vasiljević, Branko Kolarić, Branislav Jelenković

Institute of Physics, University of Belgrade, Pregrevica 118, 11080 Zemun, Serbia.

Contact: S. Savic-Sevic (savic@ipb.ac.rs)

Abstract. The change of temperature leads to thermal expansion. Most materials expand, but, some materials contract upon heating. A small number of natural materials show negative thermal expansion effects. Such negative thermal expansion (NTE) materials have great applications because they can control the thermal expansion of materials. The linear coefficient of thermal expansion, α_L, can be expressed as: $\alpha_L = (1/L_0)\,(dL/dT)$, where L_0 is the initial length at temperature T_0, dL is length change and dT is the change in temperature [1].

Photonic structure is recorded in pullulan doped with ammonium dichromate (DCP). We fabricate a one-dimensional photonic structure, pullulan layers are mutually separated and supported by nanopillars. This complex morphology is formed simultaneously by the holographic method and the nonsolvent induced phase separation [2]. Under white light illumination the grating acts as a reflector of the light for a specific band of wavelengths.

We have observed that heating leads to a reduction in the thickness of the structure, resulting in the reflectance peak shift towards shorter wavelengths. We calculated the change of thickness, corresponding to experimentally-recorded spectral shift. We have obtained the value of the negative thermal expansion coefficient, $\alpha_L = -3.8 \times 10^{-3}\ K^{-1}$.

The reflection spectra show blue shift with increasing of temperature, which originates from the contraction thickness of the air nanolayers due to the permeability of the air molecules through the pullulan nanolayers. This results in a large negative thermal expansion coefficient.

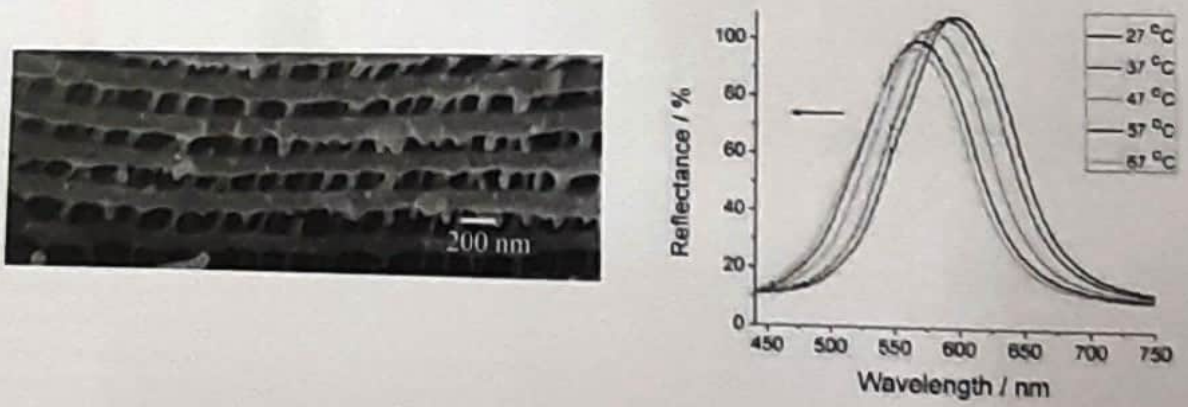

Figure 1. SEM image of a cross - section of nanolayered structure and experimentally recorded reflection spectra during heating.

REFERENCES

[1] K. Takenaka, *Frontiers in Chemistry*, **6** (2018), 267:1–13.

[2] S. Savić-Šević., D. Pantelić, Branislav Jelenković, Branislav Salatić, Dejan V. Stojanović, *Soft Matter*, **14** (2018), 5595–5603.

Micro-optical elements "à la carte"

Mihajlo D. Radmilovic[1], Branka D. Muric[1], Dejan Pantelic[1]

(1) Institute of Physics Belgrade, Pregrevica 118, 11080, Serbia

Contact: M. Radmilovic (mihajlo.radmilovic@ipb.ac.rs)

Abstract. Micro-optical elements (MOEs) have a wide range of application in different areas, including today's leading industries such as: biomedical sensing and engineering, material processing, optical telecommunications... Numerous methods are used for micro optical elements fabrications, that include grayscale photolithography, wafer based manufacturing, thermal reflow... Most of these manufacturing techniques are time, energy and financially consuming [1].

A method presented here is based on the low cost homemade material gelatin doped with tothema (a drug used to treat iron deficit) [2-3]. Thin layers are produced simply and quickly, while exhibitin biocompatibility, elasticity and environmental stability [1-2]. The main parts of fabrication system include laser (operating at 488nm) and coordinate table. Both are controlled by software, developed in our lab. MOEs are produced by laser writing, with high spatial resolution and temporal efficiency. We are able to produce different kinds of MOEs in a one step process, such as: concave micro lens arrays, diffraction gratings, micro- channels for lab on chip applications [4]. In addition, the MOEs parameters diameter, depth, size and repetition range, controlled by changing the laser power, coordinate table step size in 2D and laser exposure time. The sensitivity of material is tuned by changing the concentration of doped dye (e.g. betanine, eosine).

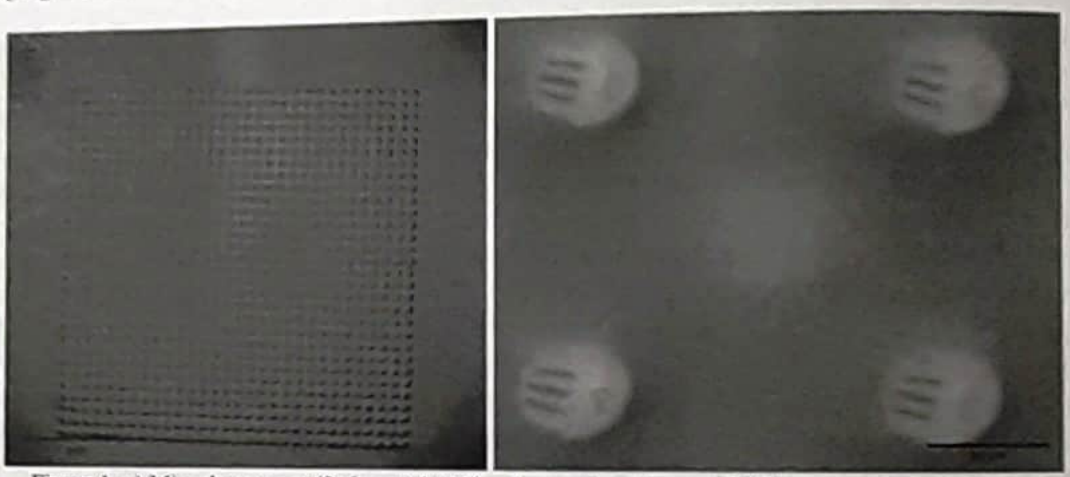

Figure 1. a) Microlens array (3x3mm), b) Microlenses imaging capabilities.

These results have shown that MOEs (microlenses) have excelent optical and imaging capabilities, with quick turnaround time (approximately 15min, for an microlens 100 x 100 array, without any additional processing), on-demand - "à la carte" - adaptability (even a single MOE can be fabricated quickly and cost effectively). The potential applications of MOEs are Shack-Hartmann wavefront sensor, document security, waveguides, optofluidic system for biosensing etc.

REFERENCES

[1] R.Voelkel, *Advanced Opt.Tech.*, **1.3** (2012): 135-150.

[2] B.D.Muric et al., *Appl.Opt* , **46**(2007): 8527-8532

[3] B.D. Muric et al., *Curr.Appl.Physi.***16**(2016): 57-62

[4] Abgrall et al., *J.of Micromech.and Microeng.* , **17.5** (2007) : R15

University of Belgrade
Institute of Physics Belgrade
Kopaonik, March 14-17, 2021

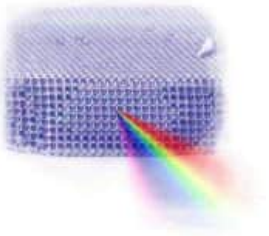

Book of Abstracts

14th Photonics Workshop

(Conference)

PHOTONICS
CENTER

14th Photonics Workshop (2021)

Book of abstracts

Kopaonik, Serbia, March 14-17, 2021

Publisher, 2021:

Institute of Physics Belgrade

Pregrevica 118

11080 Belgrade, Serbia

Editors:

Dragan Lukić, Marina Lekić, Zoran Grujić

ISBN 978-86-82441-52-6

Printed by:

NEW IMAGE d.o.o.

Tošin Bunar 185, Belgrade

Number of copies: 30

CIP - Каталогизација у публикацији - Народна библиотека Србије, Београд
535(048)
681.7(048)
66.017/.018(048)
PHOTONICS Workshop (14 ; 2021 ; Kopaonik)
Book of Abstracts / 14th Photonics Workshop, (Conference), Kopaonik, March 14-17, 2021 ; [editors Dragan Lukić, Marina Lekić, Zoran Grujić]. - Belgrade : Institute of Physics, 2021 (Belgrade : New image). - 46 str. : ilustr. ; 25 cm
Tiraž 30. - Registar.
ISBN 978-86-82441-52-6
a) Оптика - Апстракти b) Оптоелектроника - Апстракти c) Технички материјали - Апстракти

COBISS.SR-ID 33997321

Real time fabrication of microlens arrays for security applications

Mihajlo D. Radmilović, Branka Murić, Dejan Pantelić

Institute of Physics Belgrade, Pregrevica 118, 11080Belgrade, Serbia

Contact: Dejan Pantelić (pantelic@ipb.ac.rs)

Microlenses and microlens arrays have found significant applications in integral imaging, illumination and, in particular, security [1-3]. Variability under different illumination and observation conditions with associated 3D effects make microlenses excellent security alternative to holograms. A new 100 $ US bill with 3D ribbon, filled with thousands of microlenses, is a newest example of practical application of microlenses for document security.

Here we present a method for fabrication of micron-sized security QR-codes (see Fig. 1) entirely made of positive and negative microlenses. Their focal lengths, size and focal images present a new security features, which can be intertwined with the QR code contents.

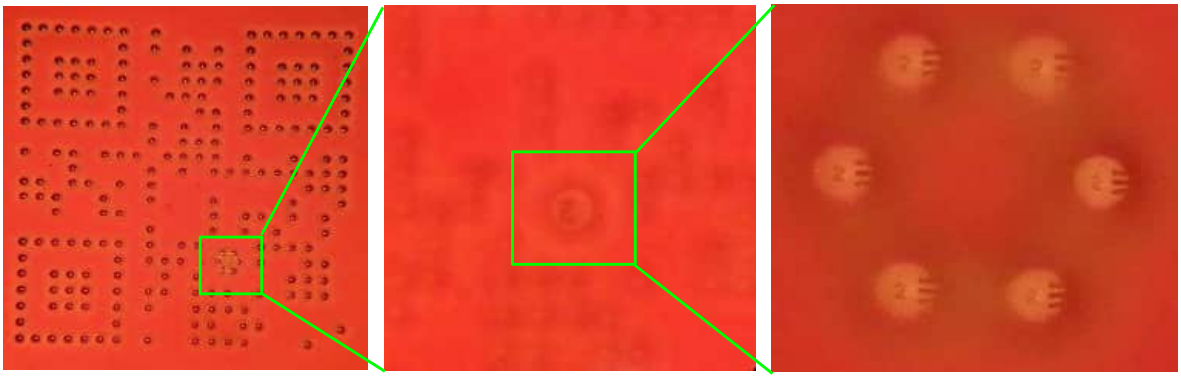

Figure 1. QR-code with positive and negative lenses

Security QR code is fabricated on a sensitized hydrogel using direct laser writing. Writing is based on local melting of hydrogel with consequtive formation of a lens like structure due to surface tension forces. Material is environmentally safe with low toxicity and microlens fabrication is fast - individual microlenses are produced in a fraction of a second - and requires no further processing. That is why security features can be fabricated in an individualized manner enabling uniquenes and complexity of security features.

By changing the laser beam profile, writing speed and pattern, complex aspherical lenses can be fabricated, thus adding to complexity of security features. Simplicity of the base material and associated laser processing technology opens way to many security applications.

REFERENCES

[1] Thomas Walger, Théophane Besson, Valentin Flauraud, Roger D. Hersch, and Juergen Brugger, "Level-line moirés by superposition of cylindrical microlens gratings,"*J. Opt. Soc. Am. A* **37** (2020): 209-218

[2] Christian Fuhse, Michael Rahm, André Gregarek, "Security element having a lenticular image", Patent US 10,105,982 B2, (2018)

[3] Hao Jiang, Bozena Kaminska, Hector Porras, Mark Raymond, Tyler Kapus,"Microlens Arrays above Interlaced Plasmonic Pixels for Optical Security Devices with High-Resolution Multicolor Motion Effects",*Adv. Opt. Mat.* 7 (2019): 1900237

Rapid protyping of microlenses based on hydrogel materials

Mihajlo D. Radmilović, Branka Murić, Dejan Pantelić

Institute of Physics Belgrade, Pregrevica 118, 11080Belgrade, Serbia

Contact: Mihajlo D.Radmilović (mihajlo.radmilovic@ipb.ac.rs)

Microlenses represent important optical components that have widespread applications in microscopy, biomedical engineering, security, etc. [1,4]. However, in most cases the production of usable microlenses is a complex technological task. Various techniques are used for microlens production such as micromolding, embossing, soft lithography [2,3,4]. Most of them don't have a high production rate, versatility, and modularity at the same time. Here we present a fast, simple, nontoxic and environmentally friendly technology for production of high-quality microlenses based on continuous wave laser processing of hydrogel materials. Direct laser writing at 488 nm is used to manufacture almost any type of microlenses within several milliseconds. Produced lenses are instantly usable without need for any further processing. We have been able to fabricate the different types of microlens: positive, negative, aspheric - and their arrays and combinations. Technology has a potential for rapid prototyping and serial production due to the modularity and versatility of the production process.

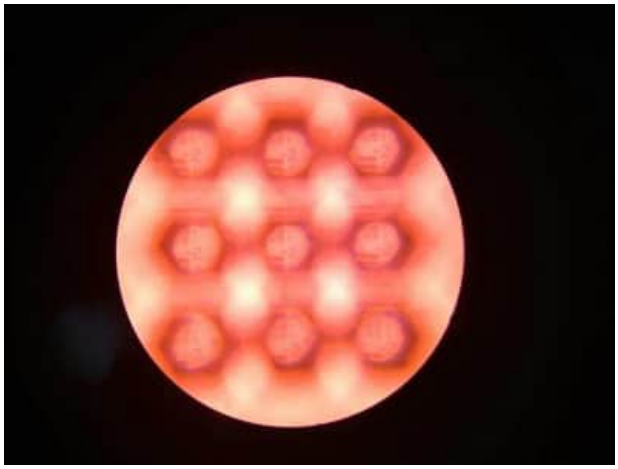

Figure 1. Positive 3x3 Microlens array

REFERENCES

[1] D. Daly, *Microlens arrays*, CRC Press, (2000).
[2] C. Ma et al., *Lab on a Chip* **16.14** (2016), 2609-2617.
[3] J. Etxebarria et al., *Sensors and Actuators B: Chemical* **190** (2014), 451-458.
[4] V. Faustino et al., *J. of biomechanics* **49.11** (2016), 2280-2292.

PHYSICAL CHEMISTRY 2021

15th International Conference
on Fundamental and Applied Aspects of
Physical Chemistry

Proceedings
Volume II

The Conference is dedicated to the

30th Anniversary of the founding of the Society of Physical Chemists of Serbia

and

100th Anniversary of Bray-Liebhafsky reaction

September 20-24, 2021
Belgrade, Serbia

Title: Physical Chemistry 2021 (Proceedings) **ISBN** 978-86-82475-40-8
Volume II: ISBN 978-86-82475-39-2
Editors: Željko Čupić and Slobodan Anić
Published by: Society of Physical Chemists of Serbia, Studentski Trg 12-16, 11158, Belgrade, Serbia
Publisher: Society of Physical Chemists of Serbia
For Publisher: S. Anić, President of Society of Physical Chemists of Serbia
Printed by: ″Jovan″, <Printing and Publishing Company, 200 Copies
Number of pages: 6+388, Format A4, printing finished in December 2021

Text and Layout: ″Jovan″

200 - *Copy printing*

MODIFIED CHITOSAN FOR RAPID FABRICATION OF MICROLENSES

B. Murić[1], D. Pantelić[1], M. Radmilović[1], D. Grujić[1], B. Zarkov[2]

[1] *Institute of Physics Belgrade, University of Belgrade, Pregrevica 118,11080 Belgrade, Serbia (muric@ipb.ac.rs)*

[2] *Directorate for Measure and Precious Metals, Mike Alasa 14, 11000 Belgrade, Serbia*

ABSTRACT

Chitosan was modified to prepare elastic, biocompatible, nontixic, and ecofriendly material (MC) for rapid fabrication of microlenses. Concave, convex, aspheric microlenses (individual or arrays) are produced on the MC layer by direct laser writing at 488 nm. Microlenses can be used directly without chemical processing for different applications such as: medicine, sensors, cameras, security...

INTRODUCTION

Microlenses are characterized by diameters from several micrometers up to nearly 1 mm and have a range of applications in microoptical devices, lab-on-a-chip, displays, sensors, smartphone cameras, artificial compound eyes, security [1-3]... Various methods were used for microlens fabrication, such as: hot embossing, direct laser writing, thermal reflow, photolithography, droplet process, and many other [4, 5]. Most of them are complex, and require use of the poisonous chemicals.

Chitosan is a partially deacetylated derivative of chitin, a natural polymer extracted from crustaceous shells. It is a linear polysaccharide composed of β-(1-4)-linked d-glucosamine and N-acetyl-d-glucosamine. Chitosan is insoluble in pure water and organic solvents. It dissolves in diluted acidic aqueous solutions where the solubility depends on pH and deacetylation degree. Chitosan as nontoxic, biocompatible and biodegradable can be used in biomedicine, bioengineering, food, pharmaceutical [6, 7]...

Our aim was to develop an ecofriendly, nontoxic, optically transparent, elastic, and durable material suitable for fabrication of microoptical components. In this paper, we present a simple and cheap method for preparing modified chitosan (MC) layer for microlenses fabrication. Microlenses, were produced on the MC layer by direct, focused blue laser radiation at 488 nm. Microlenses are produced rapidly and can be used for security, sensors, compound eyes, and so on without any additional chemical treatment.

RESULTS AND DISCUSSION

The 2% chitosan solution was prepared by dissolving chitosan (low MW, 85% deacetylated) in acetic acid (1% aq. sol.) with stirring at 50°C, until a homogeneous solution is obtained.

A water solution composed with several active ingredients (plasticizers, humectants, and preservatives) was prepared, too. This solution (PS for short) contains: glycerol, sucrose, glucose, polysorbate 80, citric acid, and sodium benzoate in appropriate proportions. 0.2 ml of PS, and 0.1 ml anthocyanin food dye (E163) were further added per 1 ml of chitosan solution, with continued stirring. After complete dissolution the MC solution was centrifuged in order to remove all undissolved impurities. As a result, both mechanical and optical properties (such as: elasticity, durability and stability, optical transparency…) of the MC layer were improved [8].

The MC layer was prepared by the gravity settling method [9, 10], and dried in the dark overnight, under ordinary environmental conditions (the temperature about 25 °C and the relative humidity 50-60%). The thickness of the MC layer depends on the quantity of PS [8]. The layer thickness was

measured using a digital micrometer, and it was determined as the average of eight random layer locations measurements. In our experiments, the layer thickness was 100 μm.

The absorption spectrum of MC layer was analyzed using a fiber-type spectrometer equipped with a tungsten-halogen lamp, and was observed that maximum absorption depends on the pH solution.

The microlenses were produced using a home-made laser writing device. The laser operating at 488 nm with maximal output power of 100 mW was focused on the MC layer, as schematically shown in Figure 1.

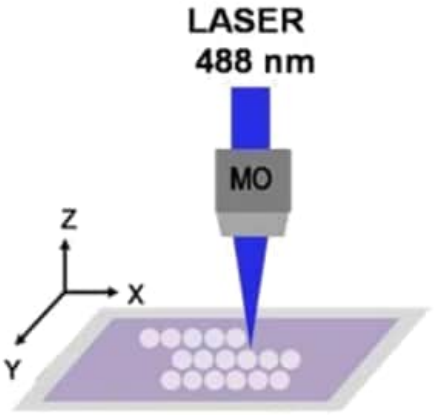

Figure 1. Microlenses array fabrication on the MC layer

The MC layer was mounted on a precise xy - linear translation stage used for the layer positioning with step resolution 25 nm and position repeatability of 2 μm. The laser beam was focused with a microscope objective - MO (50×0.55NA) on the MC layer. Software controls and synchronizes operation of laser and coordinate table using a standard g-code [11]. The microlenses array is recorded lens by lens using the program which determines the microlens array parameters from the image file. By controlling the laser power, exposure time and distance among neighbor microlenses we were able to create concave or convex microlenses (individual or closely packed arrays).

The concave dip was formed on the MC layer by its controlled and local melting. Following the laser beam profile, the surface tension forces form a lens, without any waste.

Good quality positive microlenses were produced by making an arrangement of 8 polygonally positioned spots. The spherical surface in the polygon center acts as a convex (positive) microlens. The radius of curvature, as well as the corresponding focal length of microlenses can be controlled by the diameter of a polygon.

The concave or convex microlenses are obtained with good repeatability. An image of digit “-2” taken by a digital camera through the optical microscope and 5x5 MC convex microlens array is shown in Fig. 2 (the diameter of polygon was 25 μm, while microlenses were fabricated using 50 mW of laser power and 200 ms exposure time).

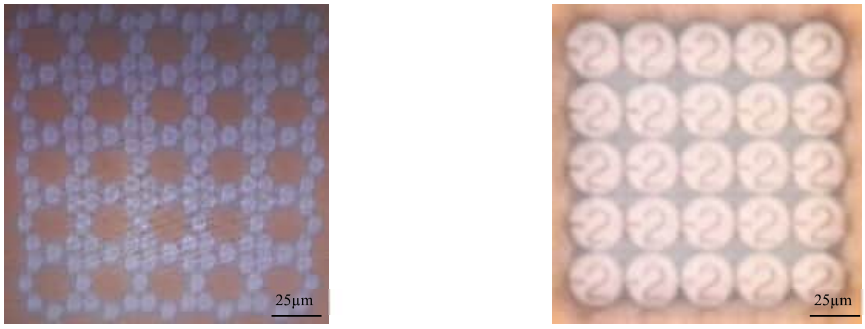

a) b)

Figure 2. Reflection image of an array of 5 x 5 convex microlenses produced on the MC layer (a). Transmission image produced by the 5x5 convex microlenses produced on the MC layer (b)

Preliminary results have shown that MC layer elongation of 100% was obtained for the already mentioned PS concentration. Based on our previous research [11], we assume that the stress-strain behavior of the layer also depends on the PS concentration. The layer elasticity is very important for the fabrication of (adaptive) tunable microstructures.

CONCLUSION

Chitosan was chemically modified to enable fabrication of microoptical components. The material is ecofriendly, nontoxic and suitable for a single-step rapid fabrication of microstructures by direct laser writing (blue radiation at 488nm).

Convex, concave, and aspherical microlenses can be used immediately, without additionally chemical treatment and waste. The individual and closely packed hexagonal or square arrays of microlenses show good optical and imaging properties. They can be used for a variety of applications such as: medical laser, optical sensors, light-field cameras, security, biological structure.

Improving the physicochemical properties of modified chitosan layer will be the focus of our future research.

Acknowledgement

This paper was supported by the Ministry of Education, Science and Technological Development of the Republic of Serbia.

REFERENCES

[1] G. Lian, Y. Liu, K. Tao, H. Xing, R, Huang, M. Chi, W. Zhou, Y. Wu, Micromachines 2020, 11, 854.
[2] F. Olivieri, M. Todino, S. Coppola, V. Vespini, V, Pagliarulo, S. Grilli, P. Ferrar, Opt. Eng. 2016, 55, 081319.
[3] H. Jiang, S. Fraser, B. Kaminska, H. Porras, M. Raymond, Adv. Opt. Materials 2019, 7,1900237.
[4] J. M. Pavia, M. Wolf, E. Charbon Opt. Express 2014, 22, 4202-4213.
[5] J. Tang, G. Qiu, X. Cao, Y. Yue, X. Zhang, J. Schmitt, J. Wang, Lab Chip 2020, 20, 2334.

[6] E. Melro, F. E. Antunes, G. J. da Silva, I. Cruz, P. E. Ramos, F. Carvalho, L. Alves, Polymers 2021,13, 13010001.
[7] B. Tian,Y. Liu, Polym Adv Technol. 2020, 1–14.
[8] B. Muric, D. Pantelic, D. Vasiljevic, B. Zarkov, B. Jelenkovic, S. Pantovic, M. Rosic, Phys. Scr. 2013, T157, 014018.
[9] B. D. Muric, D. V. Pantelic, D. M. Vasiljevic, B. M. Panicć, Appl. Opt. 2007, 46 8527-8532.
[10] B. Muric, D. Pantelic, D. Vasiljevic, B. Panic, Opt. Mater. 2008, 30, 1217-1220.
[11] ISO 6983 - 1:2009(en) Automation systems and integration – Numerical control of machines - Program format and definitions of address words - Part 1: Data format for positioning, line motion and contouring control systems.

CIP - Каталогизација у публикацији
Народна библиотека Србије, Београд

544(082)
66.017/.018(082)
502/504(082)
343.98(082)

INTERNATIONAL Conference on Fundamental and Applied Aspects of Physical Chemistry (15; 2021; Beograd)

Physical Chemistry 2021: proceedings: the Conference is dedicated to the 30th Anniversary of the founding of the Society of Physical Chemists of Serbia and 100th Anniversary of Bray-Liebhafsky reaction. Vol. 2 / 15th International Conference on Fundamental and Applied Aspects of Physical Chemistry, September 20-24, 2021, Belgrade, Serbia; [organized by The Society of Physical Chemists of Serbia in co-operation with Institute of Catalysis Bulgarian Academy of Sciences ... [et al.]]; [editors Željko Čupić and Slobodan Anić]. - Belgrade: Society of Physical Chemists of Serbia, 2021 (Belgrade: Jovan). - VI str., str. 347-732: ilustr.; 30 cm

Tiraž 200. - Bibliografija uz svaki rad. - Registar.

ISBN 978-86-82475-39-2
ISBN 978-86-82475-40-8 (niz)

а) Физичка хемија -- Зборници б) Наука о материјалима -- Зборници в) Животна средина -- Зборници г) Форензика -- Зборници

COBISS.SR-ID 53325065

Book of abstracts

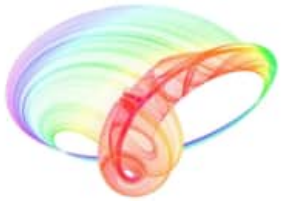

PHOTONICA2021

VIII International School and Conference on Photonics

& HEMMAGINERO workshop

23 - 27 August 2021,

Belgrade, Serbia

Editors

Mihailo Rabasović, Marina Lekić and Aleksandar Krmpot

Institute of Physics Belgrade, Serbia

Belgrade, 2021

ABSTRACTS OF TUTORIAL, KEYNOTE, INVITED LECTURES, PROGRESS REPORTS AND CONTRIBUTED PAPERS

of

VIII International School and Conference on Photonics PHOTONICA2021

23 - 27 August 2021

Belgrade Serbia

Editors
Mihailo Rabasović, Marina Lekić and Aleksandar Krmpot

Publisher
Institute of Physics Belgrade
Pregrevica 118
11080 Belgrade, Serbia

Printed by
Serbian Academy of Sciences and Arts

Number of copies
200

ISBN 978-86-82441-53-3

CIP - Каталогизација у публикацији - Народна библиотека Србије, Београд

535(048)

621.37/.39:535(048)

621.37/.39:535]:61(048)

66.017/.018(048)

INTERNATIONAL School and Conference on Photonic (8; 2021; Beograd)

Book of abstracts / VIII International School and Conference on Photonics PHOTONICA2021 & HEMMAGINERO workshop, 23 - 27 August 2021, Belgrade, Serbia; editors Mihailo Rabasović, Marina Lekić and Aleksandar Krmpot. - Belgrade: Institute of Physics, 2021 (Belgrade: SASA). - V, 192 str.: ilustr.; 30 cm

Tiraž 200. - Bibliografija uz većinu apstrakata. - Registar.

ISBN 978-86-82441-53-3

1. Hemmaginero Workshop (2021; Beograd)

a) Оптика -- Апстракти б) Оптички материјали -- Апстракти в) Оптоелектроника -- Апстракти г) Оптоелектроника -- Биомедицина -- Апстракти д) Телекомуникације -- Апстракти

COBISS.SR-ID 44290057

Thermoresponsive, biocompatible hydrogels for rapid prototyping of biomimetic microchannels

M. Radmilović[1], B. Murić[1], D. Grujić[1], B.Zarkov[2], M. Nenadić[3] and D. Pantelić[1]
[1]*Institute of Physics, Belgrade, Serbia*
[2]*Directorate for Measure and Precious Metals, Mike Alasa 14, 11000 Belgrade, Serbia*
[3]*Institute for Biological Research "Siniša Stanković" National Institute of Republic of Serbia, University of Belgrade, Serbia*
e-mail: mihajlo.radmilovic@ipb.ac.rs

Single-step prototyping of biophotonic structures that effectively mimic tissue microchannels is a complex task. A wide range of techniques is used for microchannel fabrication such as photolithography, silicon molding, etc. [1] However these techniques possess a high degree of manufacturing complexity and cost [1, 2].

We present technology that is based on locally melted nontoxic, environmentally friendly gels, and a homemade laser writing system. Microchannels are fabricated by local laser irradiation and spatial control is obtained using coordinate stage. The physical properties of microchannels are determined by: gels absorbance, surface tension and laser energy density.

Several *in vitro* assays were performed to establish biocompatibility of the gel materials. *In vitro* studies on the spontaneously immortalized human keratinocytes (HaCaT) cell line showed that the tested material had no toxic effect. Likewise, different ATCC (American Type Culture Collection) and resistant strains of pathogenic bacteria and micromycetes were cultivated. After application of the tested materials no inhibition of bacterial colonies and micromycetes growth was observed.

As a proof of concept, applicability of biomimetic microchannels (BM) was tested using a digital image of a human retinal blood vessels. Digital model is then translated to the set of G-code coordinates and imprinted in gel material by laser writing.

BM has significant potential for a wide range of applications such as noninvasive medical diagnostic, biomedical testing, security, etc. Here we suggest a retinal vascular model to study blood flow in different pathophysiological conditions. Moreover, our gel based material can be used for fast and efficient fabrication of BM and also for micro-optical components generation [3].

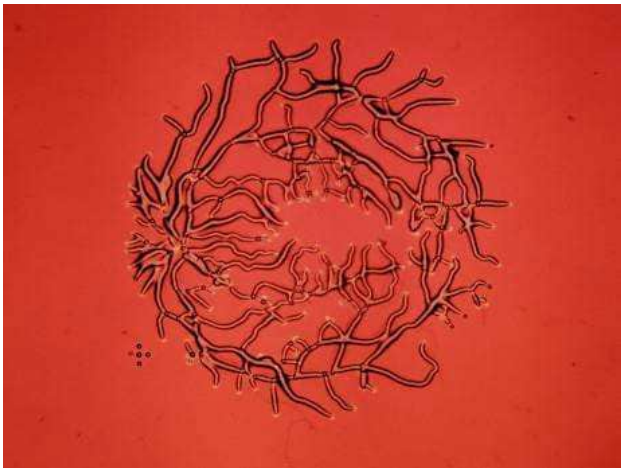

Figure 1. Biomimetic model of human retina blood vessels.

REFERENCES

[1] P. Ghassemi, J. Wang, A. Melchiorri, J. Biomed. Opt. 20, 121312 (2015).
[2] R.Long, T.King, T.Aki, Biomed. Opt. Exp. 2, 1887 (2011)
[3] B.Murić, D.Pantelić, D.Vasiljević, Appl. Opt. 46 8527 (2007)

Journal of Materials Chemistry C

ROYAL SOCIETY OF CHEMISTRY

COMMUNICATION

Cite this: J. Mater. Chem. C, 2021, 9, 8163

Received 5th March 2021,
Accepted 6th June 2021

DOI: 10.1039/d1tc01028j

rsc.li/materials-c

Thermo-osmotic metamaterials with large negative thermal expansion

Svetlana Savić-Šević, *[a] Dejan Pantelić,[a] Branka Murić,[a] Dušan Grujić,[a] Darko Vasiljević,[a] Branko Kolaric [ab] and Branislav Jelenković[a]

Negative thermal expansion (NTE) is important for compensation of thermal dilatation effects and has significant applications in high-precision devices and instruments. Several materials with intrinsic negative expansion exist but are chemically complex, difficult to manufacture and their thermal expansion coefficients (TECs) are small, typically in the order of 10^{-5}/K–10^{-6}/K. Here we present a metamaterial with a large NTE, with TEC in the order of 10^{-3}/K, enabled by thermo-osmosis of entrapped air molecules through a multitude of nanometer-thin layers. We have generated this material by holographically patterning a biopolymer (dichromated pullulan). The presented manufacturing process is quite simple and capable of generating large-area NTE materials. The concept of achieving (NTE) through thermo-osmosis is universal and can be extended to many other polymers. Our research, for the first time, introduces a relation between NTE and thermo-osmosis.

Introduction

All materials change their dimensions with temperature due to thermally dependent interatomic distances.[1] This behavior is quantified by linear (α_l) or volumetric (α_v) thermal expansion coefficients (TEC):

$$\alpha_l = \frac{1}{l}\frac{\mathrm{d}l}{\mathrm{d}T} \quad \text{and} \quad \alpha_V = \frac{1}{V}\frac{\mathrm{d}V}{\mathrm{d}T} \tag{1}$$

where $\mathrm{d}l$ and $\mathrm{d}V$ are length l and volume V changes induced by temperature difference $\mathrm{d}T$, respectively.[2] Almost all materials expand upon heating and the thermal expansion coefficient is thus positive (PTEC). Organic materials and polymers usually have a larger coefficient of thermal expansion (PTEC greater than 10^{-4}/K) than inorganic materials (such as metals and ceramics with PTEC of about 10^{-6}/K).[3]

Materials with negative thermal expansion coefficients (NTECs) are expensive, rare (except water between 273 K–277 K) and their chemical composition is very specific.[4,5] One of the main goals of NTE research is finding materials with large NTECs to compensate PTECs. In materials associated with a magnetic, ferroelectric or charge-transfer phase transition a large NTE has been discovered and such materials are used as thermal-expansion compensators.[6]

The development of a material with a large NTEC is possible by designing special structures made of several constituents.[7,8] For example, origami structures, consisting of a bi-material's 2D or 3D lattices, enable tailoring metamaterials with novel mechanical properties, including a wide range of PTECs and NTECs.[9] Such NTE materials have important applications for the control of the thermal expansion of materials. They allow adjustment of the thermal expansion of composites and can be used in microchip devices,[10] as dental fillings,[11] in optical and electronic devices,[12] for fasteners[13] and as coating materials.[14] However, such materials have a complex geometry difficult to manufacture.

Many methods have been used to fabricate metamaterials: laser interference lithography,[15] electron-beam lithography,[16] direct laser writing,[17] and focused-ion beam (FIB),[18] to mention just a few. Metamaterials can be fabricated from different substances including photoresists,[19] semiconductors,[20] and metals.[21] Holographic methods stand out as being capable of producing one-, two- and three–dimensional periodic metamaterials. Large areas can be fabricated simply and cheaply in a matter of minutes.

Here we describe a holographic method for generation of mechanical metamaterials with simple architecture and high NTECs, much higher than those of the other materials we found in the available literature. Pullulan, a biological polysaccharide, is used as a base material, which is further sensitized and holographically patterned at the nanoscale. Structural, optical and mechanical properties of the resulting metamaterial are studied, its NTEC measured and a thermo–mechanical model, explaining NTE behavior, presented. We also disclose a new physical mechanism behind such unusual behavior.

[a] Institute of Physics, University of Belgrade, Pregrevica 118, Zemun 11080, Serbia. E-mail: savic@ipb.ac.rs
[b] MNM Group, Department of Physics, UMONS, Mons, Belgium

Holographic generation of mechanical metamaterial

Doped pullulan is a home-made holographic photosensitive material used throughout this research to manufacture layered metamaterial and analyze its thermo-mechanical behavior. Pullulan is a linear polysaccharide produced from the yeast-like fungus *Aureobasidium pullulans*. The material is composed of maltotriose units connected by α-D-1,6-glycoside linkages[22] and can be photosensitized with chromium ions to produce dichromated pullulan (DCP)[23] as a transparent, thermo-stable film. Properties of DCP films as holographic material–surface gratings, its diffraction efficiency, copying and environmental stability–were previously investigated.[24,25]

DCP film was prepared by mixing an 8% aqueous solution of pullulan and 30% ammonium dichromate, which was poured on a flat glass plate. After drying, a thin film was placed in the holographic setup to produce a volume Bragg grating.[26] To do that, the laser beam from a single-frequency, a diode pumped Nd-YAG laser, at 532 nm, was expanded to expose the pullulan film at normal incidence. A mirror was set behind the film and a volume Bragg grating was recorded inside the DCP film by interference of two counter propagating beams. The interference pattern is responsible for generation of a large number of alternating DCP and air layers, parallel to the substrate. After exposure, the pullulan film was chemically processed by washing the plate in a mixture of water and isopropanol, followed by drying in pure isopropanol. Finally, the grating is slowly and fully dried in a closed vessel.

The resulting hologram is about 10 μm thick and has a complex structure, as shown in Fig. 1. On the nanoscopic level, the structure is characterized by approximately fifty Bragg layers. They are mutually separated and supported by nano-pillars with a diameter of up to 50 nm, enabling the mechanical stability of the whole structure.

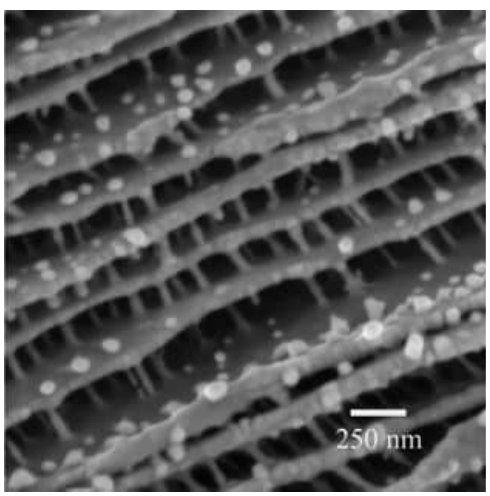

Fig. 1 A cross-section of pullulan metamaterial (recorded using a scanning electron microscope) showing pullulan layers separated by nanopillars.

The metamaterial acts as a selective reflector in the specific band of wavelengths in accordance with the Bragg's law:

$$\lambda = 2(n_a l_a + n_p l_p) \quad (2)$$

where l_a and l_p are the thicknesses of the air and pullulan layers (both about 100 nm), and refractive indices $n_a = 1$ and $n_p = 1.45$, respectively. A Bragg maximum (as defined in eqn (2)) depends on thermal variation of refractive indices and layer thicknesses. Thus, the spectral shift as a function of temperature can be found by taking the first derivative of eqn (2):

$$\frac{d\lambda}{dT} = 2\left(l_a\frac{dn_a}{dT} + n_a\frac{dl_a}{dT} + l_p\frac{dn_p}{dT} + n_p\frac{dl_p}{dT}\right) \quad (3)$$

This optical property of the DCP metamaterial was measured in a heating/cooling cycle. The sample was heated and cooled using a Peltier element (controlling temperature between 295 K and 323 K) and the reflection spectra of the white light from the halogen lamp were recorded using a fiber type spectrometer. A thermocouple was embedded within the sample to obtain accurate measurement of the temperature. As can be seen in Fig. 2a, the reflectance peaks are blue-shifted from 580 nm to 535 nm during heating, exhibiting a negative spectral shift of 45 nm for a positive temperature difference of +25 K (equivalent to 1.8 nm K^{-1}). Upon temperature decrease, a spectral maximum returns close to its initial position. Spectral shift *vs.* temperature, for the whole heating–cooling cycle, shows characteristic hysteresis, as in Fig. 2b. The hysteresis effects are inherent to many natural phenomena. In our case, we assume that hysteresis is a consequence of the nonlinear viscoelastic behaviour of the polymer,[27] *i.e.* pullulan nano-pillars, with temperature. Upon heating, air diffuses through membranes and escapes into the surrounding environment, lowering the pressure inside the multilayer. Outside pressure then compresses the layers until a new mechanical equilibrium is achieved. Due to the compression of the layers, the pullulan nano-pillars are bent. It is assumed that at higher temperatures the viscoelasticity of the pillars slightly decreases. Thanks to the capability to creep,[27] after strain due to pressure, the pillars return to their initial state, with a slightly lower temperature than the initial one.

Thermal behavior of optical systems is typically explained by thermal expansion and thermal variation of the refractive indices (as in eqn (3)). In the following, we will show that these mechanisms cannot account for the large and negative spectral shift.

First, we experimentally determined the linear TEC of a pure, unstructured DCP film. A circular, freestanding DCP membrane was produced, clamped at its perimeter, and its central zone was heated with the laser beam. The temperature of the film was measured using a thermal camera, while the resulting thermal bending was measured using digital holographic interferometry. The linear expansion coefficient was calculated from the recorded interferogram, Fig. 3, and found to be $\alpha_{DCP} = 8.8 \times 10^{-5}$/K, which is in agreement with the values obtained for other polysaccharides.[28,29]

Now we can calculate spectral shift of the Bragg maximum using eqn (3). The thermo-optic coefficient of air (dn_a/dT)[30] is

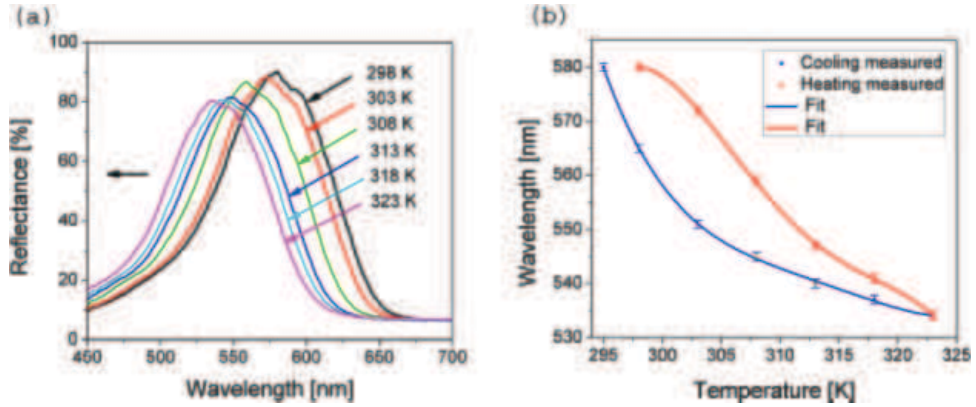

Fig. 2 (a) Reflectance spectra of DCP metamaterial during heating and (b) spectral peak shift during a heating and cooling cycle.

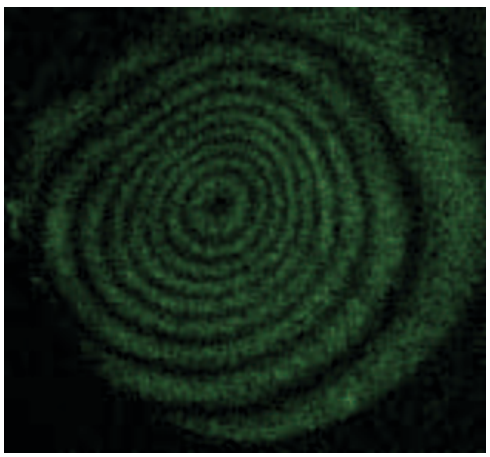

Fig. 3 Interferogram of the thermal bending of the DCP film.

very small and the first term in eqn (3) can be neglected. Additionally, thicknesses of air and pullulan layers are almost the same $l_a = l_p = l$ and eqn (3) can be simplified:

$$\frac{d\lambda}{dT} = 2\left(n_a\frac{dl}{dT} + l\frac{dn_p}{dT} + n_p\frac{dl}{dT}\right) \quad (4)$$

In a linear approximation dilatation $dl = \alpha l T$ (see eqn (1)) and finally:

$$\frac{d\lambda}{dT} = 2l\left(\frac{dn_p}{dT} + \alpha(n_p + n_a)\right) \quad (5)$$

We were not able to measure the thermo-optic coefficient of DCP, and we assumed the largest thermo-optical coefficient recorded up to now, $dn/dT = -5 \times 10^{-4}$/K.[31]

By including these values of thermal constants dn/dT and α_{DCP} into eqn (5), together with the value of the layer thickness $l = 118$ nm and refractive indices of air and pullulan, we have found that the expected temperature shift of the Bragg peak is $d\lambda/dT = -0.07$ nm K^{-1}. This value is much lower than the one recorded experimentally, $d\lambda/dT = -1.8$ nm K^{-1}, and classical thermal effects fail to explain the very large NTEC.

As shown above, while the change in the DCP film thermal expansion is small, the thickness variation of air layers must be the main contributor to the overall metamaterial contraction. From the experimentally observed spectral shift and a temperature change of +25 K, the calculated change in air layer thickness (using eqn (2)) is −22 nm. Knowing that there are fifty Bragg layers, the total thickness change is $dl = -1.1$ μm. Knowing that the initial thickness of the material is $l = 10$ μm, we estimate (using eqn (1)) that the linear thermal expansion coefficient of DCP metamaterial is $\alpha_{DCPm} = -4.4 \times 10^{-3}$/K. This value is quite large, compared to values of NTEC, available in the literature. The results presented here have been verified in a series of experiments on many different samples. We have found that the behaviour of pulullan metamaterial is the same, confirming a negative thermal expansion with NTEC of the order 10^{-3}/K.

Thermo-osmotic mechanism of negative thermal expansion

As explained above, negative and large TEC cannot be explained by usual and simple thermal effects (thermal dilatation and refractive-index variation). In this section, the peculiar behavior of DCP metamaterial is explained through thermo-osmosis,[32] a process defined as fluid or gas diffusion through a membrane due to a temperature gradient.[32,33] This phenomenon was found in many areas from biology[34] to energy harvesting.[35]

We should note that the pullulan layers are very thin (about 100 nm) and their mutual separation is of the same order of magnitude. In such a small volume, only a small number of air molecules are entrapped between the pullulan layers (the mean path length of air molecules is 67 nm under normal conditions)[36] and molecules diffuse through the layers, depending on the temperature difference between the layer and their environment. In a thermal equilibrium, a net flow of molecules between the layer and the environment is zero. If the temperature of the layer rises, more molecules escape the layer, lowering the pressure inside the layer. The resulting pressure difference compresses the layers, supported only by tiny nanopillars (Fig. 1).

Diffusion through permeable membranes is described by Fick's law,[37] which determines the diffusive flux per unit area Φ as a function of pressure p_0 and membrane thickness l:

$$\varnothing = \frac{Pp_0}{l} \quad (6)$$

where P is membrane permeability, which is an intrinsic property of the material.

Effects of temperature on gas permeability were previously analyzed.[38,39] For gases, the temperature-dependence of permeability is defined according to the Arrhenius relationship:

$$P = P_0 \exp^{\frac{-E_p}{RT}} \quad (7)$$

where P_0 is a constant (a kinetic frequency factor), R is the gas constant, and E_P is the activation energy for permeation. According to the above equation the gas permeability increases with temperature.

For simplicity of the further analysis, we will explore a single membrane separating a closed compartment from the surrounding air environment; see Fig. 4.

We suppose that the environment is a thermal reservoir with infinite capacity at constant temperature T_0 and pressure p_0. If a compartment with a membrane is at temperature T_1 and pressure p_1, we have a flux Φ_1 of molecules diffusing out of the compartment into the environment and flux Φ_0 of particles flowing from the environment into the compartment, *i.e.* by combining eqn (6) and (7):

$$\varnothing_0 = \frac{p_0}{l} P_0 \exp^{-\frac{E_p}{RT_0}} \quad (8)$$

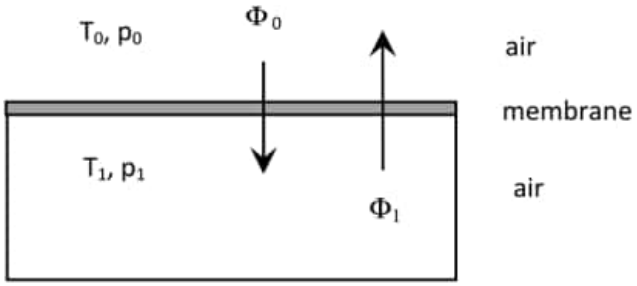

Fig. 4 Compartment with a single membrane, where T and p are temperatures and pressures, while Φ are fluxes.

$$\varnothing_1 = \frac{p_1}{l} P_0 \exp^{-\frac{E_p}{RT_1}} \quad (9)$$

Due to the temperature difference between the compartment and its external environment, ingoing and outgoing fluxes are not equal any more, and there is a net molecular flow. Suppose that the temperature inside the compartment is larger than that of the surrounding air, molecules will leak out and reduce the pressure p_1 inside the compartment. The resulting pressure difference will exert a mechanical force on the membrane and compress it until a new equilibrium is reached, *i.e.* when $\Phi_1 = \Phi_0$. From eqn (8) and (9) we can easily find that this will happen when:

$$p_1 = p_0 \exp^{-\frac{E_p}{R\left(\frac{1}{T_0} - \frac{1}{T_1}\right)}} \quad (10)$$

As stated before, this pressure difference is compensated by the mechanical resistance of nanopillars to compression.

In the case of DCP metamaterial, we have a number of pullulan membranes stacked one above the other and separated by tiny nanopillars. Air is gradually leaking from one layer to another until it goes out to the atmosphere. Air leakage is a process that takes some time, before thermo-mechanical equilibrium is reached.

Dependence of pressure p_1 on temperature was calculated from eqn (10) and is shown in Fig. 5(a). The activation energy of air permeation through the polysaccharide membrane is about 40 kJ mol^{-1}.[40] The graph shows that p_1 decreases with increasing temperature of the pullulan layers. Based on this dependence, Fig. 5(b) and (c) show the dependence of pressure p_1 on the measured time to achieve a new equilibrium state and the dependence of pressure p_1 on the air layer thickness, respectively.

Discussion and conclusions

We have shown that the proposed thermo-osmotic mechanism explains well all the experimentally recorded properties of the pullulan NTE metamaterial. However, there are other, less obvious mechanisms that could contribute to the negative thermal expansion, most notably the effect of air humidity.

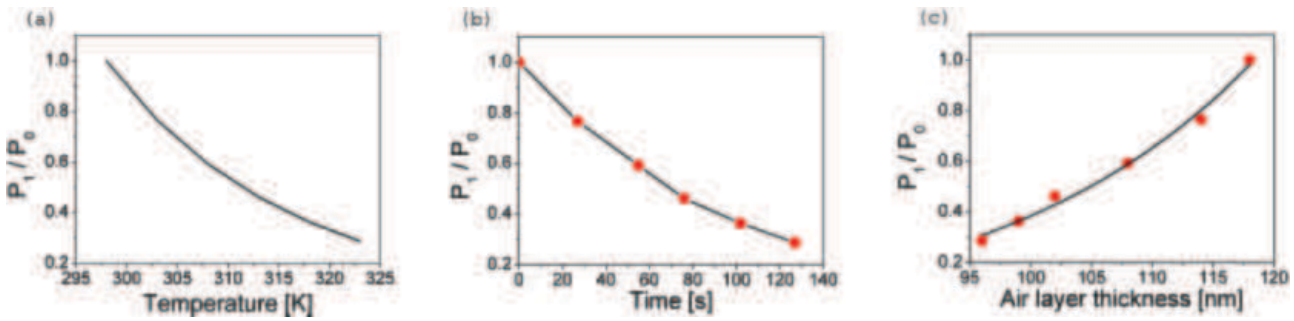

Fig. 5 Ratio of the pressure inside and outside of the compartment as a function of (a) DCP temperature, (b) time needed to reach a new equilibrium state, and (c) air layer thickness. The points on graphs (b and c) correspond to experimentally measured values.

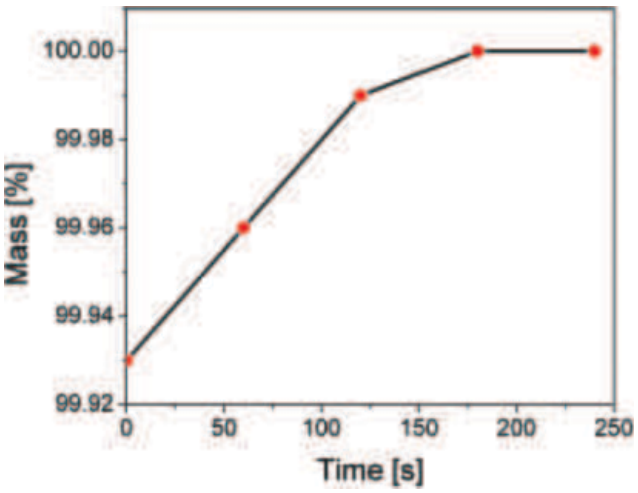

Fig. 6 The change of mass of DCP metamaterial in time due to humidity.

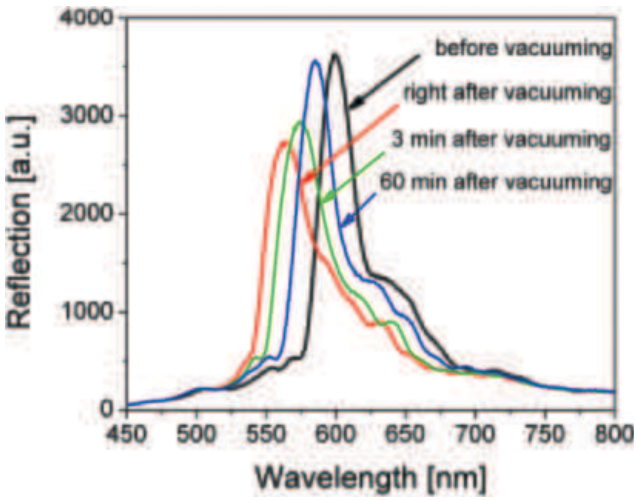

Fig. 7 Reflectance before and after vacuuming and exposing to air.

To test if pullulan absorbs water from the air we performed a simple gravimetric experiment with an analytical balance. First, the DCP metamaterial was measured under normal laboratory conditions, it was then heated to 373 K for 45 min, to eliminate moisture, and measured again. After that, the sample was kept under normal laboratory conditions and the mass was measured every hour until it reached its original value, see Fig. 6. It can be seen that the change of mass, caused by moisture, is only 0.07%. Bearing in mind that pullulan does not form the gel, and does not swell significantly, we conclude that the influence of moisture on the pullulan structure is negligible.

As a final proof of diffusion of air through pululan layers and the corresponding thermo-osmosis, as a dominant mechanism, we placed the pullulan metamaterial in a vacuum chamber, at the pressure of 4×10^{-2} Pa, for 45 minutes. During that time, entrapped air diffused out of the pullulan layers. The reflection spectra measured immediately after the sample was removed from the vacuum and placed back to the normal atmospheric conditions, were shifted towards lower wavelengths. This shift was caused by the air pressure compressing the layers due to the large pressure difference between the inside ($p \sim 0$ Pa) and outside of the metamaterial ($p_{\mathrm{atm}} \sim 100\,000$ Pa). Following the prolonged stay in the atmosphere the air diffuses into the layers, equilibrating pressures and expanding the material as evidenced by the spectral shift, see Fig. 7.

It is also important to note that when the temperature excised a certain maximum value (higher than 383 K) the DCP metamaterial loses its NTE properties. We believe that in this case there are no more air molecules entrapped within the pullulan layers, and the pressure difference is large enough to break the pullulan nanopillars, which otherwise will sustain the mechanical integrity of the whole structure. Bear in mind that all the mentioned effects (dilatation, thermo-optical, and humidity) are simultaneously present, but nevertheless our experiments show that the thermo-osmosis is a dominant one, which converts an ordinary PTE into an NTE material. Without diffusion, a pressure of entrapped air between the pullulan multilayers will follow the temperature variation–increasing upon heating, and decreasing upon cooling. This will turn the pullulan multilayer into a positive thermal expansion material, in contrast to what we observed experimentally.

Regarding the thermo-osmotic process, we emphasize the simplicity of the presented model, which very well describes the complex phenomenon responsible for NTE. First of all, the pullulan layers have a stochastic distribution of thicknesses, size and position of nanopillars, which is difficult to take into account in the model. Also, the mechanical properties of materials at the nanoscale level can be quite different, compared to those of the bulk. Additionally, for such thin layers, air cannot be treated as continuum and more complex effects come into play, such as thermophoresis and thermoconvection. In our case, the situation is further complicated by extremely small (100 nm) separation between the layers when the number of entrapped molecules is correspondingly small. This means that losing a single molecule from the layer significantly reduces the pressure. In spite of this, the proposed model is able to explain the most distinctive properties of the system: negative thermal expansion and the corresponding optical properties.

In conclusion, we have found that holographically patterned dichromated pullulan is a new mechanical metamaterial with a large NTE of $\alpha_{\mathrm{DCPm}} = -4.4 \times 10^{-3}$/K in a temperature range between 295 K and 323 K. Our investigations are in this temperature range because most of the practical interests and potential applications of organic devices are around room temperature. We show that it is simple to fabricate a stable and durable material using the holographic technique. Our explanation of the mechanism that converts an ordinary positive thermal expansion material into an NTE material is based on thermo-osmosis of the air molecules through the pullulan nanolayers. Dependence of the optical response on temperature of the pullulan metamaterials was investigated. The reflection spectra show a blue shift with increasing temperature, which originates from the contraction of air nanolayers due to the thermo-osmosis of the air molecules through the pullulan nanolayers.

The proposed mechanism can be applied to various holographic structures and materials, as well as to different gases and temperature ranges. We have performed the same measurements using holographically patterned dextran (another polysaccharide) and found NTE, too. While pullulan is linear, dextran has a branching structure but shows the same behavior as pullulan, and the reflectance peaks are blue-shifted during heating. Our multilayer design is simple and the proposed mechanism is useful for surfaces of arbitrary size. We have shown that experimental results can be explained by simple relationships, in the nanoscale, linking the structures, mechanical and optical properties, and temperature-response. The disclosed mechanism is universal and opens a range of possibilities to construct engineered materials with tailored negative thermal expansion.

Conflicts of interest

There are no conflicts to declare.

Acknowledgements

The authors acknowledge funding provided by the Institute of Physics Belgrade, through the grant by The Ministry of Education, Science, and Technological Development of the Republic of Serbia. B. Kolaric acknowledges support from the F.R.S.-FNRS.

Notes and references

1 K. Takenaka, *Front. Chem.*, 2018, **6**, 267.
2 J. P. Attfield, *Front. Chem.*, 2018, **6**, 371.
3 R. Lakes, *J. Mater. Sci. Lett.*, 1996, **15**, 475–477.
4 M. Szafránski, *J. Mater. Chem. C*, 2013, **1**, 7904–7913.
5 H. Liu, J. Chen, X. Jiang, Z. Pan, L. Zhang, Y. Rong, Z. Lin and X. Xing, *J. Mater. Chem. C*, 2017, **5**, 931–936.
6 K. Takenaka, Y. Okamoto, T. Shinoda, N. Katayam and Y. Sakai, *Nat. Commun.*, 2017, **8**, 14102.
7 L. Cabras, M. Brun and D. Misseroni, *Proc. Natl. Acad. Sci. U. S. A.*, 2019, **475**, 20190468.
8 J. Qu, M. Kadic, A. Naber and M. Wegener, *Sci. Rep.*, 2017, **7**, 40643.
9 E. Boatti, N. Vasios and K. Bertoldi, *Adv. Mater.*, 2017, **29**, 1700360.
10 J. Chen, L. Hu, J. Deng and X. Xing, *Chem. Soc. Rev.*, 2015, **44**, 3522–3567.
11 A. Versluisl, W. Douglasl and R. Sakaguchi, *Dent. Mater.*, 1996, **12**, 290–294.
12 R. Bastaits, G. Rodrigues, P. Jetteur, P. Hagedorn and A. Preumont, *Smart Mater. Struct.*, 2012, **21**, 064004.
13 O. Sigmund and S. Torquato, *J. Mech. Phys. Solids*, 1997, **45**, 1037–1067.
14 A. Sanson and J. Chen, *Front. Chem.*, 2019, **7**, 284.
15 Y. Zhou, X. Y. Chen, Y. H. Fu, G. Vienne, A. I. Kuznetsov and B. Luk'yanchuk, *Appl. Phys. Lett.*, 2013, **103**, 123116.
16 E. Almeida, O. Bitton and Y. Prior, *Nat. Commun.*, 2016, **7**, 12533.
17 M. S. Rill, C. Plet, M. Thiel, I. Staude, G. von Freymann, S. Linden and M. Wegener, *Nat. Mater.*, 2008, **7**, 543–546.
18 C. Enkrich, F. Pérez-Willard, D. Gerthsen, J. Zhou, T. Koschny, C. M. Soukoulis, M. Wegener and S. Linden, *Adv. Mater.*, 2005, **17**, 2547–2549.
19 D.-Y. Kang, W. Lee, D. Kim and J. H. Moon, *Langmuir*, 2016, **32**, 8436–8441.
20 T. K. Kormilina, E. A. Stepanidenko, S. A. Cherevkov, A. Dubavik, M. A. Baranov, A. V. Fedorov, A. V. Baranov, Y. K. Gun'ko and E. V. Ushakova, *J. Mater. Chem. C*, 2018, **6**, 5278–5285.
21 X. Zheng, W. Smith, J. Jackson, B. Moran, H. Cui, D. Chen, J. Ye, N. Fang, N. Rodriguez, T. Weisgraber and C. M. Spadaccini, *Nat. Mater.*, 2016, **15**, 1100–1107.
22 Y. Enomoto-Rogers, N. Lio, A. Takemura and T. Iwata, *Eur. Polym. J.*, 2015, **66**, 470–477.
23 D. Pantelic, S. Savic and D. Jakovljevic, *Opt. Lett.*, 1998, **15**, 807–809.
24 S. Savic-Sevic and D. Pantelic, *Appl. Opt.*, 2007, **46**, 287–291.
25 S. Savic-Sevic and D. Pantelic, *Opt. Express*, 2005, **13**, 2747–2754.
26 S. Savic-Sevic, D. Pantelic, B. Jelenkovic, B. Salatic and D. V. Stojanovic, *Soft Matter*, 2018, **14**, 5595–5603.
27 G. Strobl, *The Physics of Polymers*, Springer-Verlag, Berlin Heidelberg, 2007.
28 M. Wada and Y. Saito, *J. Polym. Sci., Part B: Polym. Phys.*, 2001, **39**, 168–174.
29 V. Ramiah and D. A. I. Goring, *J. Polym. Sci., Part C: Polym. Symp.*, 1965, **11**, 27–48.
30 B. Edlen, *Metrologia*, 1966, **2**, 71–80.
31 T. Handa, H. Tahara, T. Aharen and Y. Kanemitsu, *Sci. Adv.*, 2019, **5**, eaax0786.
32 K. G. Denbigh and G. Raumann, *Proc. R. Soc. London, Ser. A*, 1952, **210**, 377–387.
33 K. G. Denbigh, *Nature*, 1949, **163**, 60.
34 W. Groβe, *Aquat. Bot.*, 1996, **54**, 101–110.
35 A. P. Straub, N. Y. Yip, S. Lin, J. Lee and M. Elimelech, *Nat. Energy*, 2016, **1**, 1–6.
36 S. G. Jennings, *J. Aerosol Sci.*, 1988, **19**, 159–166.
37 N. Gontard, R. Thibault, B. Cuq and S. Guilbert, *J. Agric. Food Chem.*, 1996, **44**, 1064–1069.
38 C. G. Biliaderis, A. Lazaridou and I. Arvanitoyannis, *Carbohydr. Polym.*, 1999, **40**, 29–47.
39 N. Acharya, P. Yadav and Y. Vijay, *Indian J. Pure Appl. Phys.*, 2004, **42**, 179–181.
40 L. A. El-Azzami and E. A. Grulke, *J. Polym. Sci., Part B: Polym. Phys.*, 2007, **45**, 2620–2631.

Optical and Quantum Electronics (2022) 54:361
https://doi.org/10.1007/s11082-022-03681-0

Rapid direct laser writing of microoptical components on a meltable biocompatible gel

Mihajlo D. Radmilović[1] · Branka D. Murić[1] · Dušan Grujić[1] · Boban Zarkov[2] · Marija Z. Nenadić[3] · Dejan V. Pantelić[1]

Received: 15 November 2021 / Accepted: 20 March 2022

Abstract
Microoptical components are coming of age in a wide range of applications: lab-on-a-chip, imaging, detection… There are a large number of fabrication technologies capable of producing high quality individual components and their arrays. However, most of them require high-end and costly equipment, complex and time-consuming fabrication, harmful chemicals, resulting in expensive final products. Here we present a technology capable of producing high quality microoptical components, using low-end direct laser writing on a biocompatible, environmentally friendly hydrogel, without any waste substances. The gel is locally and controllably melted while surface tension forces shape the optical component, following the laser beam profile. The process is so quick that a single microlens is fabricated in less than a second, and can be used instantly without any further processing. The technology is neither subtractive nor additive, and the base material is simply displaced producing a smooth surface. We have been able to fabricate individual microlenses and their arrays (positive, negative, aspheric), gratings and diffractive components. The technology is tested by generating unique, difficult to counterfeit QR-codes. Turnaround time is fast and makes the technology suitable both for rapid prototyping and serial production.

Keywords Laser writing · Microoptics · Hydrogels · Biocompatibility · Security

This article is part of the Topical Collection on Photonics: Current Challenges and Emerging Applications.

Guest edited by Jelena Radovanovic, Dragan Indjin, Maja Nesic, Nikola Vukovic and Milena Milosevic.

✉ Dejan V. Pantelić
pantelic@ipb.ac.rs

[1] Institute of Physics Belgrade, University of Belgrade, Pregrevica 118, 11080 Belgrade, Serbia

[2] Directorate for Measure and Precious Metals, Mike Alasa 14, 11000 Belgrade, Serbia

[3] Institute for Biological ResearchSiniša Stanković",National Institute of Republic of Serbia, University of Belgrade, Bulevar despota Stefana 142, 11060 Belgrade, Serbia

Published online: 17 May 2022

1 Introduction

There is a growing need for complex microoptical devices (Kemme 2009) and their use for micro-optoelectromechanical (MOEMS) and lab-on-a-chip applications. However, their fabrication is usually a complex, time consuming, multistep process, requiring several high-end technologies: microlithography (Grigaliūnas et al. 2016), embossing (Moore et al. 2016), femtosecond direct laser writing (Deng et al. 2019), diamond turning (Zhou et al. 2011; Zhang et al. 2020). These are the reasons why prevailing microfabrication methods are not suitable for individualized production or rapid prototyping. Also, materials used for microfabrication are complex and usually toxic. A huge volume of fabricated devices enhances the problem of safe and environmentally friendly disposal of microfabricated devices.

Among other materials, gels have attracted attention as a candidate material for MOEMS. There is a wide variety of gels with characteristic solid–liquid transition induced by coil to helix transformation (Taylor et al. 2017). The transition can be induced by temperature, chemicals or electric field. Not so many of them have good optical properties and only a few appropriate ones are easy to fabricate, nontoxic and environmentally friendly. Optical gels (Duarte-Quiroga and Calixto. 2000; Li et al. 2019) have been used to manufacture dynamical and responsive microlenses. However, their response is slow and chemistry complex (Guan and Zhang 2011).

Microlenses have found application niches for illumination (Lee et al. 2013), imaging (Zhang et al. 2020) and, in particular, security (Walger et al. 2020). Applied technologies are advanced and complex favoring mass production and precluding individualization of security features (Jiang et al. 2019).

Previously (Krmpot et al. 2013), we have analyzed optical properties of negative microlenses using NLM. Here we present a technology based on nontoxic, environmentally friendly gels which are locally melted by direct laser writing. Our aim was to develop a material that is optically transparent, easily and instantly meltable by localized irradiation, durable and made from ordinary "kitchen" chemicals (by E number classification of food additives). We describe material properties, its biocompatibility, analyze the process of local laser-induced melting, demonstrate its capabilities for security purposes and envision their further use for microfluidic and lab-on-a-chip applications.

2 Materials and methods

2.1 Preparation of photo-meltable gel

Previously we have used gelatin plasticized with tot'hema (an oral solution for anemia treatment) and sensitized with eosin Y (a red fluorescent dye with absorption maximum at 530 nm) to produce microoptical components (Murić et al. 2007, 2008). We were able to manufacture negative (concave) microlenses, but the problem was gradual darkening of the material. That is why we replaced a commercial tot'hema with a water solution composed of several ingredients acting as plasticizers, humectants, and preservatives. This solution (designated PS for brevity) consists of: 0.2 ml of glycerol, 0.3 g of sucrose, 8 mg of glucose, 2 µl of polysorbate 80.6 mg of citric acid, and 2 mg of sodium benzoate (everything

is expressed per 1 ml of solution). The addition of PS improves mechanical and optical properties of the gelatin layer (elasticity, durability and stability, optical transparency…).

After swelling of gelatin in deionized water for one hour, and heating at 50 °C in the water bath (Vela™, Cole Parmer), 5% aqueous gelatin solution was prepared. Following, 0.01 g of sodium chloride and 0.16 ml of PS were further added (with stirring) to prevent gelatin layer crystallization and breaking. The preparation of photo-meltable gel (PMG) is concluded by adding 20 µl of eosin (2% aq. sol.). Quantity of all added components is expressed per 1 ml of gelatin solution. Finally, the PMG solution was centrifuged (Cole Parmer 17250–10 at 3400 rpm/min) to remove all particulates and impurities.

A PMG layer was prepared by the gravity settling method i.e., by pouring a constant volume of the prepared solution onto precisely leveled and well cleaned microscope glass slide bounded by a Plexiglas frame. After gelation, layers were left in the dark overnight, under ordinary environmental conditions (T = 25 °C, RH = 50–60%). During that time, a certain amount of water evaporated from the layer, as verified gravimetrically. After reaching the equilibrium value, the water content remains constant. The thickness of the dried layer depends on the amount of poured solution and can be chosen anywhere between several tens of microns up to several millimeters or even centimeters. In our experiments, layer thickness was kept at 100 µm.

2.2 Direct laser writing system

We used a home-made laser writing device (Zarkov et al. 2012) operating at 488 nm laser (Toptica iBEAM SMART with a maximum power of 100 mW). The laser beam is focused by the long working distance objective (Mitutoyo, 20 × 0.42 NA). Compact, color scientific CMOS camera (Thorlabs CS505CU5 Megapixel), was used to position the PMG layer at the desired position with respect to the focal point. A coordinate stage (Ludl BioPoint2, resolution 50 nm, repeatability 2 µm) with G-code enabled Arduino microcontroller was used to move the layer with respect to the laser beam. G-code (a standard programming language for CNC machines (Walger et al. 2020) was used to control movement with adjustable speed. Appropriate software was written to coordinate and synchronize the layer movement with laser switching and intensity adjustment.

2.3 Nonlinear microscopy of microoptical surfaces

To characterize the structure of microoptical components, we used a home-made nonlinear microscope (NLM) (Rabasović et al. 2015) equipped with a femtosecond Ti: Sapphire laser (Coherent, Mira, 900F). The pulse duration is 160 fs with a 76 MHz repetition rate and average power of 100 mW. A galvo-mirror scanning system was used for raster-scanning of the samples in a commercial microscope (Leica). In order to fill the entrance pupil of microscopic objective (Carl Zeiss, 20 × 0.8 air) the laser beam was expanded. A tube lens produces an image on the photomultiplier tube (PMT). Images were acquired and processed using dedicated software. The spatial resolution of scanning system was 0.6–0.9 µm in lateral direction, while the axial resolution was 2.1 µm. The device turned out to be particularly suitable for analysis of generated microstructures due to its ability to "see" internal structure of the material. Here we used two-photon excited fluorescence (TPEF) modality of NLM, which was particularly suitable due to the large penetration depth of infrared excitation beam and reduced laser damage. We were interested primarily in the surface shape of microoptical components when refraction effects do not introduce significant distortion.

2.4 Thermal analysis of micro-component manufacturing process

Throughout the research we used a thermal imaging to monitor thermal effects of the laser radiation during micro-component manufacturing. A commercial thermal camera (FLIR A65) with 640×512 pixels spatial resolution, 30 fps speed, thermal resolution/NETD 50 mK and 7.5–13 μm spectral range was utilized to record temperature and its spatial distribution. We used an additional IR (ZnS) lens, placed in front of the germanium camera lens, to further magnify the thermal image of a laser-melted zone.

2.5 In vitro biocompatibility testing

Cytotoxicity of tested PMG was determined on spontaneously immortalized keratinocyte cell line (commonly referred as HaCaT) using crystal violet assay as described previously (Stojković et al. 2020) with some modifications. A high capacity to differentiate and proliferate in vitro makes HaCaT cell lines extremely useful for the purpose (Schürer et al. 1993)). HaCaT cells were grown in high-glucose Dulbecco's Modified Eagle Medium (DMEM) supplemented with 10% fetal bovine serum (FBS), 2 mM L-glutamine and 1% penicillin and streptomycin (Invitrogen), at 37 °C in a 5% CO_2 incubator. Forty-eight hours before treatment, cells were seeded in a 96-well microtiter adhesive plate at a seeding density of 4×10^3 cells per well. PMG was dissolved in 0.01 mM PBS to a final concentration of 8 mg mL^{-1}. After 48 h, the medium was removed and the cells were treated for next 24 h with various concentrations of the dissolved gel in triplicate wells. Subsequently, the medium was removed; the cells were washed twice with PBS and stained with 0.4% crystal violet staining solution for 20 min at room temperature. Afterwards, crystal violet staining solution was removed; the cells were washed in a stream of tap water and left to air dry at room temperature. The absorbance of dye dissolved in methanol was measured in a plate reader at 570 nm (OD_{570}). The results were expressed as relative growth inhibition (GI_{50}) rate (%) indicating 50% inhibition of proliferation of HaCaT cells when compared with untreated control. Experiments were performed in triplicate for each concentration of the samples and three independent experiments were performed. The criterion used to categorize the antiproliferative activity of PMG to HaCaT cell line was as follows: $IC_{50}\leq20$ μg mL^{-1} = highly cytotoxic, IC_{50} ranged between 31 and 200 μg mL^{-1} = moderately cytotoxic, IC_{50} ranged between 201 and 400 μg mL^{-1} = weakly cytotoxic, and $IC_{50}>401$ μg mL^{-1} = no cytotoxicity (Stojković et al. 2020).

3 Results

3.1 Material characterisation

PMG is designed to be sensitive to the wavelength of the laser used in this research (488 nm) in order to enable photo-induced melting. The focused laser beam locally heated the PMG above its melting temperature and surface tension produced a concave dip. The process was observed using a thermal camera. Temperature field is localized to the vicinity of a laser beam. Within 1/5 s, the temperature reaches a maximum and decays in spite of the material being still irradiated. This is due to the bleaching of eosin and the

corresponding reduced absorption. This is associated with the layer turning transparent instead of red.

As can be seen in Fig. 1a (recorded using TPEF), the laser-produced shape is a concave asphere, while its diameter and optical characteristics depend on the laser power, irradiation time and the laser beam size (Fig. 1b). The surface of the dip is quite smooth (roughness is of the order of few nanometers) and can be faithfully approximated with a cubic polynomial, as verified by atomic force microscopy. As a result, the dip acts as a high-quality negative-power microlens (Krmpot et al. 2013).

The sensitivity threshold for a 100 μm thick PMG layer is 10^4 W/cm^2, which we achieved with only 7.5 mW of laser power. This limit depends on the layer thickness, PS and dye concentrations, focus depth. It is important to mention that layer is also sensitive below 7.5 mW, but the material is only bleached (without lens formation).

As can be seen, exposure and bleaching are intertwined. We have observed the process by measuring the decrease of PMG fluorescence during irradiation i.e., energy absorbed by the material is dissipated through fluorescence (see Fig. 2). As a consequence, after a certain irradiation time, the layer bleaches so much to drop the temperature below the melting point. In that case, material cannot remain liquid and "freezes" its lens-like shape.

We have developed a simplified thermal model which describes temperature T and its dependence on initial temperature T_0:

$$T = T_0 + \frac{A}{Kmc} + \frac{B}{C-A} \cdot exp(-At) - \left(\frac{B}{C-A} + \frac{A}{Kmc}\right) exp(-Ct) \quad (1)$$

The model includes constants A, B and C which depend on PMG layer properties: conductivity, specific heat and thickness. Additional constant K describes bleaching speed, while m is mass of the irradiated gel and c is specific heat (see Appendix).

Calculations have shown close correspondence with experimentally recorded temperature variation (compare Fig. 3a and b) and correctly describe initial temperature rise with subsequent exponential temperature drop (Eq. 1).

It is important to note that if the laser radiation is too intense it might occur that material can be bleached to fast so that melting temperature cannot be reached. We have experimentally observed this particular behaviour, which leaves material bleached without microlens being produced.

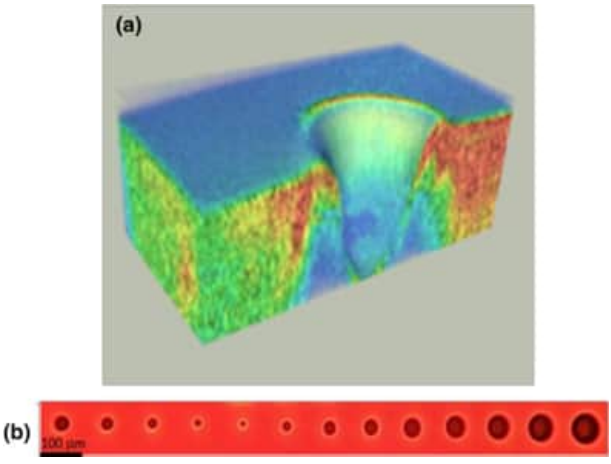

Fig. 1 **a** 3D image of a microlens shape recorded by NLM, **b** Optical microscope image showing how the size of a microlens strongly depends on the size of the laser beam.

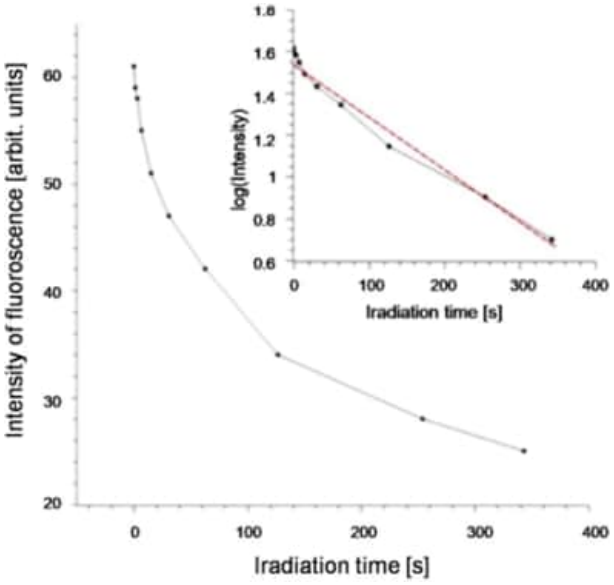

Fig. 2 Bleaching of material observed as a decrease of fluorescence intensity under irradiation with 0.05 mW focused laser beam. Fluorescence decay is represented on the linear scale. The same graph, presented on a logarithmic scale, is shown in the inset

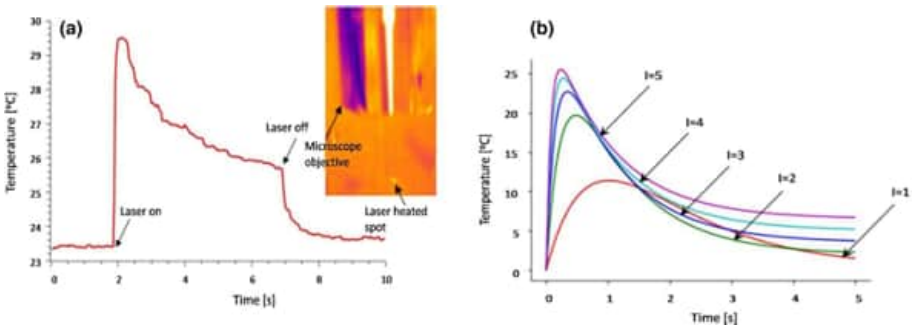

Fig. 3 **a** A temperature profile during constant-power irradiation (5 s, 15 mW laser power) of PMG layer, recorded by a thermal camera. Temperature decreases due to bleaching of eosin. After turning the laser off, temperature quickly drops to that of the environment. **b** Theoretically calculated temperature variation (using Eq. 1).

That is why we were forced to closely control the exposure in order to preclude this kind of memory effect. The effect is important if optical micro-components are too close, because the first one bleaches a certain space in its vicinity. If we try to write the next micro-component, exposure must be increased to compensate for a significant drop of absorption due to bleaching.

However, in the following we describe how more complex surface shapes can be manufactured by carefully controlling the laser focal position, beam pattern and exposure. We have manufactured good quality positive microlenses by making an arrangement six polygonally positioned spots. The material left in the center of a polygon acqures spherical surface which acts as a positive (convex) microlens. This can be seen in a NLM image of a material (Fig. 4).

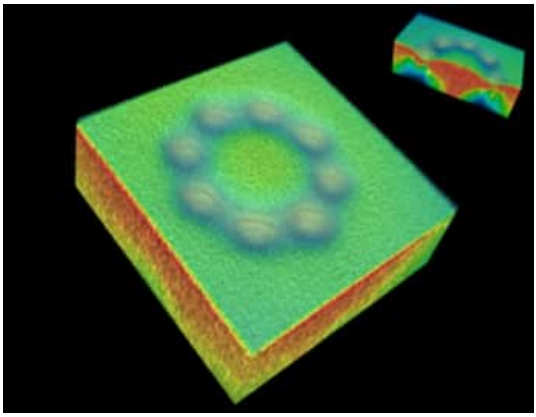

Fig. 4 A NLM image of a positive microlens produced by irradiating the PMG layer at the vertices of an octagon. 3D view together with its orthogonal cross section (inset) is shown

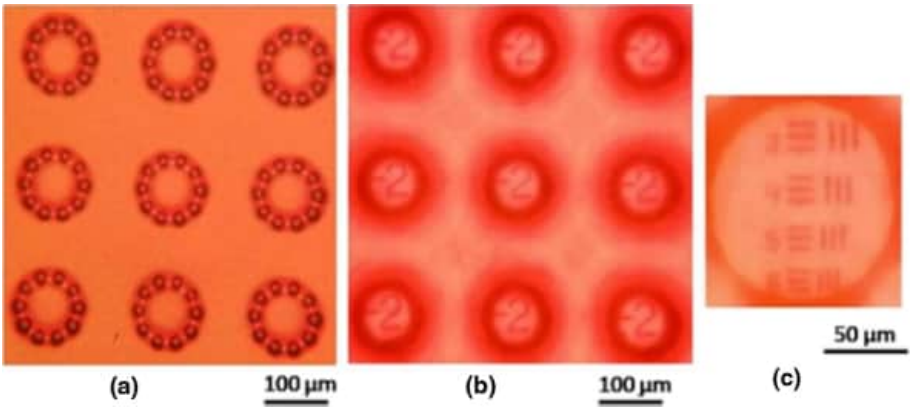

Fig. 5 **a** Reflection image of an array of 3×3 positive power microlenses produced by irradiating PMG layer at the vertices of an octagon, **b** Transmission images produced by the array, **c** A resolution chart as seen through the microlens

We were able to efficiently manufacture arrays of microlenses (Fig. 5a) with rather good imaging properties (Fig. 5b and c).

The best results were obtained with the octagonal arrangement of dots. Their radius of curvature and the corresponding focal length can be controlled by the diameter of a polygon (Fig. 6). We have measured the spatial resolution of the PMG layer by writing a series of gratings and found that we can manufacture up to 120 lp/mm.

3.2 Positive and negative microlenses for security

Microlenses have significant security applications for document protection (Walger et al. 2019, 2020; Seidler et al. 2014). In standard implementation, their effectiveness is based on Moiré effect between a microlens array and a, suitably designed, micro-pattern or another microlens array. Superposition of two overlaid arrays produces dynamic effects similar to holograms – i.e., the resulting image varies with respect to observation direction.

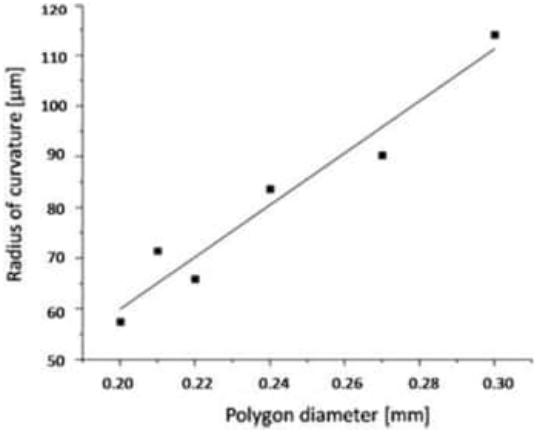

Fig. 6 A linear relation between the microlens radius of curvature and the diameter of a polygonal arrangement of dots

Difficulty of counterfeiting such a pair of arrays stems from tight tolerances of microlens parameters and the necessity of their strict alignment. While this seems to be an attractive security feature it is technologically complex to achieve in practice. That is why the corresponding technologies are economically viable only through mass production (usually by printing or embossing). Production of individualized, unique, hard-to-copy security elements is thus difficult and impractical.

Here we show that the technology presented here offers another way to produce unique security elements quickly and easily (on the fly) by changing microlens parameters (position, sag, diameter, focal length, mutual position). We demonstrate the principle by producing a microlens-based QR-code (see Fig. 7(a) and (b)).

Each dot of a standard 21×21 QR-code is a negative microlens, except for one or several selected, which are a positive. Security features are focal lengths of individual microlenses (either positive or negative) of a QR-code.

Focal length of each microlens is revealed by placing a closely positioned micro-sized object while detecting the size of its image. Here we used a butterfly wing scale as such object, positioned on the other side of a microlens substrate. Due to the wide view field of negative microlenses, image of an object is seen across several microlenses in shifted positions – yet another, difficult to copy, feature (Fig. 7(c) and (d)).

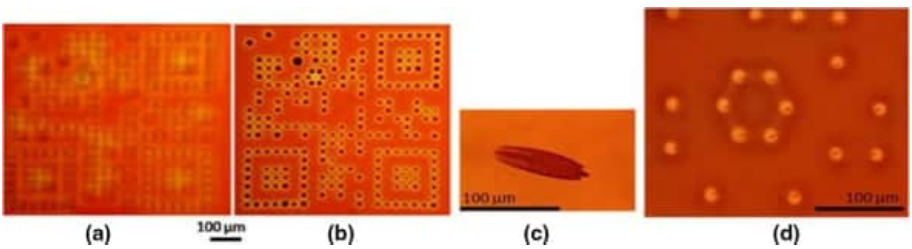

Fig. 7 **a**, **b** A microlens-based QR-code in two focal positions. **c** An image of butterfly wing scale observed through one of a QR-code lenses. **d** Multiple images of butterfly wing scale from Fig. (c) produced by QR code microlenses.

3.3 In vitro cytotoxicity of hydrogel samples towards HaCaT cells

Cytotoxic effects of PMG were investigated using HaCaT cell culture. To evaluate the cytotoxic effect of the PMG dissolved in 0.01 mM PBS on HaCaT cells, the crystal violet assay was performed. Relative growth rate of HaCaT cells in the presence of different concentrations of tested sample compared to untreated control is presented in Fig. 8. Tested sample was evaluated as non-toxic to the HaCaT cell line with respective IC_{50} values of $^{>}$ 400 mg/mL, a concentration which is considered as the limit of toxicity (Stojković et al. 2020).

4 Discussion

Microlens fabrication enables efficient control of each individual microlens by controlling a number of process parameters: laser beam size, shape, power, angle, speed and exposure, as well as physical/chemical properties of the PMG layer. There are certain limitations, drawbacks and possibilities which will be discussed in this section.

Manufacturing speed of microlenses is limited by the laser energy density (determined by the laser power and focal point size), absorbance, viscosity and surface tension of melted gel. This is a complex process difficult to model in a simple way. However, we were able to find appropriate conditions experimentally. Laser powers above 7.5 mW and exposure times longer than 100 ms gave us complete control of the process and production of predictable lens size and profile.

The material is soft and elastic due to the presence of a plasticizer. Its stress–strain behavior depends on the PS concentration, as shown earlier in the case of commercial tot'hema, when the corresponding Young's moduli were between 1 and 10 MPa (Murić et al. 2013). Also, for high-concentration (30%) of tot'hema, more than 200% elongation was achieved. In the case of PMG, the above properties are retained. Elasticity and stretchability can be utilized to manufacture tunable optical components.

On the other hand, the softness makes material sensitive to mechanical scratching and damaging. That is why it must be protected by an additional mechanically resistant layer. Alternatively, the material can be hardened by simply placing in water to let plasticizer diffuse out.

We observed the layer's surface under the polarizing microscope and noticed that there were no internal, residual stresses (material is homogeneous).

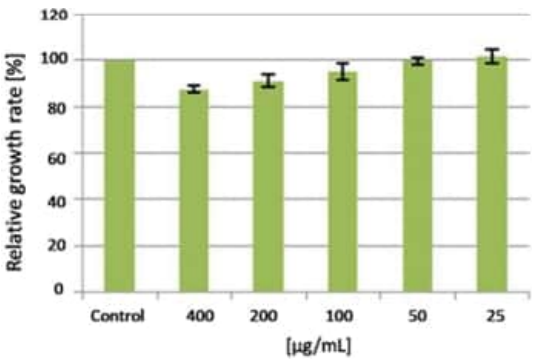

Fig. 8 Relative growth rate of HaCaT cells in the presence of different concentrations of PMG

The material remains photosensitive for a long time even if exposed to normal laboratory conditions. Its shelf life is mainly determined by slow evaporation of water and photo-bleaching of sensitizer. If the atmosphere is too dry, concentration of water diminishes and constituent chemicals start crystallizing and the layer attains a milky appearance. In that sense, it is preferable to keep material in a humid and light-tight container. From the practical experience, material processing can be performed under normal lighting without special precautions or dimmed light. However, we have a few years old gelatine layers, stored under normal laboratory conditions, which are still photosensitive and we were able to produce good quality microlenses. They are very stable, too, and the image quality remains constant during many months and even years under normal conditions. Of course, material has to be protected from scratches and dust as in the case of all the other optical surfaces.

The material presented here is not unique. Instead of eosin, we have tried gelatin sensitization with several natural fluorophores: anthocyanin, betanin and several other food dyes with excellent results. Additionally, we have tried other gels based on chitosan and pectin with very promising results. That is why we can claim that many other gels, humectants and sensitizers can further enhance microlens production speed and surface quality.

Depending on how material is prepared, buckling induced by evaporation of solvent produces unpredictable surface pattern. Even then, re-melting of material by the laser beam flattens the surface and produces good optical components. As a result, a combination of random buckling surface structure and regular optical components produce uniquely and nonreproducibly complex security features.

Yet another possibility stems from photo damage of the material, which occurs above certain power density threshold. In that case, material carbonizes, producing strongly localized damage zone in a center of the laser spot. Interestingly, this does not preclude microlens imaging, but adds a new feature to a security component.

Here we emphasize that the technology described here is neither additive nor subtractive because no material is added or removed. It is important to note that all the substances used are not volatile and the melting temperature of the material is below 50 °C, so that water evaporation is negligible. However, do to the melting, surface tension compresses and densifies the material. This is witnessed by the increased intensity of fluorescence at the circumference of the cavity. That is why the volume of the laser-induced dip is larger than the volume on the edge (Murić et al. 2009).

The material is complex mixture of nontoxic chemical aiming to fulfill several requirements: preventing crystallization, retention of constant amount of water, reducing the melting point of the gel, to enable efficient flow during laser melting, retaining plastic and elastic properties of the material, increasing the laser energy absorption. Proper composition was found experimentally and found to be stable before and after microlens fabrication.

Material has certain drawbacks too. It is soft, and can be easily damaged if unprotected. On the other hand, this property can be used to detect tampering and produce tamper sensitive tags. Material surface is sticky and dust particles easily adhere to its surface. Therefore, cleanliness is important factor in practical usage of the material.

We used gelatin as a base material, but the working principle is universal and can be applied to any material which can be locally melted, without damage on a sufficiently low temperature (preferably below 100 °C). In that respect we tested chitosan, too with quite good results which will be presented in the future publications.

Applications are not limited to microlenses and arbitrary structures can be manufactured such as microchannels, diffraction gratings, holograms (see Fig. 9).

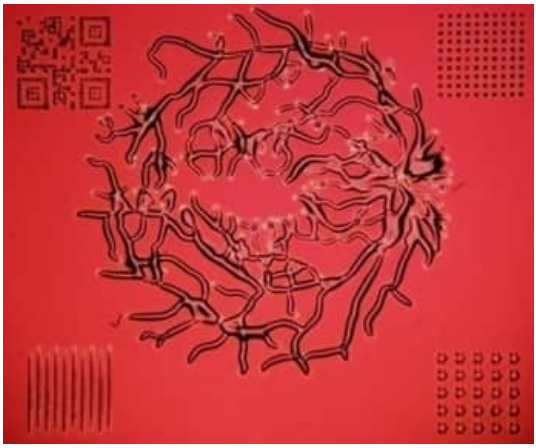

Fig. 9 A range of microoptical structures which can be fabricated on the PMG layer – retinal vessel model (center), QR-code (top left), negative microlens array (top right), positive microlens (bottom right) array, grating (bottom left)

5 Conclusions

We have presented a new, gel-based, material suitable for the fast and efficient generation of a wide range of microoptical and micromechanical components.

There are several advantages of the proposed method:

- Cheap lasers can be used as long as they have a circular laser beam profile and 2% power stability within the millisecond time interval.
- Chemicals used to produce the PMG are non-poisonous at the stated concentrations, as verified by biocompatibility tests.
- Fabrication time is fast enough to enable rapid prototyping of on-demand components.
- A variety of optical and micromechanical components can be fabricated within a single manufacturing operation.
- Components require no further processing and can be used immediately following fabrication.

Supplementary Information The online version contains supplementary material available at https://doi.org/10.1007/s11082-022-03681-0.

Acknowledgements The authors acknowledge funding provided by the Institute of Physics Belgrade, University of Belgrade, through the grant by the Ministry of Education, Science and Technological Development of the Republic of Serbia.

Author Contributions BM synthesized a photo-meltable material. DG, BZ and DP constructed a laser writing device used through this research. DP DG and MR wrote control software. BM DP and MR tested material properties. MZN. tested in vitro biocompatibility and microbial susceptibility toward synthesized gel material. DP Developed a thermal model of material bleaching. DP BM and MR jointly wrote the manuscript.

Funding This research was partially funded by the NATO Science for Peace and Security programme, project SPS G5618, Biological and bioinspired structures for multispectral surveillance.

Declarations

Conflict of interest There are no conflicts to declare.

References

Deng, C., Kim, H., Ki, H.: Fabrication of a compound infrared microlens array with ultrashort focal length using femtosecond laser-assisted wet etching and dual-beam pulsed laser deposition. Opt. Exp. **27**, 28679–28691 (2019)

Duarte-Quiroga, R.A., Calixto, S.: Dynamical optical microelements on dye-sensitized gels. Appl. Opt. **39**, 3948–3954 (2000)

Grigaliūnas, V., Lazauskas, A., Jucius, D., Viržonis, D., Abakevičienė, B., Smetona, S., Tamulevičius, S.: Microlens fabrication by 3D electron beam lithography combined with thermal reflow technique. Microelectron. Eng. **164**, 23–29 (2016)

Guan, Y., Zhang, Y.: PNIPAM microgels for biomedical applications: from dispersed particles to 3D assemblies. Soft Matter **7**, 6375–6384 (2011)

ISO 6983–1:2009(en) Automation systems and integration — Numerical control of machines — Program format and definitions of address words — Part 1: Data format for positioning, line motion and contouring control systems

Jiang, H., Kaminska, B., Porras, H., Raymond, M., Kapus, T.: Microlens arrays above interlaced plasmonic pixels for optical security devices with high-resolution multicolor motion effects. Adv. Opt. Mater. **7**, 1–10 (2019)

Kemme, S.A.: Microoptics and nanooptics fabrication. CRC Press (2009)

Krmpot, A.J., Tserevelakis, G.J., Murić, B.D., Filippidis, G., Pantelić, D.V.: 3D imaging and characterization of microlenses and microlens arrays using nonlinear microscopy. J. Phys. d: Appl. Phys. **46**, 195101 (2013)

Lee, X.-H., Moreno, I., Sun, C.-C.: High-performance LED street lighting using microlens arrays. Opt. Exp. **21**, 10612–10621 (2013)

Li, Y., Guo, M., Li, Y.: Recent advances in plasticized PVC gels for soft actuators and devices: a review. J. Mater. Chem. c. **7**, 2991–3009 (2019)

Moore, S., Gomez, J., Lek, D., You, B.H., Kim, N., Song, I.H.: Experimental study of polymer microlens fabrication using partial-filling hot embossing technique. Microelectron. Eng. **162**, 57–62 (2016)

Murić, B., Pantelić, D., Vasiljević, D., Panić, B.: Microlens fabrication on tot'hema sensitized gelatin. Opt. Mater. **30**, 1217–1220 (2008)

Murić, B., Pantelić, D., Vasiljević, D., Panić, B., Jelenković, B.: Thermal analysis of microlens formation on a sensitized gelatin layer. Appl. Opt. **48**, 3854–3859 (2009)

Murić, B., Pantelić, D., Vasiljević, D., Zarkov, B., Jelenković, B., Pantović, S., Rosić, M.: Sensitized gelatin as a versatile biomaterial with tailored mechanical and optical properties. Phys. Scr. **T157**, 014018 (2013)

Murić, B.D., Pantelić, D.V., Vasiljević, D.M., Panić, B.M.: Properties of microlenses produced on a layer of tot'hema and eosin sensitized gelatin. Appl. Opt. **46**, 8527–8532 (2007)

Rabasović, M.D., Pantelić, D.V., Jelenković, B.M., Ćurčić, S.B., Rabasović, M.S., Vrbica, M.D., Lazović, V.M., Ćurčić, B.P.M., Krmpot, A.J.: Nonlinear microscopy of chitin and chitinous structures: a case study of two cave-dwelling insects. J. Biomed. Opt. **20**, 16010 (2015)

Schürer, N., Köhne, A., Schliep, V., Barlag, K., Goerz, G.: Lipid composition and synthesis of HaCaT cells, an immortalized human keratinocyte line, in comparison with normal human adult keratinocytes. Exp. Dermatol. **2**, 179–185 (1993)

Seidler, R., Heim, M., Wiedner, B., Rahm, M.: Method for manufacturing security paper and microlens thread. US 2014/0238628 A1 (2014)

Stojković, D., Drakulić, D., Gašić, U., Zengin, G., Stevanović, M., Rajčević, N., Soković, M.: Ononis spinosa L. an edible and medicinal plant: UHPLC-LTQ-Orbitrap/MS chemical profiling and biological activities of the herbal extract. Food & Func. **11**, 7138–7151 (2020)

Taylor, M., Tomlins, P., Sahota, T.: Thermoresponsive gels. Gels **3**, 1–31 (2017)

Walger, T., Besson, T., Flauraud, V., Hersch, R.D., Brugger, J.: 1D moiré shapes by superposed layers of micro-lenses. Opt. Express. **27**, 37419–37434 (2019)

Walger, T., Besson, T., Flauraud, V., Hersch, R.D., Brugger, J.: Level-line moirés by superposition of cylindrical microlens gratings. J. Opt. Soc. Am. a. **37**, 209–218 (2020)

Zarkov, B., Grujić, D., Pantelić, D.: High-resolution dot-matrix hologram generation. Phys. Scr. **T149**, 014021 (2012)
Zhang, T., Li, P., Yu, H., Wang, F., Wang, X., Yang, T., Yang, W., Li, W.J., Wang, Y., Liu, L.: Fabrication of flexible microlens arrays for parallel super-resolution imaging. Appl. Surf. Sci. **504**, 144375 (2020)
Zhou, J., Sun, T., Zong, W.: A new approach to fabricate micro lens array using fast tool servo. Int. J. Nanomanuf. **7**, 475–487 (2011)

polymers

MDPI

Article

Characterization and Optimization of Real-Time Photoresponsive Gelatin for Direct Laser Writing

Branka D. Murić [1,*], Dejan V. Pantelić [1], Mihajlo D. Radmilović [1], Svetlana N. Savić-Šević [1] and Vesna O. Vasović [2]

[1] Institute of Physics, University of Belgrade, Pregrevica 118, 11080 Belgrade, Serbia; pantelic@ipb.ac.rs (D.V.P.); mihajlor@ipb.ac.rs (M.D.R.); savic@ipb.ac.rs (S.N.S.-Š.)
[2] Western Serbia Academy of Applied Studies, Užice Department, Trg Svetog Save 34, 31000 Užice, Serbia; bolex65@yahoo.com
* Correspondence: muric@ipb.ac.rs

Abstract: There is an abundance of plastic materials used in the widest range of applications, such as packaging, machine parts, biomedical devices and components, etc. However, most materials used today are non-decomposable in the environment, producing a huge burden on ecosystems. The search for better, safer alternatives is still on. Here we present a detailed analysis of a simple, cheap, non-toxic, even edible, eco-friendly material, which can be easily manufactured, laser patterned and used for the fabrication of complex structures. The base substance is gelatin which is made photoresponsive by adding plasticizers and sensitizers. The resulting films were analyzed with respect to their optical, thermal and mechanical properties, which can be modified by a slight variation of chemical composition. The material is optimized for rapid laser-manufacturing of elastic microstructures (lenses, gratings, cantilevers, etc.) without any waste or residues. Overall, the material properties were tailored to increase photothermal responsivity, improve the surface quality and achieve material homogeneity, transparency and long-term stability (as verified using electron microscopy, infrared spectroscopy and differential scanning calorimetry).

Keywords: gelatin; bio-eco-polymers; physicochemical properties; optical elastomers; rapid laser printing; microstructures

Citation: Murić, B.D.; Pantelić, D.V.; Radmilović, M.D.; Savić-Šević, S.N.; Vasović, V.O. Characterization and Optimization of Real-Time Photoresponsive Gelatin for Direct Laser Writing. *Polymers* **2022**, *14*, 2350. https://doi.org/10.3390/polym14122350

Academic Editor: Oh Seok Kwon

Received: 29 April 2022
Accepted: 5 June 2022
Published: 9 June 2022

1. Introduction

The mechanical strength, low production cost and manufacturability of petroleum-based plastics established them as the most popular packaging materials [1]. Unfortunately, their non-biodegradability makes them an important source of pollution [2]. The ecological impact of petroleum-based plastics has accelerated the worldwide interest in biodegradable polymers from renewable resources. Despite the great potential of biodegradable polymers to solve the problem of plastic waste, they are rarely used, considering that their production is relatively expensive and they do not possess all the other properties (e.g., mechanical, optical, and electrical) required by various end-applications [3]. Additionally, such materials may have quite variable properties. For example, tensile strength, strain at break and elasticity (Young's modulus) depend on the raw material source, additives, molecular structures, etc. [4,5].

A good example of a natural biodegradable polymer from renewable resources is starch which is inexpensive, readily available and biodegradable. However, its mechanical strength is strongly modulated by its moisture sensitivity while being difficult for thermal processing (it thermally decomposes before being melted). To modify these characteristics, starch is blended with other polymers [6–8]. Unfortunately, these blends can affect biodegradability. Furthermore, there is a direct relationship between the starch-based bioplastic properties and different starch botanical sources. Namely, the amylose and amylopectin proportion, which depends on starch biosynthesis enzymes, soil type, and

climatic conditions during plant growth, strongly influences the bioplastic gelation temperature and mechanical and rheological properties [9]. Nevertheless, significant research and technological work invested in the development of starch-based polymers in the packaging sectors of food, cosmetics, pharmaceuticals, etc. [10–12].

Gelatin, yet another biocompatible and biodegradable polymer, is widely used in photography, food, pharmaceutical, biomedical and many others applications [13–17]. It has poor mechanical properties that limit its potential applications. A variety of chemical agents (formaldehyde, epoxy, glutaraldehyde and some others) are capable of crosslinking gelatin, consequently overcoming the brittleness of gelatin films, improving its flexibility, reducing the degree of swelling and enhancing its thermal stability. Glutaraldehyde [18] is usually used but is being replaced with genipin because of its lower cytotoxicity [19,20].

Besides gelatin, many other natural polymers (such as albumen, alginate, cellulose, chitosan, pullulan, etc.) can be used too [21,22]. We emphasize that the photoresponsiveness and photosensitivity of most materials stem from harmful and poisonous chemicals (such as dichromate compounds).

Also, gelatin is often mixed with other substances, e.g., chitosan, poly(vinyl alcohol), alginate and carbon nanotubes. These hybrid materials are specifically of interest in biomedicine for drug delivery, wound healing, cell culture and tissue engineering [23–25].

Gelatin hydrogels are photosensitized by various dyes, making them suitable for laser writing of microstructures (such as microfluidic channels, microlenses, micro-optoelectromechanical systems (MOEMS), lab on a chip, etc.) intended for a wide variety of applications [26–28]. Gelatin was widely used previously in optics, primarily as a photosensitive material for holography. Photo-crosslinking was achieved by adding ammonium dichromate or potassium dichromate, which resulted in holograms of excellent quality. It is known that gelatin doped with ammonium dichromate (dichromated gelatin—DCG) represents an almost ideal high-resolution holographic photosensitive material [29]. Additionally, DCG can be used as a material for the production of micro-optical components [30,31]. Most of them are toxic, difficult to manufacture and require complex chemical postprocessing. Various silicate-based materials (silicones, silica glass, etc.) were used for the fabrication of micro-optical components [32,33]. Compared to gelatin, they have higher thermal and chemical stability, but the fabrication processes are manly complex, multistep, time-consuming and costly, frequently including the use of poisonous chemicals.

Emerging applications in biomedicine, micro-mechanics, micro-optics, energy storage, and sensors require new materials, simultaneously possessing advanced optical, electrochemical, mechanical and biological properties [34–36]. Previously, we have described photosensitive tot'hema-gelatin as a good candidate material for applications requiring real-time manufacturing of micro-optical and micro-mechanical components [37–40]. Gelatin was modified with a complex aqueous mixture of various salts, plasticizers, humectants and preservatives (commercially sold under the trade name tot'hema, which is used to treat iron anemia). The material is simple to prepare, low-cost, non-toxic, biodegradable and can be patterned by direct laser writing (DLW—widely used non-contact high-precision processing technique [41,42]). Here, a variety of micro-optical and microfluidic structures were fabricated using DLW, and threshold laser energy was established. This kind of microprocessing is neither additive nor subtractive as the material is only redistributed without any waste.

Therefore, in order to fully explore and optimize the capabilities of tot'hema-gelatin films for real industrial applications, the physicochemical characteristics of the film were studied in more detail and disclosed in this paper. We correlated the applied concentration of tot'hema with the film properties, such as color, thickness, light transmission, mechanical (tensile strength, elongation at break and Young's modulus), thermal properties, moisture content, swelling, the functional group on the film surface as well as surface morphology. These properties are essential for establishing optimal conditions of material used as an elastomer for adaptive, rapid prototyping of micro-optics and micro-mechanics.

2. Materials and Methods

2.1. Materials

All chemical components were analytical grade, well known, easily available, cheap and non-toxic. Commercial gelatin from bovine skin (gel strength ~225 g Bloom, Type B) and NaCl (puriss, p.a.) were purchased from Sigma Aldrich. Tot'hema, an oral solution for the treatment of human anemia, was manufactured by Laboratoire Innotech International, France. According to the manufacturer's data [43], this is a complex water solution of gluconate (iron, manganese and copper) and excipients (glycerol, glucose liquid, saccharine, citric acid, polysorbate 80, etc.). Saline solution was purchased from Hemofarm (Serbia).

2.2. Film Preparation

A 5% water solution of gelatin with added NaCl (20% by weight of dry gelatin) was prepared as described in previous papers [37,38]. The tot'hema (ranging from 0% to 30% v/v) was mixed with gelatin solution by a magnetic stirrer. The series of five solutions (denoted as TG_X, where the letter X indicates the tot'hema percentage in solution) were prepared and centrifuged in order to remove all remaining impurities.

TG_X films were prepared by the gravity settling method [39]. Namely, the accurately measured volume of TG_X solution was pipetted onto a very clean, horizontally leveled microscope glass slide and dried in a stable environmental condition over the night.

2.3. Mechanical Properties

A film thickness was determined using a digital micrometer (an accuracy of 0.01 mm) at eight randomly selected points in the center and edges of the films. Measurements were averaged and taken as the film thickness.

The surface morphologies of the tot'hema-gelatin films were analyzed using a high-resolution scanning electron microscope equipped with a high brightness Schottky field emission gun (FEGSEM) and using non–contact profilometry (3D optical surface profiler—Zygo New View 7100).

The mechanical properties of the films were determined using a tensile testing machine, at a strain rate of 20 mm/min, as previously described for photosensitive tot'hema-gelatin, with minor modifications [44]. The dried film was cut by a brass mold, designed according to the ASTM standard [45], into a dog-bone-shaped specimen (see Figure 1). Three measurements were made for each film, and the average value was calculated. The tensile strength, elongation at break and Young's modulus were determined.

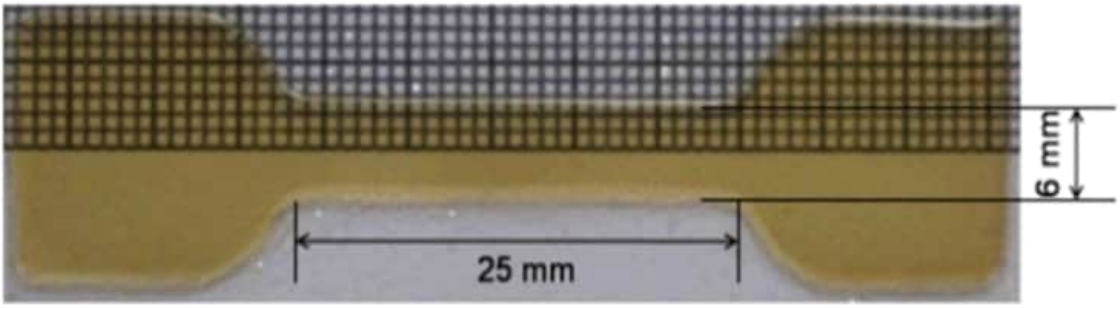

Figure 1. Optically transparent TG_20 film is used for tensile testing with dimensions according to the ASTM standards (gauge length 25 mm, width 6 mm).

2.4. Optical Properties

The transmittance of the TG_X films was analyzed using a fiber-type spectrometer (Ocean Optics) with a tungsten-halogen light as an illumination source in the wavelength range from 200 nm to 800 nm at room temperature.

A home-made direct laser writing system was used to fabricate microfluidic, micro-mechanic and micro-optical components on tot'hema modified gelatin film. A laser beam (488 nm wavelength, up to 100 mW power–iBEAM SMART, manufactured by Toptica)

was focused through the long-working-distance microscope objective. The samples were mounted on an xyz-coordinate stage to enable precise movement of the material along with the arbitrary pattern. The system was computer-controlled using G-code (standard programming language for CNC machines). More details about the system are given in a previous publication [46].

2.5. Physicochemical Properties

To determine how the number of water changes during the drying–dehydration of the film, the water content (WC) was measured. The TG_X films were weighted (w_1), then dried for 24 h at normal laboratory conditions, and weighted again (w_2). The WC for each film was determined as an average value of three measurements by the equation: $WC(\%) = [(w_1 - w_2)/w_1] \cdot 100$ [47].

In order to determine the influence of tot'hema concentration on the film swelling, TG_X films were immersed in saline solution for different intervals at laboratory conditions. Wet, swollen samples, after wiping with filter paper to remove excess liquid, were weighted again (w_w). The swelling factor (SF) of the films was calculated as the average value of three measurements by the equation: $SF(\%) = [(w_w - w_d)/w_d] \cdot 100$ where (w_d) corresponds to the weight of TG_X films before immersion [48].

Functional groups on the films were inspected by Fourier transformed infrared (FTIR) spectroscopy. The spectra were recorded on a Nicolet iS10 FTIR Spectrometer (Thermo Scientific Instruments) equipped with an attenuated total reflectance (ATR) accessory. ATR/FTIR measurements were done in the wavenumber interval from 500 to 4000 cm^{-1} with a resolution of 4 cm^{-1}.

The thermal stability of the films was analyzed by differential scanning calorimetry (DSC). An amount of about 2.5 mg of each film sample was packed in an aluminum pan (30 µL). The pan was sealed and analyzed using a DSC 131 EVO (SETARAM Instrumentation) differential scanning calorimeter previously calibrated with indium. An empty sealed pan was used as a reference. Both pans were placed in a chamber under the nitrogen flow of 20 mL/min, kept at 20 °C for 5 min and subsequently heated from 20 to 250 °C with a heating rate of 10 °C/min. To construct a baseline, two empty pans were placed in the chamber and measured under the same experimental conditions. The baseline subtraction was performed using the CALISTO Processing software (SETARAM Instrumentation).

3. Results

The pure gelatin film (TG_0) has a uniform, relatively smooth and flat surface, which indicates that the gelatin has a good film-forming ability. We have found that there is no noticeable difference in the gelatin film surface after tot'hema adding. Films still keep a rather smooth, uniform and homogeneous surface (without pores or cracks), indicating that there is good compatibility between tot'hema and gelatin molecules. Smoothness remains high after laser processing, as verified by SEM analysis of hexagonal concave microlenses array fabricated on photoresponsive tot'hema-gelatin film (Figure 2a). The lens-shaped dip is very symmetric (verified by the concentric shape of the corresponding interferogram in Figure 2b), and its roughness is of the order of several tens of nanometers (see Figure 2c). This makes photoresponsive tot'hema-gelatin an excellent material for the fabrication of micro-optical components.

To study mechanical properties, equal volumes of solution were used to prepare all TG_X films. An increase in tot'hema concentration resulted in the film thickening from 25 µm (pure gelatin) to 200 µm (30% of tot'hema) as a result of the plasticizer's interaction with the polymer chains. Tot'hema added to gelatin increases the distance between protein chains, increasing the film thickness. It can be noticed that the highest tot'hema concentration (30%) results in the thickest film due to the fact that most tot'hema ingredients are hydrophilic molecules that retain water and further increase the film thickness. Moreover, increased tot'hema content in gelatin film decreases the stress at break (reaching a minimum of 0.72 MPa at 30% of tot'hema) and increases the strain at break (turning tot'hema-gelatin

into an elastomer—maximum elasticity of about 220% was obtained). Mechanical properties of TG_X films, as a function of the concentration of tot'hema, are summarized in Table 1. The tot'hema addition (which is a mixture of different plasticizers and humectants) to the gelatin matrix improves the film flexibility and, consequently, makes it less rigid. Namely, glycerol is well known as a plasticizer. As a hydrophilic molecule with low molecular weight, glycerol can easily fit into protein chains creating hydrogen bonds [49]. Furthermore, tot'hema provides additional mobility of protein chains by increasing their distance, influencing a significant decrease of Young's modulus of elasticity, from 1933 MPa for pure gelatin (TG_0) to 948 MPa for the 5% tot'hema concentration (TG_5). As the tot'hema content increases further, Young's modulus value decreases even more (see Table 1). As demonstrated, the TG_30 film has Young's modulus of 0.32 MPa (which is very close to 0.35 MPa for PDMS), making it suitable for contact copying. Elastic properties of TG_X films are very important for the production of adaptive micro-optical components.

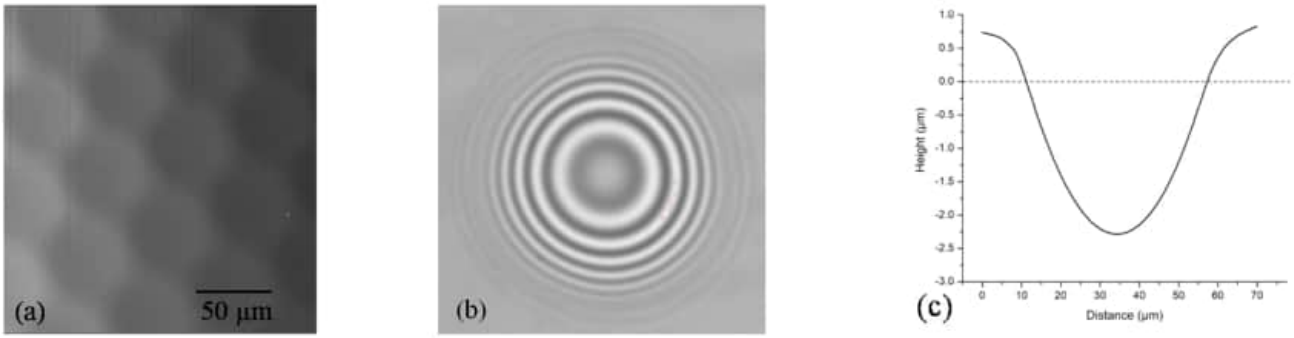

Figure 2. (**a**) SEM image of hexagonal microlenses array; (**b**) Interference fringe pattern of a microlens; and (**c**) 2D surface profile of a microlens.

Table 1. The film thickness, stress at break, strain at break and Young's modulus.

Film	Tot'hema (%)	Thickness (µm)	Stress at Break (MPa)	Strain at Break (%)	Young's Modulus (MPa)
TG_0	0	25 ± 10	58 ± 1	2 ± 0.1	1933 ± 40
TG_5	5	35 ± 10	37.92 ± 0.76	4 ± 0.2	948 ± 10
TG_10	10	50 ± 10	4.89 ± 0.10	40 ± 2	12.23 ± 0.06
TG_20	20	100 ± 10	1.71 ± 0.03	140 ± 6	1.22 ± 0.02
TG_30	30	200 ± 10	0.72 ± 0.01	224 ± 10	0.32 ± 0.01

Results are expressed as mean value ± standard deviation.

The change of color and transparency of the films varied from transparent (pure gelatin) and slightly yellow to yellow with increasing tot'hema content (see Figure 3).

Figure 3. Colors of TG_X films − (gelatin with 0%, 5%, 10%, 20%, and 30% of tot'hema).

The corresponding spectral light transmittance of the TG_X films as a function of wavelength is presented in Figure 4. Light transmission (in the visible range of 350–800 nm) of the pure gelatin (TG_0) film was above 80%, and the transmission increased with increasing wavelength (see Figure 4). By adding tot'hema, a layer is transformed into a spectral filter whose characteristics strongly depend on the concentration. In all cases, UV

radiation is strongly suppressed, making tot'hema-gelatin films an excellent filter for UV-sensitive applications. As we see, pure gelatin film transmits light very well at wavelengths from 350 nm to about 800 nm, but this can be changed at will using appropriate colorants.

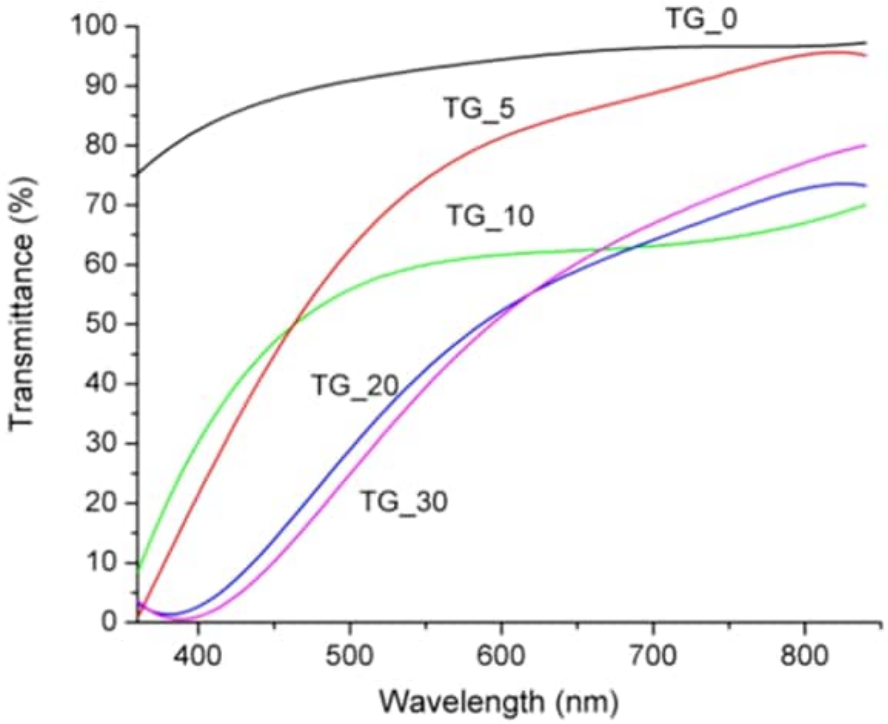

Figure 4. Spectral transmittance of the TG_X films (X− 0, 5, 10, 20, and 30% of tot'hema).

It was noticed that, after the initial rapid decrease of water content for all TG_X films during the drying process (see Figure 5a), the water content remains constant after 24 h of drying. After that, all the other properties remain stable, and the film is ready for further use (e.g., direct laser writing). Pure gelatin film had the lowest water content that exponentially increased with tot'hema content (see Figure 5b). This behavior is consistent irrespective of film thickness. The increase in water content in the presence of a tot'hema can be attributed to the additional hydrogen bonds formed between water molecules and gelatin chains. Water content can influence the physical properties of films (low-humidity films are generally stiff, while films with increased humidity are flexible and malleable). However, relatively high water content does not necessarily mean better physical properties in films [50] but makes the material suitable for a range of applications in biomedicine.

The influence of tot'hema concentration on the swelling of TG_X films during 1 h, 4 h and 24 h are shown in Figure 6.

The longer the film is immersed in the saline solution, the higher swelling (without deterioration) was observed (after 24 h, the film is fully saturated). Water content and swelling factor of the films were correlated. Opposite to the water content, the film swelling (see Figure 6) decreases with increasing concentration of tot'hema: pure gelatin film has the highest swelling factors (around 220%), while the tot'hema addition reduces the film swelling. This might be due to the limited spaces in film (gelatin network) for absorbing water as already occupied by tot'hema (plasticizer) molecules. The lowest swelling factor for TG_30 is correlated with the largest water amount in the film. Namely, in contact with the film, water diffuses into it, which results in the movement of polymer chains, incorporating between them and the dissolving of added ingredients. In this way, swelling enhances the release effect of some ingredients added to the film, which later diffuse into the system, manifesting different roles (for example, protective) [51].

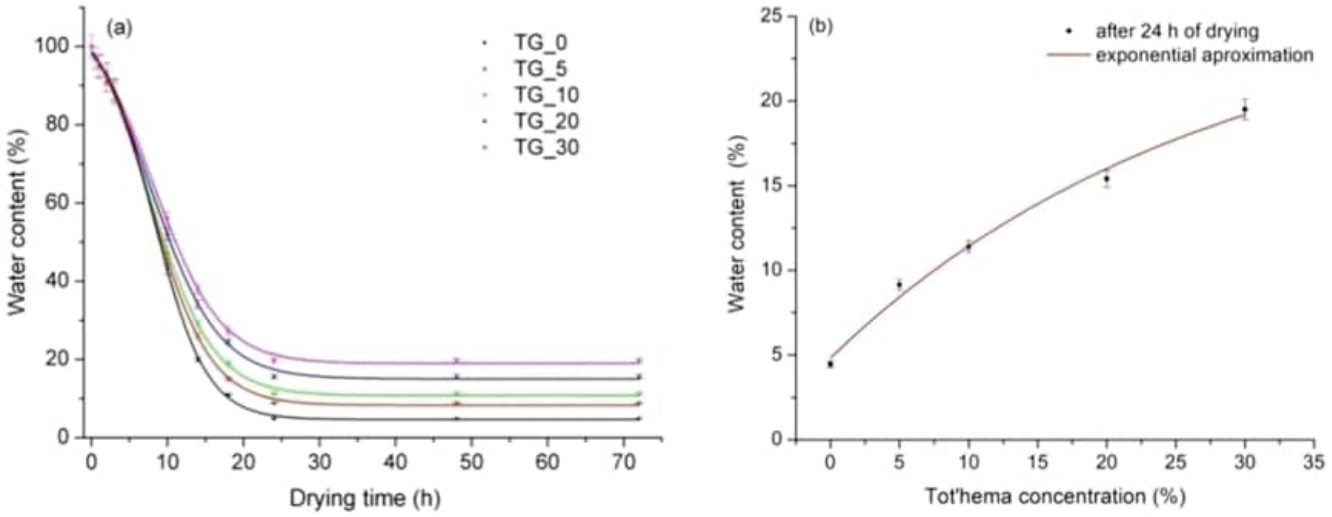

Figure 5. (**a**) Influence of drying time on the water content of TG_X films (X − 0, 5, 10, 20, and 30% of tot'hema); (**b**) The equilibrium water content as a function of tot'hema concentration.

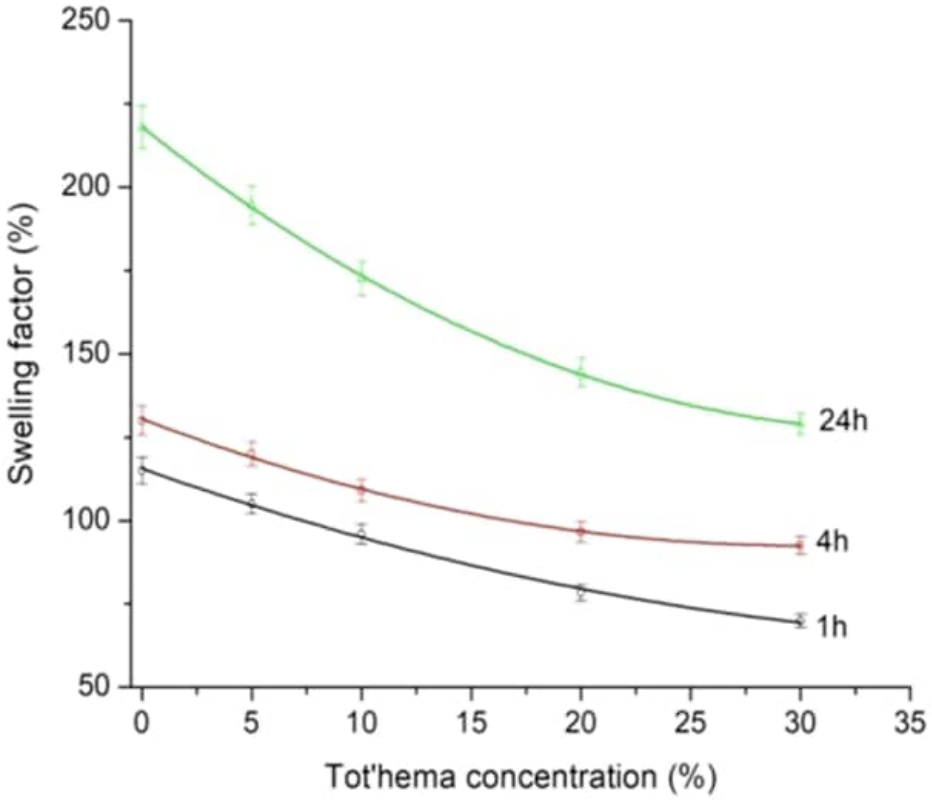

Figure 6. TG_X film (X− 0, 5, 10, 20, and 30% of tot'hema) swelling (during 1, 4 and 24 h) as a function of tot'hema concentration.

FTIR analysis was performed to study the interactions between tot'hema and gelatin matrix, i.e., to illustrate possible conformational changes in the gelatin films containing tot'hema. FTIR spectra of TG_X films are presented in Figure 7. A wide band in the range of 3500–3000 cm^{-1} can be attributed to O–H stretching and N–H bending, which are able to form a hydrogen bond with the carbonyl group of the peptide bond in the gelatin, as suggested by a literature review [52,53].

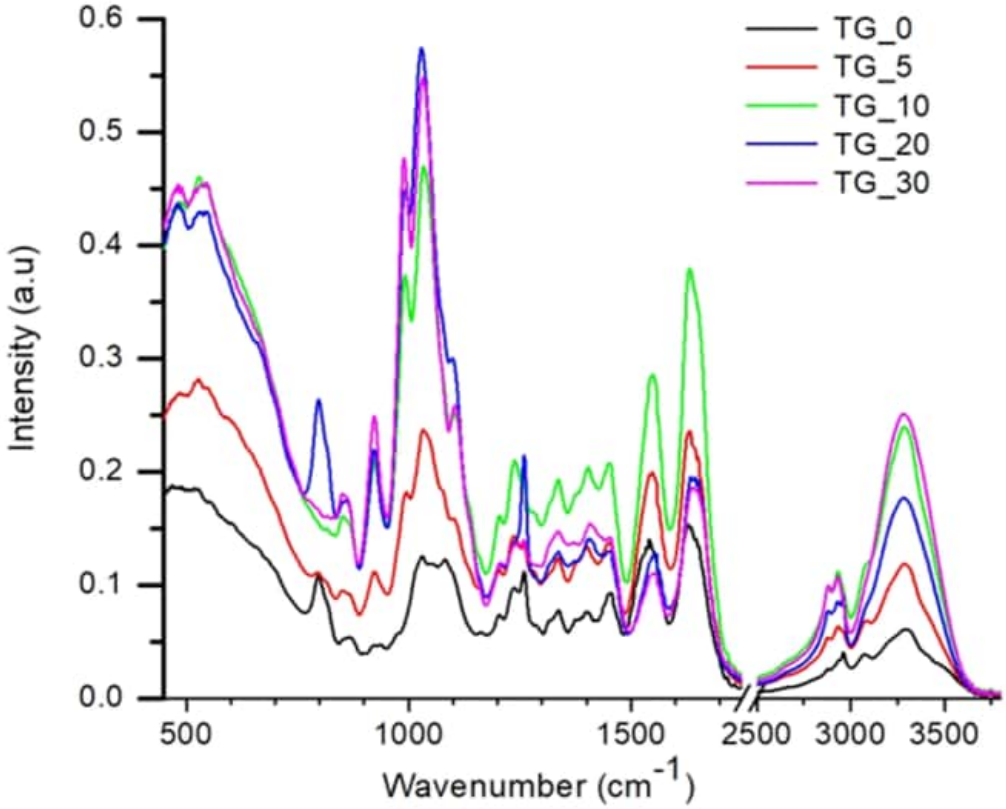

Figure 7. FTIR spectra of TG_X films (X− 0, 5, 10, 20, and 30% of tot'hema).

The FTIR spectrum of the pure gelatin film contains characteristic peaks at 3297 cm^{-1} and 2963 cm^{-1}, which can be attributed to –OH and –CH vibration stretching peaks. Further, it showed the characteristic amide I, amide II and amide III bands [54]. It is observed that the main absorption of the gelatin film such as C=O stretching at 1629 cm^{-1} (Amide I), N–H bending at 1542 cm^{-1} (Amide II), C–H deformation at 1403 cm^{-1}, and C–N stretching (Amide III) at 1237 cm^{-1} remains present in all films.

Compared to pure gelatin film, it was noticed that there are no new peaks in the spectrum of TG_X films. At the same time, the addition of tot'hema caused noticeable changes in the intensity of the Amide I, Amide II, and Amide III band. The peaks characteristic of C–H stretching of CH_2 and CH_3 at 2963 cm^{-1} and 2876 cm^{-1} in TG_X films vary significantly in intensity relative to the TG_0. Further, there is a slight shift in the peak's position, which can be explained by the formation of hydrogen bonds. The shift of these bands to a lower wavelength can be explained by the crosslinking between the components of TG_X films. These data indicate that the polar groups of tot'hema solution interact with the amino acids of the protein chains via inter-and intra-molecular hydrogen bonding and hydrophobic interaction. Therefore, tot'hema adding does not change the chemical composition of gelatin, but it changes the structure of gelatin due to intermolecular hydrogen bonding.

DSC is used to establish thermal stability due to changes in the physical and chemical properties of a material as a function of temperature or time [55]. It is well known that heat can cause structural transitions in protein networks that break chemical bonds [56]. The thermal properties of the film are closely related to their applications. The DSC thermograms of the TG_X films up to a temperature of 250 °C are shown in Figure 8.

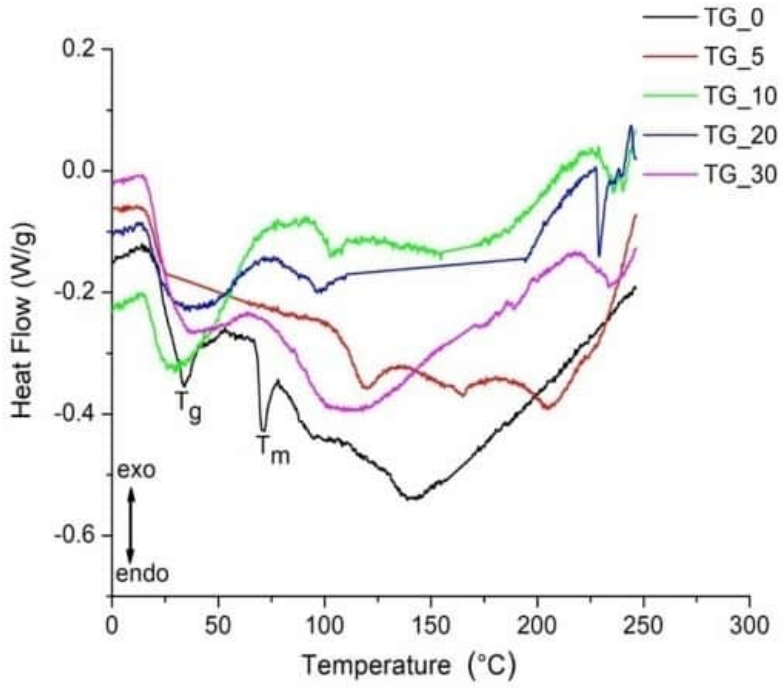

Figure 8. DSC curves of the TG_X films (X− 0, 5, 10, 20, and 30% of tot'hema). Tg and Tm − Endothermic peaks (denoted for pure gelatin film −TG_0) represent glass transition and melting temperature, respectively.

The first endothermic peak of pure gelatin film (TG_0) is recorded at a temperature of about 40 °C (see Figure 8). This endothermic peak represents glass transition (T_g) and is attributed to the transition from the glassy state to rubber. The endothermic peak that follows T_g, at a temperature around $T_m \approx 70$ °C is attributed to the melting and dissociation of arranged polymer parts. Some authors attribute this peak to the overlap of various processes such as the water evaporation, melting and recrystallization of small and/or imperfect gelatin crystals [57,58].

It was found that the peak temperatures and the enthalpies of these endothermic processes depend on the film preparation and drying conditions [57]. The endothermic peak at about 160 °C represents the gelatin decomposition temperature. It was observed that by adding and increasing the tot'hema content, the endothermic peaks become significantly wider and larger than that of the pure gelatin film. In addition, DSC analysis demonstrated that tot'hema addition, depending on its content, improves gelatin thermal stability. The melting temperature (T_m) increased when compared to pure gelatin film for all concentrations of tot'hema. T_m is typically associated with thermal stability: a high value of T_m corresponds to high thermal stability. It is already established that the thermal stability of polymers is related to crosslinking density [59]. In Figure 8, it is noticed that pure gelatin film (TG_0) has the lowest melting temperature (T_m). This temperature increases after crosslinking gelatin by tot'hema. The highest value of T_m was obtained for TG_5 film, while the T_m for films prepared with 10–30% of tot'hema show lower values. This behavior is attributed to the hydrophobicity of the gelatin molecular structure resulting from the addition of a large quantity of tot'hema. The improved thermal stability of TG_X films indicates that the temperature range of the use has been extended to about 100 °C, which is very important for practical applications.

To summarize—tot'hema is added to gelatin in order to increase the light absorption, modify its melting temperature and make it permanently elastomeric. Tot'hema concentration was optimized in order to make a compromise between gelatin thermal (e.g., melting temperature), mechanical (flatness) and optical (transparency) properties.

4. Discussion

The gelatin-based material described above has a number of useful optical, thermal and mechanical properties, which can be modulated by slight variations of its chemical composition. In this way, it becomes suitable for a range of applications, primarily dealing with micro-mechanics, microfluidics and micro-optics.

The most important property is photo-responsiveness. The photoresponsivegelatin studied here belongs to the class of waste and natural biopolymers (such as alginates and eggshells already reported for the electronics industry [35,36]), which is very important for developing non-toxic, eco-friendly materials. In contrast to the classical photosensitive materials (for example, silver-halide films, photoresists, dichromatedgelatin), the response of tot'hemamodified material is a consequence of physical, rather than chemical, processes. Here, absorbed light locally heats the material above the melting point, and surface tension pushes the fluidized layer, thus producing a dip (concave, lens-shaped recess), as can be seen in Figure 2. After the light is turned off, rapid cooling "freezes" the surface shape. Due to the low melting point of the gel (approximately 50 °C), the effect is easily achieved by a few milliwatt laser beams and millisecond irradiation times. Depending on the focal point size, micron-sized structures are easily formed. It is important to note that there is no material ablation because the melting point is much higher, and the material is simply displaced [60].

This makes the material extremely useful for rapid fabrication of micron-sized features using direct laser writing (DLW)—see Video S1 in a Supplementary Material of this paper demonstrating manufacturing of a complex array of microlenses. By controllably guiding the laser beam across the surface, virtually any shape can be formed (see Figure 9), where a rather complex microchannel structure (with three Tesla valves) is shown [61,62]. The whole pattern was fabricated in less than a minute using a 488 nm laser with 10 mW power (focused by 0.4 NA microscope objective).

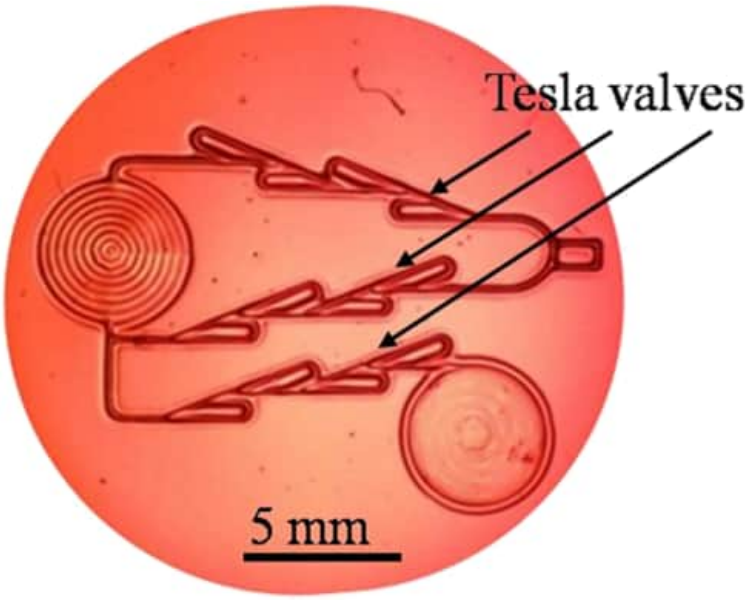

Figure 9. Complex microfluidic channels, with three Tesla valves formed on a tot'hema-gelatin.

Physicochemical processes during interaction with light depend strongly on the laser beam power and focus. The sensitivity threshold is reached at approximately 7.5 nJ/μm^2 of laser energy, which is easily achieved by focusing the laser beam through the long-working–distance microscope objective (Mitutoyo 20×, 0.4 NA). By appropriately controlling the laser beam size and power, irradiation time and writing speed, features can be fabricated with characteristic widths between 10 μm and 1000 μm and depths up to several hundred micrometers. By using high-power lasers, fabrication time can be significantly reduced

to milliseconds for the fabrication of individual microlenses or seconds for more complex structures like the one in Figure 9. Of course, the scanning speed of the laser beam must be increased to prevent material destruction. In most cases, there is no postprocessing, so the optical structures are usable immediately after fabrication.

We have mostly studied optical applications of the material [37,38], which simultaneously offers several key features—optical homogeneity, transparency, surface quality, easy fabrication and environmental friendliness. We have found that tot'hema ingredients mostly determine the material properties. As shown above, spectral absorption and melting point enable tailoring of the material to efficiently absorb the DLW beam.

The concept of microfabrication using meltable gels can be easily extended by replacing tot'hema with a suitable combination of plasticizers, humectants, preservatives and sensitizing dyes (e.g., betanin, eosin, anthocyanin, etc.) to achieve improved characteristics (faster melting, improved sensitivity, optical transparency after laser processing), which we described elsewhere [37].In this way, we were able to fabricate a range of optical components, such as diffraction gratings and arrays of positive and negative microlenses.

Gelatin-based materials are biocompatible, and additional chemicals used in this research are non-toxic (even food grade), giving the advantage of quick and natural biodegradability. We have covered a piece of the material with a few centimeters of soil and found that it was completely absorbed, without a trace, within a few days. For some applications, this might be a problem as we observed fungi growing on the material after some time (several days). To prevent that, we added table salt (NaCl), which made it durable and usable over a long period of exposure time to normal room conditions. Normal laboratory conditions (humidity, temperature) do not affect the material properties, and laboratory illumination does not diminish the material sensitivity (i.e., the material does not have to be kept in darkness). Dust is the major problem because of the stickiness of the film, and the material surface must be protected by an additional cover glass.

Softness is yet another possible disadvantage. Surfaces should not be scratched or punched with hard objects as this will certainly damage the structure. On the positive side, films can be easily cut, peeled from the substrate, stacked together and transferred. Mechanical hardness can be further significantly increased by removing the plasticizer (by submerging the films in cold water and letting the plasticizer diffuse out) or by hardening (tanning) with, e.g., alum [63]. In addition, we have been able to use tot'hema-gelatin as a template for contact copying into harder materials (epoxies, photopolymer composites).

The usable temperature range is limited by the melting point to somewhere between 50 °C and 100 °C, depending on tot'hema concentration. For the majority of applications, this is quite satisfactory and makes the material usable in the widest range of applications: lab-on-a-chip, sensors and micro-optics. We have also found that above the critical power density of the laser beam, material locally carbonizes and can be used as a blocking filter [39] and, possibly, as an electrical conductor.

Finally, the fabrication cost is really low. Materials used here are cheap and ubiquitous. Most of them can be found in the kitchen, while the fabrication of layers is straightforward and simple. Production methods are well known in the film industry and can be used both in low-and large-scale production.

5. Conclusions

To conclude, here we disclosed an innovative combination of well-known substances producing really versatile material for safe, real-time, low-cost, rapid microfabrication. Physicochemical properties of the material have been thoroughly studied, aiming to establish operational limits and optimize properties for the desired application. Application potential is high due to the simplicity of fabrication of highly complex structures, good optical properties, and manufacturability by direct laser writing without any further postprocessing, micrometers resolution, elastomeric characteristics, environmental friendliness, and non-toxic character—a rare combination of properties concentrated in a single material. Elasticity, uniform and homogeneous surface and optical transparency were achieved,

making the material suitable for the production of adaptive micro-optical components and protective filters. The temperature range of the material's applicability is extended up to 100 °C.

Supplementary Materials: The following supporting information can be downloaded at: https://www.mdpi.com/article/10.3390/polym14122350/s1, Video S1: Microoptics fabrication.

Author Contributions: B.D.M.: Conceptualization, methodology, investigation, visualization, writing original draft, reviewing, editing, resources, project administration; D.V.P.: Software, supervision, writing, editing, reviewing; M.D.R.: Software, data curation, reviewing; S.N.S.-Š.: Investigation, editing, reviewing; V.O.V.: Editing, project administration. All authors have read and agreed to the published version of the manuscript.

Funding: The authors acknowledge funding provided by the Institute of Physics University of Belgrade through the grant by the Ministry of Education, Science and Technological Development of the Republic of Serbia.

Data Availability Statement: Not applicable.

Acknowledgments: We thank Smilja B. Marković from the Institute of Technical Sciences of the Serbian Academy of Sciences and Arts, Belgrade, Serbia for help with FTIR and DSC measurements.

Conflicts of Interest: The authors declare no conflict of interest.

References

1. Chaudhary, V.; Bangar, S.P.; Thakur, N.; Trif, M. Recent advancements in smart biogenic packaging: Reshaping the future of the food packaging industry. *Polymers* **2022**, *14*, 829. [CrossRef] [PubMed]
2. Tokiwa, Y.; Calabia, B.P.; Ugwu, C.U.; Aiba, S. Biodegradability of plastics. *Int. J. Mol. Sci.* **2009**, *10*, 3722–3742. [CrossRef] [PubMed]
3. Vroman, I.; Tighzer, L. Biodegradable polymers. *Materials* **2009**, *2*, 307–344. [CrossRef]
4. Shamsuddin, I.M.; Jafar, J.A.; Shawai, A.S.A.; Yusuf, S.; Lateefah, M.; Aminu, I. Bioplastics as better alternative to petroplastics and their role in national sustainability: A review. *Adv. Biosci. Bioeng.* **2017**, *5*, 63–70. [CrossRef]
5. Rosenboom, J.G.; Langer, R.; Traverso, G. Bioplastics for a circular economy. *Nat. Rev. Mater.* **2022**, *7*, 117–137. [CrossRef] [PubMed]
6. Hassan, M.M.; Le Guen, M.J.; Tucker, N.; Parker, K. Thermo-mechanical, morphological and water absorption properties of thermoplastic starch/cellulose composite foams reinforced with PLA. *Cellulose* **2019**, *26*, 4463–4478. [CrossRef]
7. Souza, C.R.; Andrade, C.T. Processing and properties of thermoplastic starch and its blends with sodium alginate. *J. Appl. Polym. Sci.* **2001**, *81*, 412–420. [CrossRef]
8. Abe, M.M.; Martins, J.R.; Sanvezzo, P.B.; Macedo, J.V.; Branciforti, M.C.; Halley, P.; Botaro, V.R.; Brienzo, M. Advantages and disadvantages of bioplastics production from starch and lignocellulosic components. *Polymers* **2021**, *13*, 2484. [CrossRef]
9. Rivadeneira-Velasco, K.E.; Utreras-Silva, C.A.; Díaz-Barrios, A.; Sommer-Márquez, A.E.; Tafur, J.P.; Michell, R.M. Green nanocomposites based on thermoplastic starch: A review. *Polymers* **2021**, *13*, 3227. [CrossRef]
10. Onyeaka, H.; Obileke, K.; Makaka, G.; Nwokolo, N. Current research and applications of starch based biodegradable films for food packaging. *Polymers* **2022**, *14*, 1126. [CrossRef]
11. Jiang, T.; Duan, Q.; Zhu, J.; Liu, H.; Yu, L. Starch-based biodegradable materials: Challenges and opportunities. *Adv. Ind. Eng. Polym. Res.* **2020**, *3*, 8–18. [CrossRef]
12. Estrada-Monje, A.; Alonso-Romero, S.; Zitzumbo-Guzmán, R.; Estrada-Moreno, I.A.; Zaragoza-Contreras, E.A. Thermoplastic starch-based blends with improved thermal and thermomechanical properties. *Polymers* **2021**, *13*, 4263. [CrossRef] [PubMed]
13. Chauhan, S.; Bansal, M.; Khan, G.; Yadav, S.K.; Singh, A.K.; Prakash, P.; Mishra, B. Development, optimization and evaluation of curcumin loaded biodegradable crosslinked gelatin film for the effective treatment of periodontitis. *Drug Dev. Ind. Pharm.* **2018**, *44*, 1212–1221. [CrossRef] [PubMed]
14. Yang, J.; Sun, X.; Kang, Q.; Zhu, L.; Qin, G.; Chen, Q. Freezing-tolerant and robust gelatin-based supramolecular conductive hydrogels with double-network structure for wearable sensors. *Polym. Test.* **2021**, *93*, 106879. [CrossRef]
15. Liu, J.; Li, Y.; Hu, D.; Chao, X.; Zhou, Y.; Wang, J. An essential role of gelatin in the formation process of curling in long historical photos. *Polymers* **2021**, *13*, 3894. [CrossRef]
16. Lu, Y.; Luo, Q.; Chu, Y.; Tao, N.; Deng, S.; Wang, L.; Li, L. Application of gelatin in food packaging: A review. *Polymers* **2022**, *14*, 436. [CrossRef]
17. Maiti, S.; Khillar, P.S.; Mishra, D.; Nambiraj, N.A.; Jaiswal, A.K. Physical and self–crosslinking mechanism and characterization of chitosan-gelatin-oxidized guar gum hydrogel. *Polym. Test.* **2021**, *97*, 107155. [CrossRef]
18. Farris, S.; Song, J.; Huang, Q. Alternative reaction mechanism for the cross-linking of gelatin with glutaraldehyde. *J. Agric. Food Chem.* **2010**, *58*, 998–1003. [CrossRef]

19. Bigi, A.; Cojazzi, G.; Panzavolta, S.; Roveri, N.; Rubini, K. Stabilization of gelatin films by crosslinking with genipin. *Biomaterials* **2002**, *23*, 4827–4832. [CrossRef]
20. Zhao, Y.; Sun, Z. Effects of gelatin-polyphenol and gelatin–genipin cross-linking on the structure of gelatin hydrogels. *Int. J. Food Prop.* **2017**, *20*, S2822–S2832. [CrossRef]
21. Savić, S.; Pantelić, D.; Jakovijević, D. Real-time and postprocessing holographic effects in dichromated pullulan. *Appl. Opt.* **2002**, *41*, 4484–4488. [CrossRef] [PubMed]
22. Haniffa, M.A.C.M.; Ching. Y., C.; Abdullah, L.C.; Poh, S.C.; Chuah, C.H. Review of Bionanocomposite Coating Films andTheir Applications. *Polymers* **2016**, *8*, 246. [CrossRef] [PubMed]
23. Salahuddin, B.; Wang, S.; Sangian, D.; Aziz, S.; Gu, Q. Hybrid gelatin hydrogels in nanomedicine applications. *ACS Appl. Bio Mater.* **2021**, *4*, 2886–2906. [CrossRef] [PubMed]
24. Rakhshaei, R.; Namazi, H.; Hamishehkar, H.; Kafil, H.S.; Salehi, R. In situ synthesized chitosan−gelatin/ZnO nanocomposite scaffold with drug delivery properties: Higher antibacterial and lower cytotoxicity effects. *J. Appl. Polym. Sci.* **2019**, *136*, 47590. [CrossRef]
25. Afnas, V.M.; Unnikrishnan, G.; Budhe, S.; Manaf, O.; Ameen, J. PVA/gelatin/chitin ternary blend as a humidity sensing material. *J. Mater. Sci. Mater. Electron.* **2022**, *33*, 2031–2043. [CrossRef]
26. Nawroth, J.C.; Scudder, L.L.; Halvorson, R.T.; Tresback, J.; Ferrier, J.P.; Sheehy, S.P.; Cho, A.; Kannan, S.; Sunyovszki, I.; Goss, J.A.; et al. Automated fabrication of photopatterned gelatin hydrogels for organ-on-chips applications. *Biofabrication* **2018**, *10*, 25004. [CrossRef] [PubMed]
27. Liu, J.; Su, C.; Chen, Y.; Tian, S.; Lu, C.; Huang, W.; Lv, Q. Current understanding of the Applications of photocrosslinked hydrogels in biomedical engineering. *Gels* **2022**, *8*, 216. [CrossRef]
28. Pinto-Iguanero, B.; Olivares-Perez, A.; Mendez-Alvarado, A.W.; Fuentes-Tapia, I.; Trevino-Palacios, C.G. Non-hydroscopic vanilla doped dichromated gelatin holographic material. *Opt. Mater.* **2003**, *22*, 397–404. [CrossRef]
29. Pantelić, D.; Murić, B. Improving the holographic sensitivity of dichromated gelatin in the blue–green part of the spectrum by sensitization with xanthene dyes. *Appl. Opt.* **2001**, *40*, 2871–2875. [CrossRef]
30. Yao, J.; Cui, Z.; Gao, F.; Zhang, Y.; Guo, Y.; Du, C.; Zeng, H.; Qiu, C. Refractive micro lens array made of dichromate gelatin with gray-tone photolithography. *Microelect. Eng.* **2001**, *57–58*, 729–735. [CrossRef]
31. Calixto, S.; Scholl, M.S. Relief optical microelements fabricated with dichromated gelatin. *Appl. Opt.* **1997**, *36*, 2101–2106. [CrossRef] [PubMed]
32. Pan, A.; Gao, B.; Chen, T.; Si, J.; Li, C.; Chen, F.; Hou, X. Fabrication of concave spherical microlenses on silicon by femtosecond laser irradiation and mixed acid etching. *Opt. Express* **2014**, *22*, 15245–15250. [CrossRef] [PubMed]
33. Marcinkevičius, A.; Juodkazis, S.; Watanabe, M.; Miwa, M.; Matsuo, S.; Misawa, H.; Nishii, J. Femtosecond laser-assisted three-dimensional microfabrication in silica. *Opt. Lett.* **2001**, *26*, 277–279. [CrossRef] [PubMed]
34. Calixto, S.; Ganzherli, N.; Gulyaev, S.; Figueroa-Gerstenmaier, S. Gelatin as a photosensitive material. *Molecules* **2018**, *23*, 2064. [CrossRef]
35. Minakshi, M.; Higley, S.; Baur, C.; Mitchell, D.R.G.; Jonesd, R.T.; Fichtner, M. Calcined chicken eggshell electrode for battery and supercapacitor applications. *RSC Adv.* **2019**, *9*, 26981–26995. [CrossRef]
36. Wickramaarachchi, K.; Minakshi Sundaram, M.; Henry, D.J.; Gao, X. Alginate Biopolymer Effect on the Electrodeposition of Manganese Dioxide on Electrodes for Supercapacitors. *ACS Appl. Energy Mater.* **2021**, *4*, 7040–7051. [CrossRef]
37. Murić, B.D.; Pantelić, D.V.; Vasiljević, D.M.; Panić, B.M. Properties of microlenses produced on a layer of tot'hema and eosin sensitized gelatin. *Appl. Opt.* **2007**, *46*, 8527–8532. [CrossRef]
38. Murić, B.; Pantelić, D.; Vasiljević, D.; Panić, B. Microlens fabrication on tot'hema sensitized gelatin. *Opt. Mater.* **2008**, *30*, 1217–1220. [CrossRef]
39. Murić, B.D.; Pantelić, D.V.; Vasiljević, D.M.; Savić-Šević, S.N.; Jelenković, B.M. Application of tot'hema eosin sensitized gelatin as a potential eye protection filter against direct laser radiation. *Curr. Appl. Phys.* **2016**, *16*, 57–62. [CrossRef]
40. Murić, B.; Pantelić, D.; Vasiljević, D.; Zarkov, B.; Jelenković, B.; Pantović, S.; Rosić, M. Sensitized gelatin as a versatile biomaterial with tunable mechanical and optical properties. *Phys. Scr.* **2013**, *T157*, 14018. [CrossRef]
41. Krmpot, A.J.; Tserevelakis, G.J.; Murić, B.D.; Filippidis, G.; Pantelić, D.V. 3D imaging and characterization of microlenses and microlens arrays using nonlinear microscopy. *J. Phys. D Appl. Phys.* **2013**, *46*, 195101. [CrossRef]
42. Wu, Z.-L.; Qi, Y.-N.; Yin, X.-J.; Yang, X.; Chen, C.-M.; Yu, J.-Y.; Yu, J.-C.; Lin, Y.-M.; Hui, F.; Liu, P.-L.; et al. Polymer-Based Device Fabrication and Applications Using Direct Laser Writing Technology. *Polymers* **2019**, *11*, 553. [CrossRef] [PubMed]
43. Available online: www.vidal.fr/medicaments/tot-hema-sol-buv-en-ampoule-16626.html (accessed on 10 February 2022).
44. Keinonen, T.; Riihola, P.; Huttu, K.; Parkkonen, S. Dye films for optical demonstrations in the undergraduate laboratory. *Opt. Mater.* **1998**, *11*, 79–86. [CrossRef]
45. *ISO 527–3:2018*; Plastics—Determination of Tensile Properties—Part 3: Test Conditions for Films and Sheets. ISO: Geneva, Switzerland, 2018. Available online: https://www.iso.org/standard/70307.html (accessed on 12 March 2022).
46. Radmilović, M.D.; Murić, B.D.; Grujić, D.; Zarkov, B.; Nenadić, M.Z.; Pantelić, D.V. Rapid direct laser writing of microoptical components on a meltable biocompatible gel. *Opt. Quantum Electron.* **2022**, *54*, 361. [CrossRef]
47. Tabatabaei, S.D.; Ghiasi, F.; Gahruie, H.H.; Hosseini, S.M.H. Effect of emulsified oil droplets and glycerol content on the physicochemical properties of Persian gum-based edible films. *Polym. Test.* **2022**, *106*, 107427. [CrossRef]

48. Gahruie, H.H.; Eskandari, M.H.; Meeren, P.V.; Osseini, S.M.H. Study on hydrophobic modification of basil seed gum-based (BSG) films by octenyl succinate anhydride. *Carbohydr.Polym.* **2019**, *219*, 155–161. [CrossRef]
49. Rivero, S.; García, M.A.; Pinotti, A. Correlations between structural, barrier, thermal and mechanical properties of plasticized gelatin films. *Innov. Food Sci. Emerg. Technol.* **2010**, *11*, 369–375. [CrossRef]
50. Blanco-Pascual, N.; Fernández-Martín, F.; Montero, M.P. Effect of different protein extracts from Dosidicus gigas muscle co-products on edible films development. *Food Hydrocoll.* **2013**, *33*, 118–131. [CrossRef]
51. Siepmann, J.; Streubel, A.; Peppas, N.A. Understanding and predicting drug delivery from hydrophilic matrix tablets using the "Sequential layer" model. *Pharm. Res.* **2002**, *19*, 306–314. [CrossRef]
52. Queiroz, M.F.; Rachel, K.; Melo, T.; Sabry, D.A.; Sassaki, G.L.; Alexandre, H.; Rocha, O. Does the use of chitosan contribute to oxalate kidney stone formation. *Mar. Drugs* **2014**, *13*, 141–158. [CrossRef]
53. Farahnaky, A.; Dadfar, S.M.M.; Shahbazi, M. Physical and mechanical properties of gelatin–clay nanocomposite. *J. Food Eng.* **2014**, *122*, 78–83. [CrossRef]
54. Coates, J. Interpretation of infrared spectra, A practical approach. In *Encyclopedia of Analytical Chemistry: Applications, Theory and Instrumentation*; John Wiley & Sons, Ltd.: Hoboken, NJ, USA, 2006; pp. 1–23. [CrossRef]
55. Lin, S.-Y.; Wang, S.-L. Advances in simultaneous DSC–FTIR microspectroscopy for rapid solid-state chemicalstability studies: Some dipeptide drugs as examples. *Adv. Drug Deliv. Rev.* **2012**, *64*, 461–478. [CrossRef] [PubMed]
56. Liu, F.; Majeed, H.; Antoniou, J.; Li, Y.; Ma, Y.; Yokoyama, W.; Zhong, F. Tailoring physical properties of transglutaminase-modified gelatin films by varying drying temperature. *Food Hydrocoll.* **2016**, *58*, 20–28. [CrossRef]
57. Dai, C.A.; Chen, Y.-F.; Liu, M.-W. Thermal properties measurements of renaturated gelatin using conventional and temperature modulated differential scanning calorimetry. *Appl. Polym. Sci.* **2006**, *99*, 1795–1801. [CrossRef]
58. Mendieta-Taboada, O.; Sobral, P.J.A.; Carvalho, R.A.; Habitante, A.M.B.Q. Thermomechanical properties of biodegradable films based on blends of gelatin and poly(vinyl alcohol). *Food Hydrocoll.* **2008**, *22*, 1485–1492. [CrossRef]
59. Skopinska-Wisniewska, J.; Tuszynska, M.; Olewnik-Kruszkowska, E. Comparative Study of Gelatin Hydrogels Modified by Various Cross-Linking Agents. *Materials* **2021**, *14*, 396. [CrossRef]
60. Murić, B.; Pantelić, D.; Vasiljević, D.; Panić, B.; Jelenković, B. Thermal analysis of microlens formation on a sensitized gelatin layer. *Appl. Opt.* **2009**, *48*, 3854–3859. [CrossRef]
61. Hong, C.-C.; Choi, J.-W.; Ahn, C.H. A novel in-plane microfluidic mixer with modified Tesla structures. *Lab Chip* **2004**, *4*, 109–113. [CrossRef]
62. Tesla, N. Valvular Conduit. U.S. Patent 1329559, 3 February 1920. Available online: https://www.freepatentsonline.com/1329559.html (accessed on 12 March 2022).
63. Murić, B.D.; Panić, B.M. Microlenses with focal length controlled by chemical processes. *Phys. Scr.* **2012**, *T 149*, 14071. [CrossRef]